

THERMOHALINE VARIABILITY IN THE
UPPER LAYERS OF THE ARABIAN SEA

by

HAREESH KUMAR P. V.

Naval Physical and Oceanographic Laboratory, Cochin

Thesis submitted in partial fulfilment of the requirements
for the degree of Doctor of Philosophy
in Physical Oceanography

at

Cochin University of Science and Technology
Cochin

January, 1992

to my father

DECLARATION

I hereby declare that the thesis entitled "Thermohaline variability in the upper layers of the Arabian Sea" has not previously formed the basis of the award of any degree, diploma or associateship in any university.



HAREESH KUMAR P.V.

Scientist - C

Cochin - 682 021

January, 1992.

Naval Physical and Oceanographic Lab.

C E R T I F I C A T E

This is to certify that this Thesis is an authentic record of research work carried out by Mr. Hareesh Kumar P.V. under my supervision and guidance in the Naval Physical and Oceanographic Laboratory for the Ph.D. Degree of the Cochin University of Science and Technology and no part of it has previously formed the basis for the award of any other degree in any university.



Dr. BASIL MATHEW
(Research Supervisor)
Scientist-C

Cochin - 682 021
January, 1992

Naval Physical and Oceanographic Lab.

A C K N O W L E D G E M E N T S

I wish to express my deepest sense of gratitude to Dr. Basil Mathew for his valuable guidance and constant encouragement provided throughout the course of this work. I am very grateful to Dr. G.S. Sharma, Retired Professor, Cochin University of Science and Technology for his guidance in the early part of this study.

I am grateful to Shri.A.S. Ramamoorthy, Director, NPOL and Dr.V.K. Aatre, former Director, NPOL and Shri.K.R.G.K. Murthy, Head, Ocean Sciences Group for providing the necessary facilities to carryout this work. It would be a lapse on my part if I do not express my profound gratitude to Dr.R.R. Rao who has been a source of encouragement throughout this study and also for many fruitful discussions.

My thanks are also due to Shri.C.K.B. Kurup for kindly providing the necessary data sets utilised in this study. I also acknowledge the help received from Shri.N. Mohan Kumar, Shri.K.V. Sanil Kumar and Dr.Rao V.S.N Tatavarti at various stages of the preparation of this work. The support provided by my other colleagues in the Ocean Sciences Group is gratefully appreciated.

I am thankful to Shri.R. Sivakumar, Shri.R. Prasithlal and Shri.C.K. Joseph for providing the necessary expertise and facilities at the DRDO-Cochin University Computer Centre.

The help provided by Shri.P.C. Abraham, Shri.M.P. George, Shri.P.K. Sunil and Shri.K.S. Sahadevan in draughting the diagrams is gratefully acknowledged.

Finally I wish to thank my wife and mother for affording me the time and helpful supportive environment necessary for writing this thesis.

P R E F A C E

The Arabian Sea is an area of complex air-sea interaction processes with seasonal reversing monsoons. The associated thermohaline variability in the upper layers appears to control the large scale monsoon flow which is not yet completely understood.

The variability in the thermohaline fields is known to occur in temporal domain ranging from intra-diurnal to inter-annual time scales and on spatial domains of few tens of kilometers to few thousands of kilometers. In the Arabian Sea though the surface temperature was routinely measured by both conventional measurements and satellites, the corresponding information on the subsurface thermohaline field is very sparse due to the lack of adequate measurements. In such cases the numerical models offer promise in providing information on the subsurface features given an initial thermohaline field and surface heat flux boundary conditions.

This thesis is an outcome of investigations carried out on the various aspects of the thermohaline variability on different time scales. In addition to the description of the mean annual cycle, the one dimensional numerical models of Miller (1976) and Price et al (1986) are utilised to simulate the observed mixed layer characteristics at selected locations in the Arabian Sea on time scales ranging from intra-diurnal to synoptic scales under variable atmospheric forcing.

The thesis is divided in to seven chapters. The first chapter deals with general introduction and objectives of the study.

The mean annual cycle of mixed layer depth and salinity fields in the upper 200m of the Arabian Sea and T-S diagrams for typical regions are discussed in chapter II.

Chapter III deals with the annual cycle of the heat budget components of the Arabian Sea, with special emphasis on summer cooling based on net surface heat fluxes, rate of oceanic heat storage and heat change due to vertical motion.

A detailed investigation on the monthly variation of thermohaline structure at selected locations off the west coast of India is presented in chapter IV. The importance of upwelling/sinking in modifying the thermohaline field is discussed.

In chapter V, the response of the upper ocean under variable atmospheric forcing at typical locations in the Arabian Sea is studied. The mixed layer temperature and depth are simulated using the one dimensional numerical model of Miller (1976).

Chapter VI deals with the evolution of diurnal thermal cycle at a typical location in the eastern Arabian Sea. The one dimensional numerical model of Price et al (1986) is utilised to simulate the diurnal thermal cycle.

The summary, conclusions and future outlook are presented in chapter VII.

CONTENTS

Chapter I	Introduction	1-9
Chapter II	Some Aspects of the Seasonal Variability of the thermohaline fields in the Arabian Sea	10-20
Chapter III	Heat Budget of the Arabian Sea	21-39
Chapter IV	Seasonal Variation of thermohaline fields off the west coast of India	40-57
Chapter V	Simulation of the short-term variability of the mixed layer characteristics	58-71
Chapter VI	Intra-diurnal variability in the upper ocean Observations and Simulations	72-87
Chapter VII	Summary and Conclusions	88-95

CHAPTER I

INTRODUCTION

1.1 Introduction

The Arabian Sea is unique among the world oceans in several aspects. The wind field over the Arabian Sea reverses semi-annually, blowing from southwest during northern summer and from northeast during northern winter (Fig.1.1). The winds are weak and variable during transition periods, i.e. March/April and October/November. Of the two monsoons, the southwest monsoon prevails over a much longer period of the year and is stronger and steadier than the northeast monsoon.

The seasonal variation in the wind field is reflected in the distribution of temperature, salinity and the near surface circulation. Under the influence of this wind field a clockwise gyre is present in the Arabian Sea during southwest monsoon, while an anti-clockwise gyre prevails during northeast monsoon (Fig.1.2). During southwest monsoon a strong western boundary current known as Somali Current appears off Somalia which is by far the strongest current in the world oceans with speeds exceeding 7 knots (Swallow et al,1983). Recent observations (Bruce,1979; Swallow et al,1983; Schott,1983) have revealed the eddy nature of the Somali Current. Throughout the year a number of clockwise and anti-clockwise eddies of varying dimensions are found in the Arabian Sea which are maximum during transition months (Duing,1970). The Equatorial Undercurrent is known to be present during the early part of the year (Taft and Knauss,1967; Leetmaa and Stommel,1980). The Equatorial Jet appear only in the eastern part of the Arabian Sea during April-May and October-November (Wyrтки,1973).

The sea surface temperature (SST) in the Arabian Sea exhibits a bi-modal distribution, a warming phase during pre- and post- summer monsoon periods and cooling during winter and

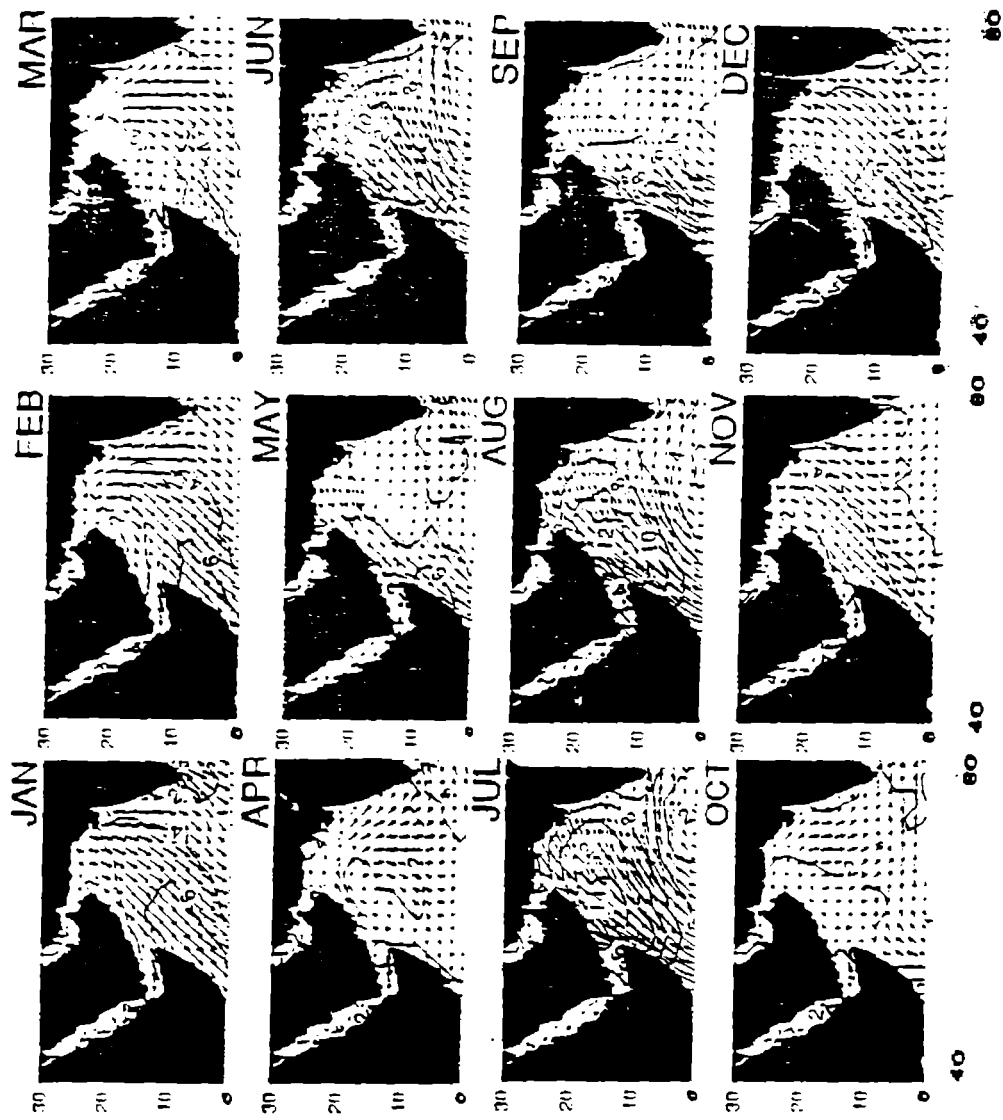


FIG. 1.1. OBSERVED MEAN SURFACE WIND VECTORS(m/s)

Rao et al (1991)

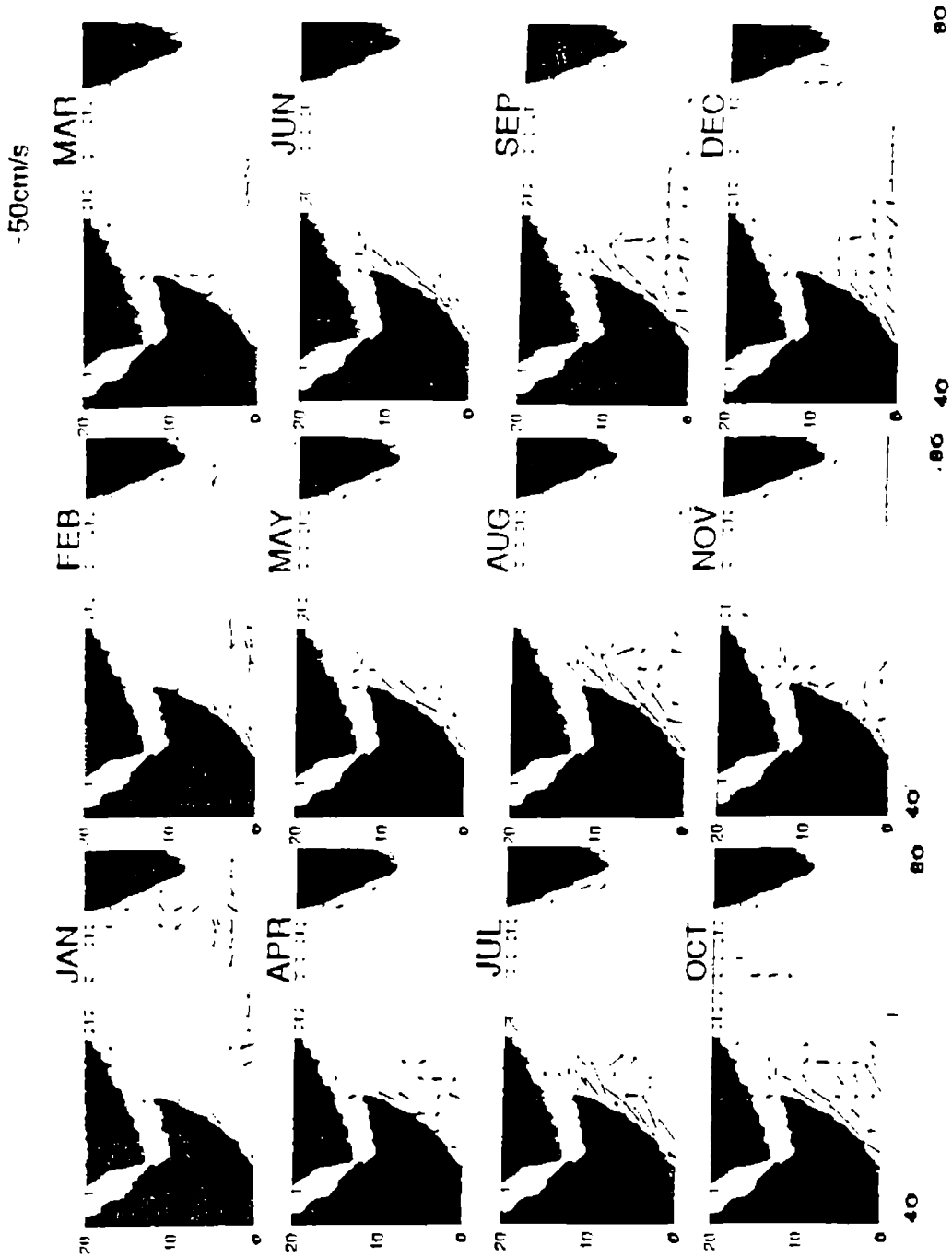


FIG. 1-2. OBSERVED SHIP DRIFT CURRENT VECTORS

Rao et al (1991)

summer (Wyrтки, 1971; Colborn, 1975; Hastenrath and Lamb, 1979a; Rao et al, 1989). The sea surface temperature and its relationship with the air-sea fluxes have been the objective of a large number of studies in the last few decades (Colon, 1964; Saha, 1974; McPhaden, 1982b; Rao et al, 1990; McCreary and Kundu, 1989). A mini warm pool, known as Indian Ocean warm pool, with temperature greater than 30°C is noticed in the eastern Arabian Sea during May, just prior to the onset of summer monsoon (Seetaramayya and Master, 1984; Sadler et al, 1987; Joseph, 1990). The studies of Hastenrath and Lamb (1979b) reveal that the Arabian Sea is a region of annual net heat gain at the surface. Hence to maintain equilibrium in the annual thermal cycle, physical processes like horizontal and vertical advection should contribute to the removal of the surplus heat from the ocean.

A unique feature of the Arabian Sea is the cooling of the surface layers during summer. Associated with the onset and progress of summer monsoon, the surface mixed layer cools and deepens in the Arabian Sea (Wyrтки, 1971; Robinson et al, 1979; Molinari et al, 1986a; Shetye, 1986; Rao et al, 1989) except near the coasts where though the mixed layer cools, it shoals due to coastal upwelling (Banse, 1968; Currie et al, 1973; Schott, 1983). The cooling in the Arabian Sea is mostly manifested by the increased turbulent heat fluxes due to strong winds and decreased insolation under the monsoon cloud cover (Colon, 1964; Krishnamurti, 1981; McPhaden, 1982a; Rao, 1984), coastal upwelling (Duing and Leetmaa, 1980), advection of these cold upwelled water into the interior basin (Tunnel, 1963; Saha, 1974) and entrainment of colder waters from thermocline into the mixed layer due to wind, wave and buoyancy mixing (Murthy et al, 1983; Ramesh Babu and Sastry, 1984). The layer deepening is mostly attributed to mixing in the upper layers caused by wind/wave action and

convective overturn caused by buoyancy flux, convergence due to clockwise surface wind stress curl and enhanced vertical shear in the horizontal flow etc. (Wyrski,1971; Colborn,1975; Rao et al,1976; Sastry and Ramesh Babu,1979; Robinson et al,1979; Rao,1987; Rao and Mathew,1990). However, detailed information is meagre on the relative importance of these processes during the summer monsoon in producing these changes in the spatial and time domain. Duing and Leetmaa (1980) suggested that the cooling in the Arabian Sea is mainly caused by upwelling and the offshore spreading of the cold upwelled water into the interior Arabian Sea. They also concluded that the rate of cooling due to upwelling is two to three times larger than the advection of cold water across the equator and more than sufficient to offset the gain of heat from the atmosphere. On the other hand, Shetye (1986) found that downwelling (sinking) will have only marginal effect on SST but it influences the vertical distribution of heat by pushing down the thermocline.

In the Arabian Sea, the process of upwelling is noticed mainly during southwest monsoon season. The major areas of upwelling in the Arabian Sea are off Somalia (Warren et al,1966; Swallow and Bruce,1966; Bruce,1974; Swallow et al,1983; Schott,1983), Arabia (Currie et al,1973; Smith and Bottero,1977) and the southwest coast of India (Ramasastri and Myrland,1959; Ramamirtham and Jayaramam,1960; Banse,1968; Sharma,1968,1978; Narayna Pillai et al,1980; Mathew,1983; Johannessen et al,1981; Shetye,1984; Shetye et al,1990). However, upwelling along the equator is less pronounced unlike in the Pacific and Atlantic Oceans (Leetmaa and Stommel,1980). Downwelling (sinking) is noticed near the coastal belt during winter.

The spatial and temporal variability of the thermohaline fields of the Arabian Sea have been the objective of a few research investigations. In comparison to thermal structure, information on the salinity distribution is extremely sparse in the Arabian Sea, though some investigators have described the mean seasonal or annual variation of salinity in the coastal regions (Darbyshire, 1967; Warren et al, 1966; Ramam et al, 1968, Wyrтки, 1971; Ramesh Babu et al, 1980; Varma et al, 1980; Shetye et al, 1990). However, most of the work carried out using observed salinity data is mainly to study the structure of watermasses. Analysis on the spreading of the watermasses suggest that some of the prominent watermasses which have their origin in the northwest Arabian Sea spread along the west coast of India (Rochford, 1964; Wyrтки, 1971). Based on hydrographic data sets, Varadachari et al (1974) and Ramesh Babu et al (1980) studied the variation in the watermass characteristics along the west coast of India and found that the Arabian Sea High Saline Watermass spreads southward along the coast with its core around 90m. Varma et al (1980) studied the temperature and salinity distribution in the northern Arabian Sea during February-April and concluded that the Arabian Sea High Saline Water is noticed around 60m depth in the eastern part of the study area. Darbyshire (1967) studied the annual cycle of watermasses off the Kerala c Warren et al (1966), Quadfasel and Schott (1982) and Swallow et al (1983) discussed the characteristics of watermass and flow pattern in the Somali Basin. During winter, the northward flowing current off the west coast of India brings low saline Bay of Bengal waters into the Arabian Sea (Darbyshire, 1967; Wyrтки, 1971, Pankajakshan and Ramaraju, 1987).

The most important feature of the salinity distribution in the Arabian Sea is the presence of a core of high salinity

(>36%) in the upper 200m. With the onset and progress of the monsoon, intense turbulent mixing destroys this subsurface maxima and increase surface salinity (Rao et al,1990; Rao and Kumar,1991). Rainfall, evaporation and river discharge also contribute to the variation in the salinity field. Few studies were carried out to highlight the distribution of salinity in the Arabian Sea during southwest monsoon season (Sastry and D'Souza,1972; Rao et al,1990; Rao and Kumar,1991). Wooster et al (1967) prepared an atlas showing the climatological distribution of temperature and salinity. Rao et al (1990) discussed the intra-seasonal variability in the thermohaline characteristics in the upper layers of the Arabian Sea with the aid of repeat zonal and meridional transects made during pre- and post- monsoon season. However, no attempts were made to document the observed changes in the salinity field on a monthly scale.

The major limitations of these studies are that they are confined to specific seasons or specific oceanic regions in the Arabian Sea and were based on sparse data sets. Hence any specific conclusion drawn from these studies has to be interpreted cautiously to explain the variability of thermohaline structure.

Recently, oceanographers have given a great deal of importance to understand the dynamics of the upper layer of the ocean, because it is in this layer exchanges of heat, moisture and momentum occur. The absorption of energy from the sun within this layer is the major source of energy for all oceanic processes. The convergence and divergence in this layer leads to circulation in deeper water. It has been realised that improved long range prediction is possible with better prediction of the mixed layer characteristics. Several studies were carried out to understand the variability of

mixed layer (Wyrтки,1971; Molinari et al,1986; Rao et al 1990; Rao and Mathew,1990). However, due to the non-availability of systematic data sets in the Arabian Sea, knowledge on the time dependent behaviour of the mixed layer characteristics is fragmentary.

A number of investigators have made attempts to simulate numerically the mixed layer characteristics taking into account the net surface heat flux, wind stress and entrainment across the base of the mixed layer. There are in general, two types of mixed layer models, the integral models (Kraus and Turner,1967; Pollard et al,1973; Denman,1973; Denman and Miyake,1973; Miller,1976; Niiler and Kraus,1977), and the diffusion models (Mellor & Durbin,1975; Kondo et al,1979). In the first type of models, relatively simple expressions for bulk mixed layer characteristics are obtained by eliminating the eddy diffusivities and assuming surface layer to be homogeneous. The second type of models are based on turbulence closure scheme. Here the vertical profiles of the turbulent variables are obtained from the solutions of a closed system of turbulence and thermocline equations. The solution of these equations depends on the values assigned to the eddy diffusivity which is highly uncertain. Since more computational time and finer data sets are needed for the turbulence closure models, these type of models are not frequently used.

Munk and Anderson (1948) developed the first realistic model of the mixed layer with stratification. Later Kraus and Turner (1967) extended this approach and developed a 1-D numerical model for the oceanic area based on energy arguments. Denman (1973) modified the work of Kraus and Turner (1967) by including time varying meteorological inputs and simulated the time dependent behaviour of the surface

mixed layer. Miller (1976) further extended this work by including salinity effects. The most significant effect produced by the inclusion of salinity is the reduction of deepening rate and the corresponding change in the heating characteristics of the mixed layer when salinity increases with depth. Later several authors extended this work by including processes causing mixing in the upper ocean (Pollard et al, 1973; Miller and Kraus, 1977; Kundu, 1980; Garwood, 1977; Price et al, 1986).

Until recently, the performance of these models are not tested in the Arabian Sea. Shetye (1986) used Denman's (1973) model to simulate the annual cycle of mixed layer temperature (MLT) along a zonal strip across the Arabian Sea using climatological inputs. He concluded that MLT can be simulated reasonably accurately from the surface fluxes alone, except during southwest monsoon season, when the horizontal and vertical advection is very significant. McCreary and Kundu (1989) developed a numerical model to study the thermodynamic processes of the Arabian Sea on an annual cycle. The model simulated the observed SST pattern reasonably well with errors less than 0.5°C . But on a synoptic time scale only a few studies are reported in the literature on the simulation of the mixed layer characteristics in the Arabian Sea (Rao, 1986; Rao and Mathew, 1990; Joseph et al, 1990). But the model simulations were based on an arbitrary extinction coefficient of 0.002 cm^{-1} , which is four times higher than the observed value (0.0005 cm^{-1}). Attempts are also made to test the performance of this model at selected locations in the coastal waters, where in addition to the one dimensional forcings, the tidal effects, fresh water discharge and the internal waves also affect the mixed layer dynamics on a synoptic time scale (Hareesh Kumar et al, 1990; Murthy and Kumar, 1991). Even during the periods of a deep depression, Murthy and Kumar

(1991) obtained a reasonably good simulation of the mixed layer characteristics using the model of Miller (1976) with r.m.s. error of 0.2°C and 5m for MLT and MLD respectively.

1.2 Objectives of the study

In the present study attempts have been made to bring out the salient features of thermohaline variability in the upper layers of the Arabian Sea and off the west coast of India on an annual cycle.

The present knowledge on the role of horizontal and vertical motion, which influence the thermal structure significantly, on the heat budget of the Arabian Sea is very limited. An investigation on the importance of various physical processes such as net surface heat flux and vertical and horizontal advection on the heat balance of the Arabian Sea on an annual cycle is carried out. The summer cooling of the mixed layer in the Arabian Sea is parameterised in terms of net air-sea heat flux, heat change due to upwelling and horizontal advection.

The synoptic and diurnal scale variabilities in the mixed layer characteristics at selected locations in the Arabian Sea is carried out to understand the effects of atmospheric forcing on short time scales. The significance of one-dimensional processes (net air-sea heat flux and wind stress) in controlling the mixed layer dynamics is studied utilising the mixed layer model of Miller (1976). Following the scheme of Price et al (1986), the intra-diurnal variability of the thermal structure is simulated under summer heating

conditions at a location off the southwest coast of India. Scale analysis is done to understand the relative importance of net air-sea heat flux and surface wind stress.

CHAPTER II

CERTAIN ASPECTS OF THE THERMOHALINE VARIABILITY IN THE UPPER LAYERS OF THE ARABIAN SEA

2.1 Introduction

Studies on thermohaline variability of the Arabian Sea received considerable momentum after the International Indian Ocean Expedition (IIOE). Based on IIOE data sets, the watermass structure in the Arabian Sea was analysed by Rochford (1964), Gallagher (1966), Darbyshire (1967), Wyrski (1971), Sastry and D'Souza (1971,72) and Sharma (1972,1976). However, most of these studies focussed only on the thermal structure or limited to either selected locations or season (Colon,1964; Warren et al,1966; Taft and Knauss,1967; Banse,1968; Saha,1974; Colborn,1975; Duing and Leetmaa,1980; Rao et al,1989). The data sets collected during other observational programmes, particularly INDEX-79 and MONEX-79 have considerably improved our understanding of the thermohaline variability of the Arabian Sea although these experiments were confined to certain locations for pre-monsoon or monsoon seasons (Quadfasel and Schott,1982; Swallow et al,1983, Schott,1983; Rao et al,1990; Rao and Kumar,1991).

Recently, Molinari et al (1986a,b) and Rao et al (1989) described the annual cycle of mixed layer depth climatology with the relevant meteorological and oceanic parameters. However, still many aspects like pre-monsoon warming, summer cooling, seasonal variation of the subsurface salinity maxima pertaining to the thermohaline variability of the Arabian Sea are not adequately resolved. Hence in this study attempts are made to bring out certain aspects of the seasonal evolution of the thermohaline structure, especially the salinity variability in the Arabian Sea. The modification induced by the summer monsoon on the thermohaline field in the upper 200m water column is also studied.

2.2 Data

The temperature and salinity data utilised for this study are obtained from the National Oceanographic Data Centre (NODC), Washington, Indian National Oceanographic Data centre (INODC), Goa, First Global GARP Expedition (FGGE), Oceanovax Indo-Polish expedition and from ships of opportunity. The domain of study extends from the equator to 25°N, 40° to 80°E and excludes the marginal seas, Red Sea and Persian Gulf. The data averaged on 2°x2° (latitude x longitude) for the study area following Rao et al (1989) was used in the analysis

2.2.1 Data qualification

The major difficulty in the analysis is the quality control and true representativeness of the data. Since all the available historical data (1931-1991) are utilised for this study, any 2°x2° grid can contain data from different years and collected using different instruments. In the temperature file, data sets collected using Mechanical Bathythermograph (MBT), Expendable Bathythermograph (XBT), Salinity-Temperature-Depth (STD) recorder and Nansen cast are merged together, whereas the salinity file consists of data obtained from Nansen cast and STD. Based on standard statistical checks and certain empirical criteria, quality control is performed to remove spurious data. The details are discussed below.

As a first step, locations, date, and ship codes of all stations are checked to eliminate duplicate data. Then the data which are grossly in error is eliminated by range checking. Various range criteria are used for temperature and salinity at different depth levels following Levitus (1982). Further, each temperature profile is checked for inversion.

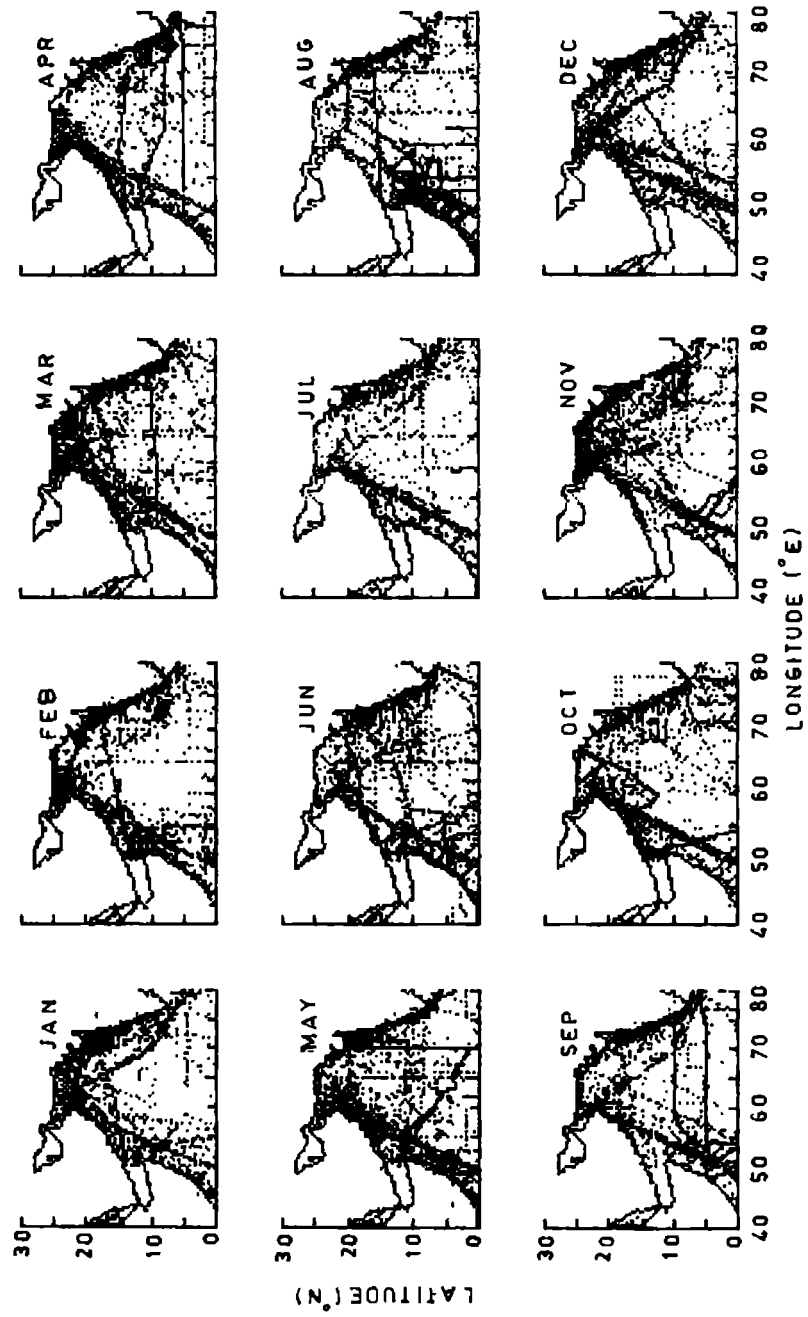


Fig. 2.1 Monthly data distribution of temperature (each dot represents a vertical temperature profile)

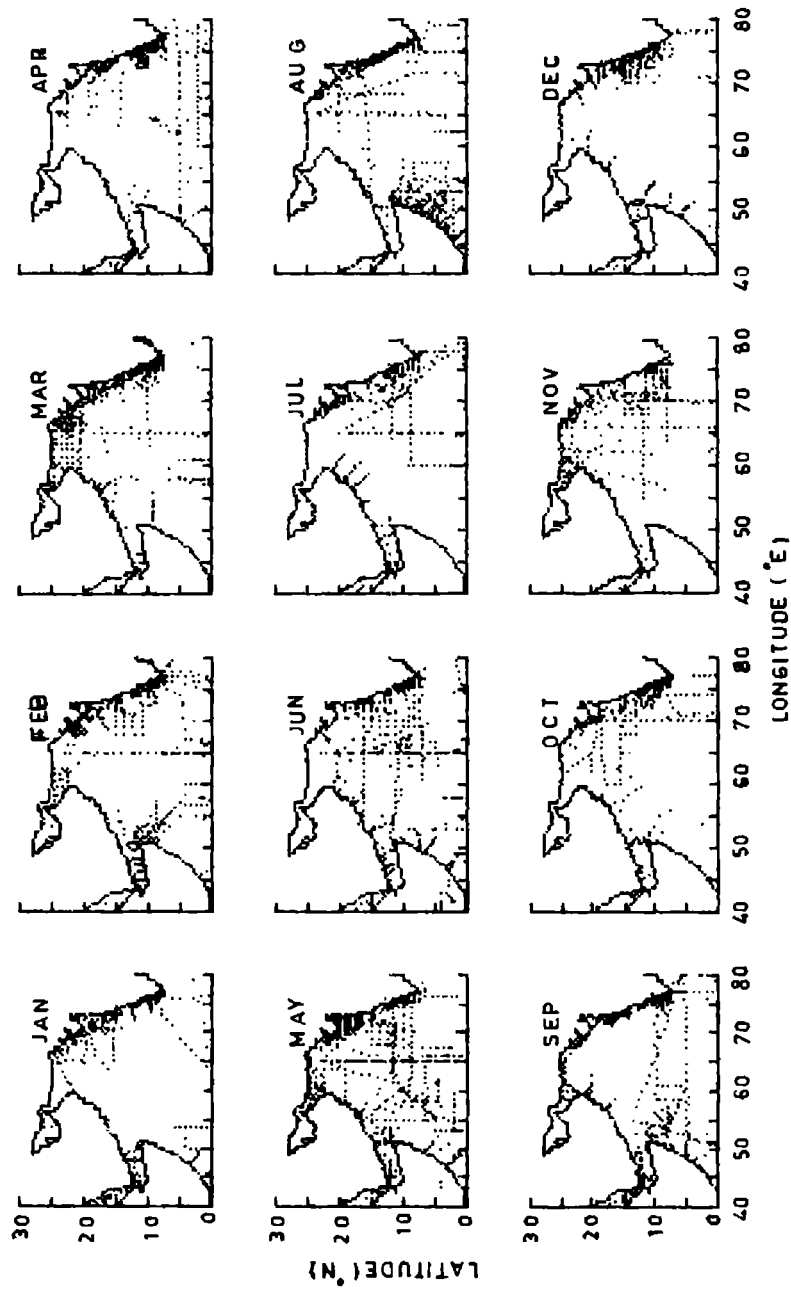


Fig. 2.2 Monthly data distribution of Salinity (each dot represents a vertical salinity profile)

Except in selected areas like the vicinity of Red Sea and Persian Gulf, the profiles having thermal inversion greater than 1°C are eliminated. Then the vertical profiles of temperature and salinity are interpolated using Lagrangian interpolation scheme to obtain values at every 10m and the mean (\bar{X}) and standard deviation (σ) at these depth are computed for each $2^{\circ}\times 2^{\circ}$ grid. Following Levitus (1982) statistical check is performed to eliminate erroneous data. The standard deviation check is performed twice to the data. The second check is more effective in eliminating erroneous data. The temperature data sets contain approximately 40,000 profiles whereas the salinity data sets contain only 10,000 profiles after the quality control. The monthly distribution of the station location of temperature and salinity profiles after the quality control are presented in Figs.2.1 and 2.2 respectively. Finally, the monthly mean profiles of temperature and salinity for each $2^{\circ}\times 2^{\circ}$ grid was computed.

2.3 Thermal structure of the Arabian Sea

2.3.1 Pre-monsoon heating and summer cooling

It is well known that the sea surface temperature (SST) in the Arabian Sea shows a bi-modal distribution on an annual cycle with cooling during winter and summer monsoons and warming during transition periods (Colborn,1975; Hastenrath and Lamb,1979a; Rao et al,1989). To study the pre-monsoon warming in the Arabian Sea, SST changes between May and January (May-January) are presented in Fig.2.3a. During this period, warming is maximum in the northwestern Arabian Sea particularly off the Arabian Coast and is minimum near the equator. Between March and May the Arabian Sea is mostly cloud free with weak winds around 2 to 3m/s (Hastenrath and Lamb,1979a). This leads to higher insolation and negligible

turbulent heat losses resulting in an increase in the net heat input into the ocean thereby reducing the mixed layer depth (Fig.2.4). Large accumulation of heat over shallower mixed layers (<25m) in the northwestern Arabian Sea leads to a warming of the order of 4°C from January to May (Rao et al,1991). A typical mixed layer of 40m in the northwestern Arabian Sea and a corresponding net heat flux of 100 W.m⁻² (Hastenrath and Lamb,1979b) would produce a warming of over 4°C which is consistent with the climatological SST distributions. In the southeastern Arabian Sea the warming rates are minimum due to weak heat input over deep mixed layer.

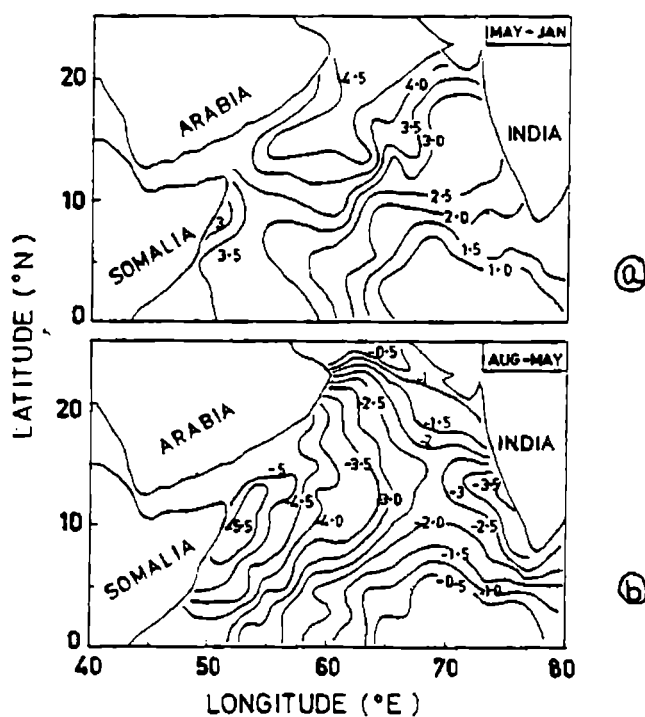


Fig.2.3. (a) Pre monsoon warming (May-January) and (b) Summer Cooling (August-May) in the Arabian Sea (° C)

The Arabian Sea is probably the only region of the world oceans which cools during summer eventhough the Arabian Sea as a whole gains heat through air-sea interaction processes (Hastenrath and Lamb,1979b; Duing and Leetmaa,1980). To understand the magnitude of summer cooling in the Arabian Sea, SST variability between August and May (August-May) is

presented in Fig.2.3b. The surface cooling is maximum off the Somalia Coast ($>5^{\circ}\text{C}$) and off the southwest coast of India ($>3^{\circ}\text{C}$) whereas minimum cooling ($<1^{\circ}\text{C}$) is noticed in the northern and southeastern Arabian Sea. The cooling in the Arabian Sea is mostly attributed to coastal upwelling and horizontal advection of this cold upwelled water (Tunnel,1963; Saha,1974; Duing and Leetmaa,1980). More details of summer cooling in the Arabian Sea are discussed in chapter 3.

2.3.2 Seasonal variation of surface mixed layer

Usually the upper few meters of the ocean are well mixed having uniform temperature and salinity, known as the surface mixed layer. This is the region of high primary productivity and all weather activities are closely related to storage and removal of heat from the mixed layer. The thickness of this layer determines the thermal and mechanical inertia of the layer in direct contact with the atmosphere. The mixed layer significantly affect the oceanic response to surface forcing and the evolution of the coupled ocean-atmosphere system. Hence, knowledge of mixed layer variability has great importance in understanding the thermal and velocity fields of the upper ocean. Several different approaches have been followed in defining the mixed layer depth (MLD) from vertical temperature profiles (Stevenson and Niiler,1983; Rao et al,1989). However, in this study MLD is taken as the deepest depth at which SST- 1°C occur in the vertical temperature profile following Wyrтки (1971). The MLD computed for individual stations are averaged for each $2^{\circ}\times 2^{\circ}$ grid and the monthly distribution of MLD is presented in Fig.2.4.

On an annual cycle the mixed layer shows considerable variations in the Arabian Sea. During heating season (April-May), MLD shows very little temporal changes throughout

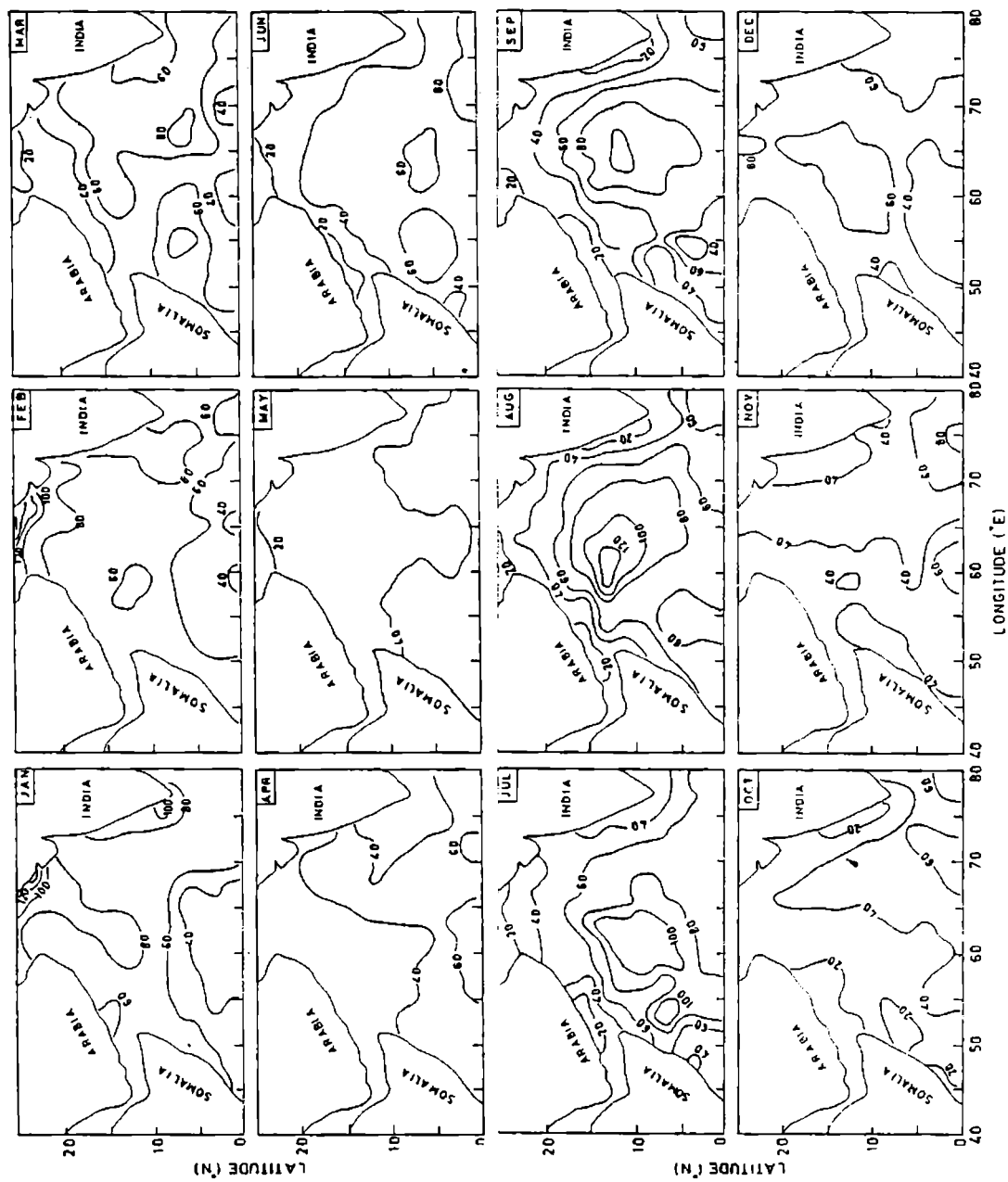


Fig. 2.4 Meanmonthly mixed layer depth distribution(meters)

the Arabian Sea. In general, shallow mixed layers (<50m) are noticed during this period under intense solar heating (Hastenrath and Lamb,1979b). On the otherhand, the mixed layer deepening during cooling seasons (summer monsoon and winter) is variable across the basin. The deepest mixed layers (>140 m) are observed in the northern Arabian Sea during January-February when winter cooling (Hastenrath and Lamb,1979b) and sinking (Banse,1968) in the coastal belt pushes the thermocline deeper. During July-August the mixed layer deepens over 120m in the central Arabian Sea when surface cooling and convergence due to negative wind stress curl (Hastenrath and Lamb,1979a) dominate. However, shallower layers (<20m) are noticed near the coasts under the influence of coastal upwelling during this period.

2.4 Salinity structure in the Arabian Sea

2.4.1 The subsurface salinity maxima

One of the characteristic features of the salinity structure in the upper layers (upper 200m) of the Arabian Sea is the subsurface salinity maxima (Rochford,1964; Wyrcki,1971). Since these subsurface maxima are located close to surface, seasonal variation in the surface wind field will significantly affect the distribution of the maxima. To understand the seasonal variation of this subsurface salinity maxima, its core depth and salinity are presented in Figs.2.5 and 2.6 respectively. The salinity and temperature range of these subsurface maxima correspond to a thermosteric anomaly of approximately 400 cl/t. Rochford (1964) called this water as the Arabian Sea High Salinity Watermass (ASHSW). In the northeastern Arabian Sea, the core depth of this salinity maxima is generally less than 25m with core salinities greater than 36.4‰. in all months. Moreover, the higher core values

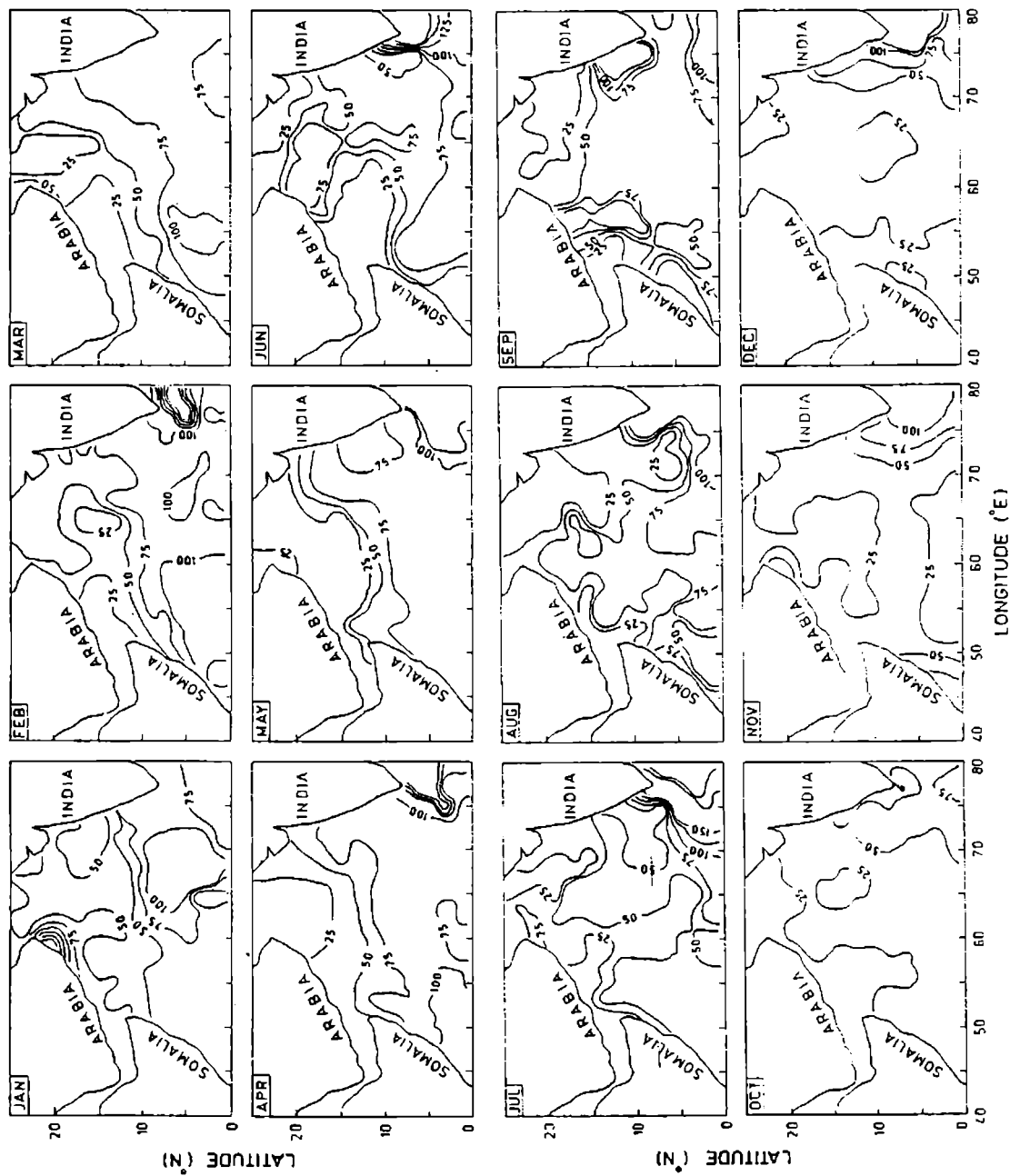


Fig. 2.5 Mean monthly distribution of the core depth (meters) of the subsurface salinity maxima



Fig. 2.6 Mean monthly distribution of the subsurface salinity maxima (parts per thousand)

(>36.6%) and shallow core depth (< 25m) in the northeastern Arabian Sea especially during winter and summer suggest that the ASHSW is formed during these seasons, when evaporation is higher or heat loss is maximum (Hastenrath and Lamb, 1979b). The core depth increases southward, particularly southeastward to over 75m south of 10°N during all months suggesting that the ASHSW is formed only in the northern Arabian Sea and sinks to subsurface depths and occupies deeper levels as it traverses southwards/southeastwards.

To understand the significance of this subsurface salinity maxima (S_{max}), difference between S_{max} and S_o ($\Delta S = S_{max} - S_o$), where S_o is surface salinity, for all months are presented in Fig.2.7. On an annual cycle, the northern and western Arabian Sea is characterised by small ΔS (<0.1%). The maximum values of ΔS are noticed during summer monsoon season (over 1.4% during July-September) and winter (over 1.4% during December-March) off the west coast of India. Marked difference is noticed in the aerial extent of the maximum values of ΔS . Since there is not much difference in the core value of this maxima, the increase in ΔS suggests the importance of surface dilution. Sastry and D'Souza (1972) attributed the surface dilution during southwest monsoon to the increased precipitation and river discharge. However, during winter the dilution in the surface layers is caused by the influx of low saline Bay of Bengal/Equatorial waters into the eastern Arabian Sea (Darbyshire, 1967; Pankajakshan and Ramaraju, 1987). However, during May-June, ΔS shows minimum values (<0.6%) in the eastern Arabian Sea. As there is no conspicuous difference in the core value of S_{max} compared to other months, this reduction in ΔS is related to the increase of surface salinity due to the presence of waters of northern Arabian Sea and under the influence of southerly coastal current and increased evaporation.

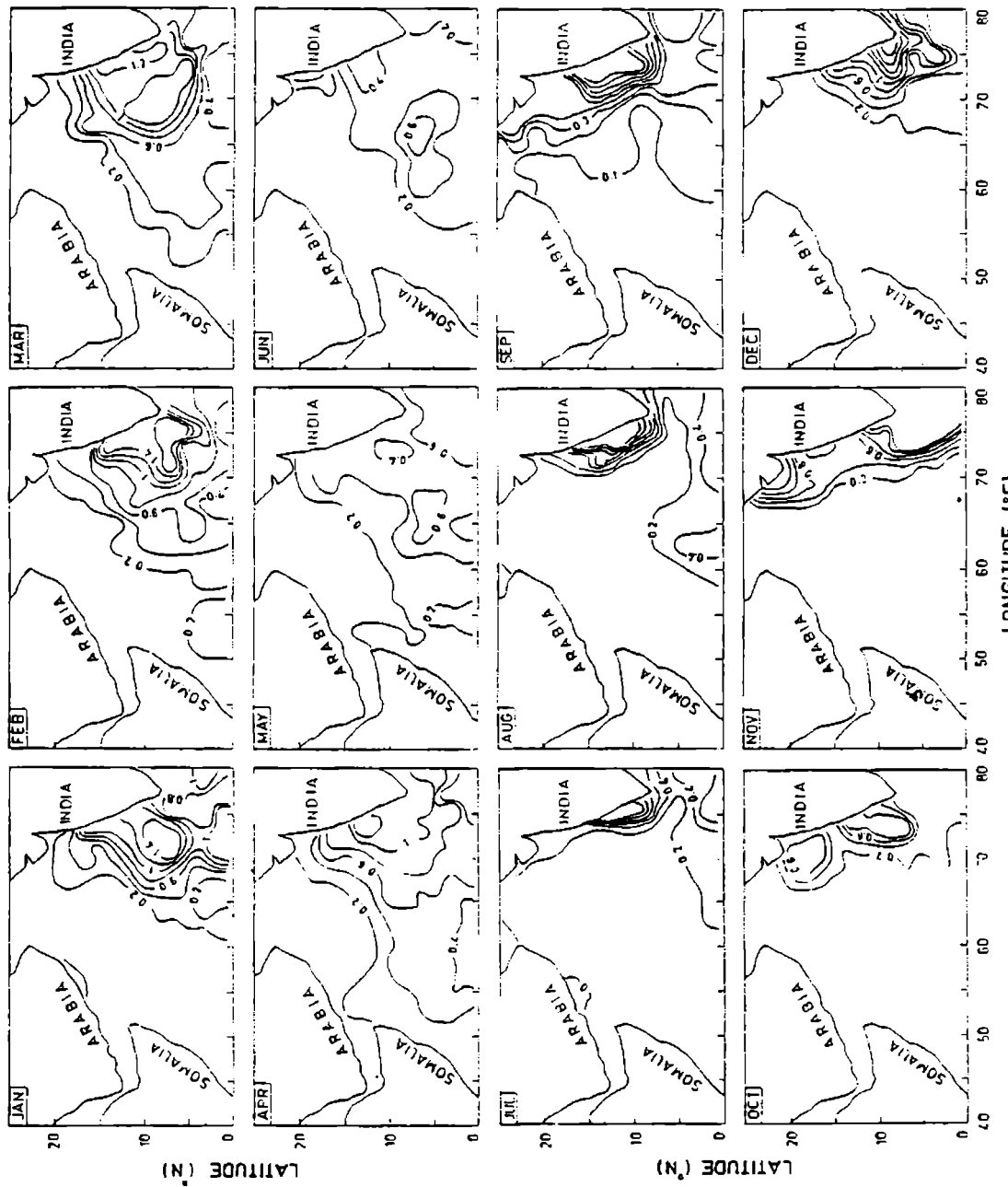


Fig. 2.7 Mean monthly distribution of S_{max}-S₀ (parts per thousand)
 (S_{max}, maximum salinity; S₀, surface salinity)

2.4 T-S diagrams for typical areas of the Arabian Sea

The main feature of the watermass structure in the upper layers of the Arabian Sea is the subsurface salinity maxima associated with the ASHSW. The seasonal variation of subsurface maxima and its core depth reveals that this high salinity zones are found in different depths at different region. To understand more about the structure of the watermasses in the upper 200m of the Arabian Sea, the average temperature and salinity profiles at selected $4^{\circ} \times 4^{\circ}$ grid for February, May, August and November are plotted on T-S diagrams (Fig.2.8) with isopleths of thermosteric anomaly. The areas selected are off Somalia coast (area I), off the Arabia coast (area II), central Arabian Sea (area III), equatorial Arabian Sea (area IV), off the Gujarat coast (area V) and of the southwest coast of India (area VI).

The analysis brings out some interesting similarities and contrasts in the thermohaline fields in the upper 200m of the Arabian Sea. A close examination of the T-S diagrams reveals that there is only one salinity maximum above 100 cl/t surface. The salinity values at this subsurface maximum is higher (>36‰) in the northern regions (areas I, III and V) compared to southern Arabian Sea. This subsurface salinity maxima lies around 400 cl/t in areas IV, V and VI during all seasons, attributed to the ASHSW (Rochford, 1964; Wyrski, 1971). Very low salinities are noticed in the surface layers of area VI during February and August. The inflow of low saline Bay of Bengal water into the southeastern Arabian Sea reduces the surface salinity during northeast monsoon. However, the low surface salinity confined to the upper 10m during August is due to large dilution caused by the precipitation and river discharges. On the otherhand,

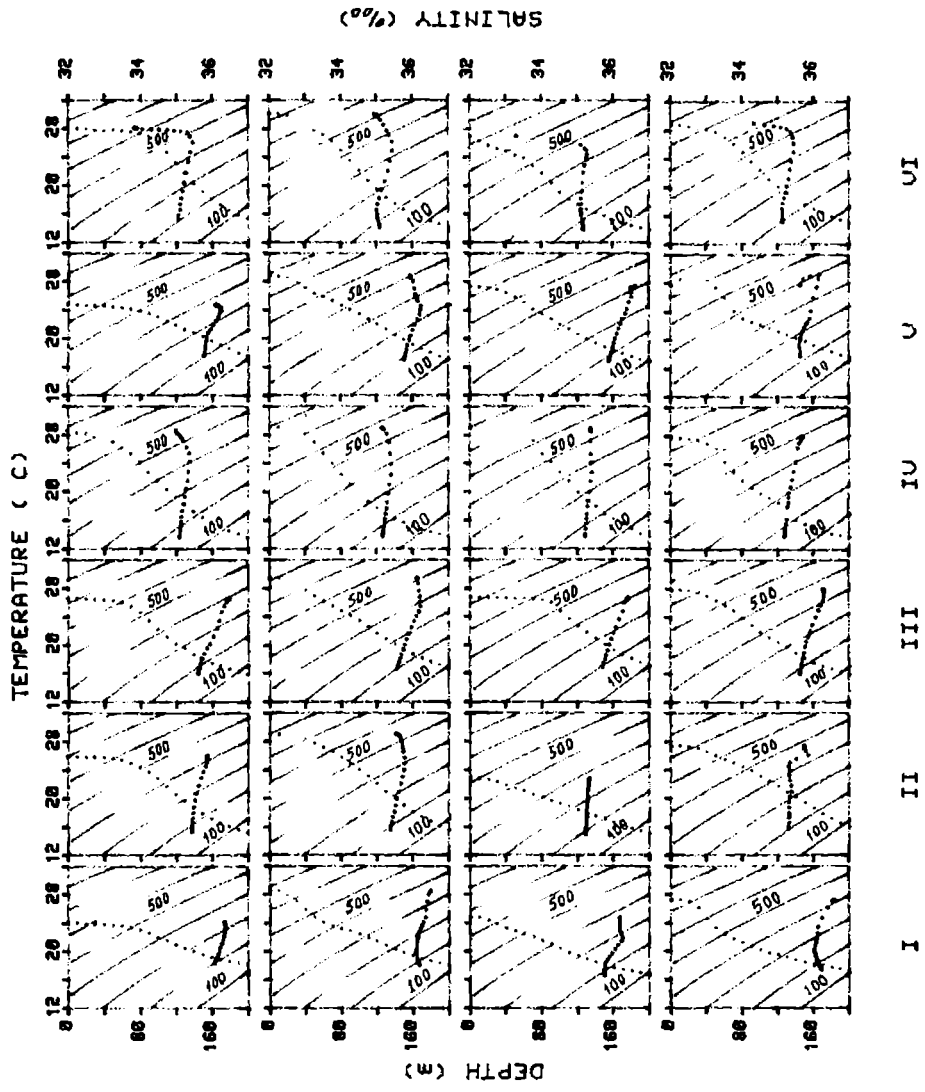


Fig.2.8. T-S diagrams at selected 4 x 4 grids in the Arabian Sea for February, May, August and November

moderately low salinities (35‰) are noticed in area II during August to November. This may be due to the influence of low saline equatorial water carried by Somali Current (Swallow et al, 1983). In area IV moderately low salinities are noticed on all seasons. However, in area III an increase in the surface salinity is noticed during southwest monsoon. This is attributed to the combined effect of the southward advection of ASHSW, increased evaporation and vertical mixing (Rao et al, 1990; Rao and Kumar, 1991).

2.5 Thermohaline variability with the onset and progress of monsoon

The onset and progress of the summer monsoon produces large scale modification in the thermohaline fields of the upper 200m water column in the Arabian Sea. Hydrographic data collected along $8^{\circ}30'N$, $11^{\circ}30'N$ and $16^{\circ}N$ latitudes and one meridional transect along $65^{\circ}E$ longitude (at an interval of approximately 1° latitude/longitude) repeated by USSR ships during end May 1973 and end June/early July 1973 (Fig.2.9a) are utilised to study the changes brought by the summer monsoon in the thermohaline structure (Figs.2.9(b-e)). The stations utilised are repeated after an interval of 2 weeks along $16^{\circ}N$, 7 weeks along $11^{\circ}30'N$ and $8^{\circ}30'N$.

The summer monsoon of 1973 produced only slight variations in the thermal structure off the Arabia coast (along $16^{\circ}N$), whereas a cooling of $0.5^{\circ}C$ and a layer deepening of 10-20m is noticed towards east (Fig.2.9b).

A mild salinity minimum is noticed along this section just below the isohaline layer during pre-monsoon (Fig.2.9b). This minimum diffused and its depth of occurrence increased eastward and disappeared east of $60^{\circ}E$. Swallow et al (1983)

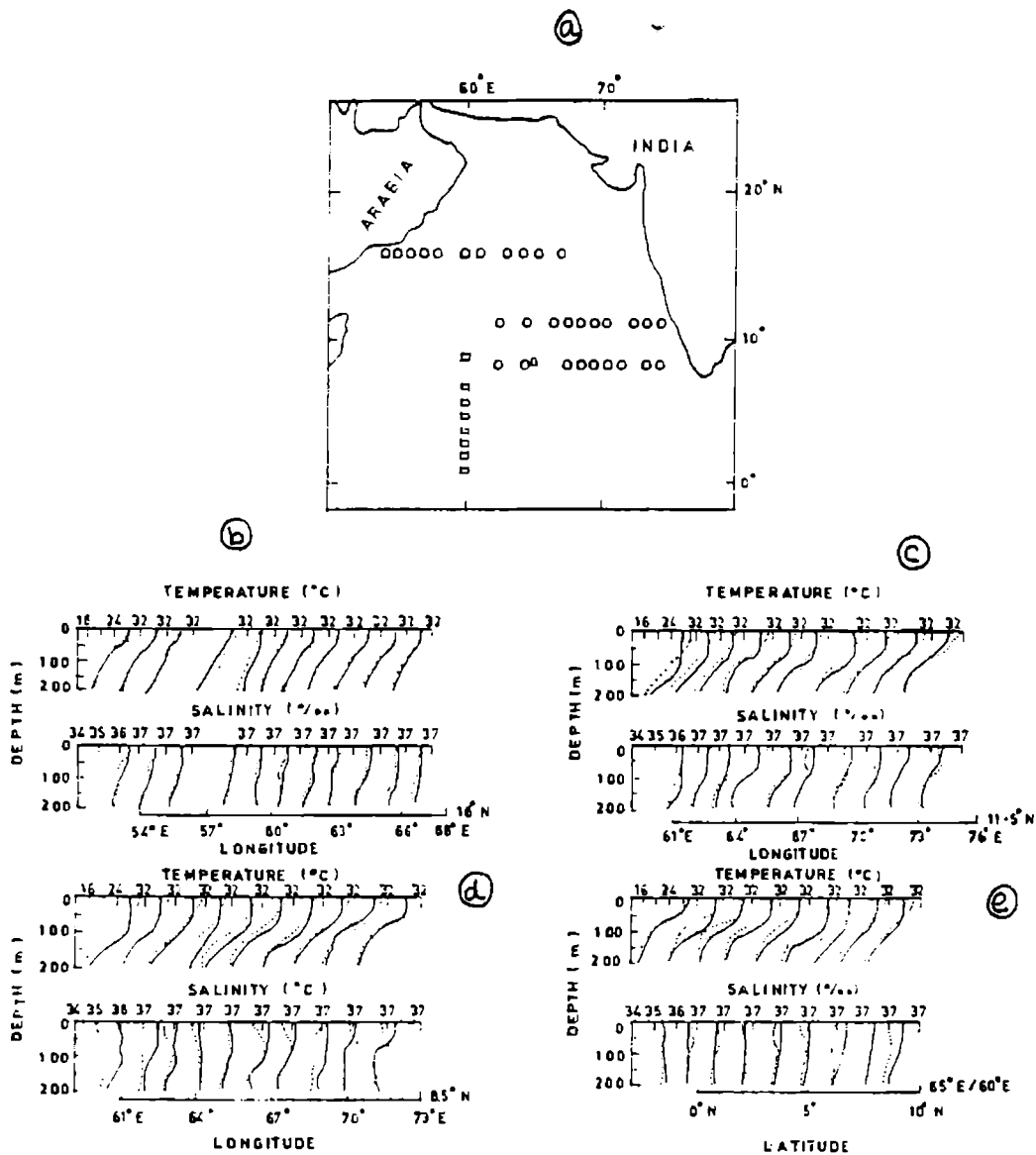


Fig. 2.9 (a) Station Location map; Vertical profiles of temperature ($^{\circ}\text{C}$) and Salinity (‰) during pre-(continuous line) and post-(Dotted line) monsoon along (b) 16°N (c) 11.5°N (d) 8.5°N (e) $60^{\circ}/65^{\circ}\text{E}$.

suggested the presence of low saline waters near the surface in the Somali Basin during southwest monsoon of 1979. It is not clear whether these low saline waters have encountered any mixing while advecting northeastward. This minimum disappeared during post-onset period and the isohaline layer deepened due to vertical mixing under strong monsoon winds.

Along $11^{\circ}30'$ (Fig.2.9c), maximum layer deepening is noticed west of $70^{\circ}E$ ($>70m$) whereas it is relatively weak east of $70^{\circ}E$ ($<30m$) as the effects of coastal upwelling appeared to have inhibited the deepening. One interesting feature of the thermal structure along this transect is that cooling is confined to the uppermost layers in the central Arabian Sea while it is evident up to 200m east of $70^{\circ}E$.

A subsurface salinity maxima is evident along $11^{\circ}30'$ (Fig.2.9c) during pre-onset period which obviously correspond to the ASHSW (Rochford,1964; Wyrтки,1971). This subsurface salinity maxima disappeared during the post-onset period producing an increase in the salinity of the near surface water column. This increase appears to be due to the advection of high saline waters from north and vertical mixing with subsurface high saline waters and evaporation (Rao and Kumar,1991). The rise in the mean salinity of the near surface water column showed a decrease eastward, implying that the advection of high saline water is mostly confined to east central Arabian Sea. The pre-onset salinity maxima descended eastward occupying deepest depth around $72^{\circ}E$ and further east it ascended under the influence of coastal upwelling.

Maximum layer deepening in the Arabian Sea is noticed along $8^{\circ}30'N$ (Fig.2.9d) in the central Arabian Sea ($>100m$) and decreased eastward ($<50m$). Under the influence of coastal upwelling, the two eastern stations off the southwest coast of

India shows weaker mixed layer deepening. In the central Arabian Sea, noticeable warming is observed in the upper thermocline as warmer near surface water downwelled in association with the mixed layer deepening and convergence due to clockwise surface wind stress curl (Yoshida and Mao, 1957; Sastry and Ramesh Babu, 1979; Hastenrath and Lamb, 1979a). Bruce (1982) also noticed good geographic correspondance between the maxima of the surface wind stress curl and mixed layer deepening in the central Arabian Sea.

Along $8^{\circ}30'N$ the subsurface salinity maxima is less organised during pre- and post- onset period (Fig.2.9d). During post- onset regime deeper isohaline layers with increased surface salinity is noticed. At the two eastern stations off the southwest coast of India stronger haloclines produced by the presence of low saline waters in the surface layers are noticed (Levitus, 1986).

As the ship traversed along $60^{\circ}E$ and $65^{\circ}E$ longitudes during pre- and post- monsoon periods, repeat transects are not available. In this case meridional sections are seperated by about 300 nautical miles and were covered over a span of 6 weeks. Under the assumption of weak zonal variations in the thermal response in the central Arabian Sea, the profiles made along these two sections may be compared to study the thermal response to the summer monsoon. Mixed layer cooling increased from equator ($1^{\circ}C$) to $10^{\circ}N$ ($2.5^{\circ}C$) while MLD shows a deepening trend from the equator to $10^{\circ}N$ (Fig.2.9e).

A general increase is noticed in the subsurface salinity maximum from the equator to $10^{\circ}N$ with few exceptions. This subsurface salinity maximum disappeared during the post- onset period and the mean salinity of the water column showed an increase towards north.

CHAPTER III

HEAT BUDGET OF THE ARABIAN SEA

3.1 Introduction

Knowledge of the various processes that affect the upper ocean thermal structure is useful to understand the global climate. In the tropics, temperature of the ocean shows considerable variation both in temporal and spatial domains. These variations suggest that heat may be added or removed from the ocean by various processes, which include air-sea exchange processes, horizontal advection, coastal and mid ocean upwelling/sinking etc. Of these processes, air-sea interaction has received considerable attention. Hastenrath & Lamb (1979b) and McCreary and Kundu (1989) found that on an annual cycle, the Arabian Sea is characterised by a net heat gain, with maximum off Somalia and Arabian coasts and in the equatorial region. McPhaden (1982b) found that about 80% of the variance in the SST in the central Indian Ocean can be accounted by the air-sea fluxes alone. Along a strip across the Arabian Sea, Shetye (1986) studied the relative importance of net air-sea flux and horizontal and vertical advection on the observed thermal structure. Molinari et al (1986b) also studied the relative importance of net air-sea flux and horizontal advection in the SST variability for the entire Arabian Sea. However, most of these studies dealt with the surface temperature (SST) variation and its relationship with air-sea fluxes and vertical advection. But the role of the above discussed factors in controlling the temperature variation in the upper 200m water column has received only little attention. Rao (1988) discussed the heat budget of the upper 200m water column for a $10^{\circ} \times 10^{\circ}$ box in the central Arabian Sea in terms of air-sea heat fluxes, oceanic heat storage and divergence of heat. In this study, the contribution of net surface heat flux and vertical advection in the oceanic heat storage is discussed on a monthly scale

for the Arabian Sea. An attempt is also made to parameterize the summer cooling in the Arabian Sea.

3.2 Computational procedure of heat budget components

The heat balance equation (in $W.m^{-2}$) of the water column can be written as (Etter, 1983),

$$Q = Q_T + Q_{div} + Q_{ADV} \quad (3.1)$$

where Q , net air-sea heat flux; Q_T , rate of oceanic heat storage; Q_{div} , heat change due to vertical motion and Q_{ADV} , heat change due to horizontal advection.

3.2.1 Net Air-Sea Heat Flux (Q)

In the tropics, ocean gains heat through the absorption of solar radiation (Q_I) and loses heat by effective back radiation (Q_B), latent heat flux (Q_E) and sensible heat flux (Q_H). The net oceanic heat flux (Q) can be written as (Pickard and Emery, 1982)

$$Q = Q_I - Q_B - Q_E - Q_H \quad (3.2)$$

Negative values of Q indicates heat loss to ocean.

To estimate the solar radiation at sea surface, direct radiation at the top of the atmosphere (Q_o), mean transmittivity of the atmosphere and the correction for cloudiness and reflectivity of the sea surface are required. Q_o is also known as the clear sky radiation and is computed from astronomical and geographical factors (Seckel and Beaudry, 1973) with coefficients appropriate for the latitudes from $20^{\circ}S$ to $40^{\circ}N$. This formula has gained general acceptance

and has been widely used by Reed (1977), Weare et al (1981), Stevenson and Niiler (1983) and Hsiung (1986).

$$Q_o = A_o + A_1 \cos \beta + B_1 \sin \beta + A_2 \cos 2\beta + B_2 \sin 2\beta \quad (3.3)$$

$$A_o = -15.82 + 326.87 \cos \phi$$

$$A_1 = 9.63 + 192.44 \cos(\phi + \pi/2)$$

$$B_1 = -3.27 + 108.7 \sin(\phi)$$

$$A_2 = -0.64 + 7.8 \sin 2(\phi - \pi/4)$$

$$B_2 = -0.5 + 14.42 \cos 2(\phi - \pi/36)$$

$$\beta = (t - 21) \frac{360}{365}$$

Here ϕ is the latitude and 't' is the Julian day.

Q_o is then corrected for cloud effects (Reed, 1977) and reflectivity of the sea surface (Payne, 1972) by the relation

$$Q_I = Q_o (1 - 0.62 c_l + 0.0019 \alpha_n) (1 - A) \quad (3.4)$$

where c_l , fractional cloud cover ($0 \leq c_l \leq 1$); α_n , noon altitude of the sun in degrees and ξ , declination of the sun.

$$\sin(\alpha_n) = \sin(\phi) \sin(\xi) + \cos(\phi) \cos(\xi) \quad (3.5)$$

$$\xi = -23.45 \cos(t + 11) \quad (\text{Oke, 1987}) \quad (3.6)$$

The effective outgoing long wave radiation from the ocean (Q_b) is the balance between the long wave radiation from the sea surface and from the atmosphere. Cloud cover, sea-air temperature difference, water vapour content of the atmosphere immediately above the sea surface are the important factors controlling Q_b . Several semi-empirical expressions are available in the literature to estimate Q_b . Simpson and Paulson (1979) found better agreement of measurement with the

Brunt's formulation of outgoing radiation and the correction factor for sea-air temperature by Beriland (Budyko,1963).

$$Q_B = \epsilon \sigma T_S^4 (0.39 - 0.05 e_{10}^{0.5}) (1 - 0.59cl) + 4\epsilon \sigma T_S^3 (T_S - T_{10}) \quad (3.7)$$

where ϵ , emissivity of the sea surface (0.98); σ , Stefan-Boltzman constant ($5.67 \times 10^{-8} \text{ W.m}^{-2}\text{K}^{-1}$); T_S , sea surface temperature (K); T_{10} , air temperature (K); e_{10} , vapour pressure (mb) at a height 10m; cl , fractional cloud cover ($0 \leq cl \leq 1$).

The turbulent heat fluxes from the ocean are the heat loss/gain due to latent heat (Q_E) and sensible heat (Q_H) fluxes. In the tropical ocean Q_E contributes to the heat loss due to evaporation while Q_H can be either gain or loss. The latent and sensible heat fluxes are parameterised with widely used bulk aerodynamic method.

$$Q_E = \rho_a C_E L_E (q_S - q_{10}) V \quad (3.8)$$

$$Q_H = \rho_a C_H C_P (T_S - T_{10}) V \quad (3.9)$$

where ρ_a , density of air (Kg.m^{-3}); L_E , latent heat of evaporation (J.Kg^{-1}); q_S , specific humidity corresponding to T_S (Kg.Kg^{-1}); q_{10} , specific humidity at 10m (Kg.Kg^{-1}); V , wind velocity (m.s^{-1}); C_P , specific heat of air at constant pressure ($\text{J.Kg}^{-1}.\text{°C}$); and C_E and C_H are the non-dimensional transfer coefficients for moisture and heat respectively. C_E and C_H are derived from a review of previous determinations following McCreary and Kundu (1989) and Friehe and Schmitt (1976) respectively. These formulation takes into account of the atmospheric stability.

$$C_E = 0.0015 + 0.00033 (T_S - T_{10}) \quad (3.10)$$

$$\begin{aligned} C_H &= 0.97 \times 10 ; T_{10} - T_S < 0 \\ &= 0.86 \times 10 ; T_{10} - T_S > 0 \end{aligned} \quad (3.11)$$

3.2.2 Rate of Oceanic Heat Storage (Q_T)

The rate of oceanic heat storage (Q_T) is the time derivative of the heat content of the water column over a depth D . For each month Q_T ($W.m^{-2}$) is computed as (Etter, 1983)

$$(Q_T)_i = \frac{H_{i+1} - H_{i-1}}{2 \text{ months}} \quad (3.12)$$

$$H_i = \rho_v C_p \int_{-D}^0 (T_w)_i dz \quad (3.13)$$

where i is the month index (1 to 12). $(T_w)_i$ is the temperature of the water column of thickness dz corresponding to the i^{th} month and H_i ($Kcal.cm^{-2}$) is the heat content corresponding to i^{th} month.

3.2.3 Divergence of Heat (Q_{div})

The divergence of heat (Q_{div}) account for the heat change due to vertical motion. The influence of vertical advection in the oceanic heat balance has not been studied in detail for the Arabian Sea. In the present study an attempt is made to incorporate the vertical advection in the heat balance equation following Emery (1976)

$$Q_{\text{div}} = \frac{W_D}{D} (H - \rho_w C_p D T_{wD}) \quad (3.14)$$

The magnitude of the vertical velocity W_D at the fixed depth level 'D' is defined as the negative ratio of the monthly temperature change at D (∂T) to the mean vertical temperature gradient at D ($\partial T / \partial z$).

$$W_D = - \frac{\partial T}{(\partial T / \partial z)} \quad (3.15)$$

In the absence of adequate subsurface current data, the effect of horizontal advection is taken as the residual term in the heat balance equation.

3.3 Data

The surface marine meteorological data used in this study was obtained from the India Meteorological Department (IMD), Delhi, covering a period of ten years (1961-1970). The domain of analysis extends from the equator to 30°N and 40° to 80°E and excludes the marginal seas as Red Sea and Persian Gulf. The data set consists of atmospheric pressure, surface wind speed and direction, air and wet bulb temperature, sea surface temperature, total and low cloud amount. As suggested by Esbensen and Reynolds (1981), the data points were averaged over 2°x2° (latitude x longitude) on monthly time scale for computing the monthly mean net heat flux (Q). Quality control was performed on the raw data to eliminate erroneous and spurious observations. As a first step, each parameter was checked for duplication. Then the data that were grossly in error was removed by range checking. Further, statistical check was carried out by computing mean (\bar{X}) and standard deviation (σ) of each parameter for each 2°x2° grid. The

observation deviating more than 2σ from \bar{X} are rejected. After the quality control the final data set contains around 500,000 data points.

3.4 Results

Due to the lack of adequate subsurface temperature data, the heat storage of the 200m water column has received only little attention until recently. The earlier studies on heat storage rate were carried out either with limited data sets or were restricted to specific regions (Hastenrath and Lamb, 1980; Duing and Leetmaa, 1980; Rao, 1988). Hence, the monthly rate of heat storage in the upper 200m water column for the entire Arabian Sea is computed and presented in Fig.3.1. Positive values imply accumulation of heat.

In March, warming is noticed in the entire Arabian Sea ($>250 \text{ W.m}^{-2}$), except off the southwest coast of India, where slight cooling of the water column is noticed and coincides with the commencement of coastal upwelling (Sharma, 1978). By June, the entire coastal waters experience significant cooling with maximum values of 250 W.m^{-2} occurring in the upwelling region. However, a region of warming extends from the central Arabian Sea to the southeastern Arabian Sea (east of 60°E). In July, the region of warming shifts to west of 70°E in the equatorial Arabian Sea whereas the coastal waters continues to cool. Rao (1988) noticed a cooling of $2\text{-}3^\circ\text{C}$ in the surface temperature of the central Arabian Sea during southwest monsoon season. But the rate of heat storage revealed warming of the 200m water column caused by mixed layer deepening and convergence in the central Arabian Sea. By October, the situation is completely opposite to that in July with warming in the coastal waters and cooling in the central and equatorial (east of 72°E) Arabian Sea. During this period,

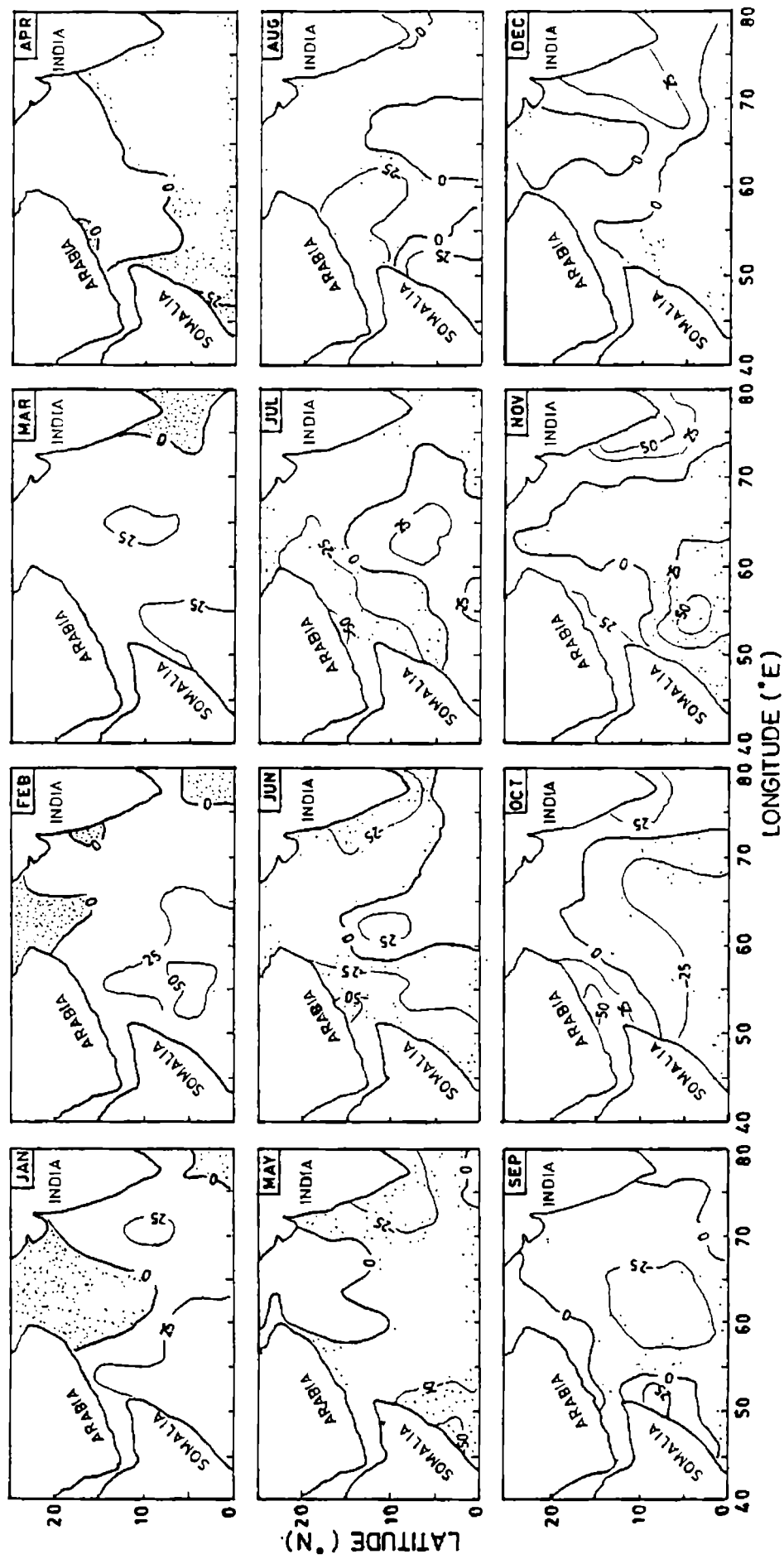


Fig. 3.1 Monthly distribution of the heat storage of upper 200m water column ($\times 10 \text{ Wm}^{-2}$)

maximum warming is noticed off the southwest coast of India and Arabia Coast (over 500 W.m^{-2}) where sinking was dominant, whereas cooling of the water column extends further northwards from central Arabian Sea. In December, a clear cut demarkation exists between cooling in the northern Arabian Sea (north of 10°N) and western equatorial Arabian Sea. The cooling in the northern Arabian Sea attains maximum in January and thereafter the intensity of cooling decreases and the water column starts gaining heat.

The heating/cooling in the Arabian Sea is mainly caused by the surface energy exchange processes and lateral and vertical advection. An attempt is made to study the possible influence of these processes in the heat balance of the Arabian Sea. Of the various processes that contribute to changes in the heat storage rate, air-sea exchange processes have received the major attention (Hastenrath and Lamb, 1979b; Rao et al, 1989). The monthly variation of the net air-sea heat flux (Q), computed following equation 3.2.1 is presented in Fig.3.2. Positive values of Q indicate heat gain by ocean. During northern winter (November to January), northern Arabian Sea experiences drastic heat loss (-100 W.m^{-2} in December) whereas heat gain was noticed in the equatorial Arabian Sea (south of 5°N) and the coastal waters of India south of 10°N . The increased latent heat loss due to the large air-sea temperature difference (Hastenrath and Lamb, 1979a) largely contribute to the heat loss in the northern Arabian Sea.

Arabian Sea starts gaining heat from February onwards and attains maximum in April, when values in excess of 125 W.m^{-2} are noticed. In May, a reduction in the net heat gain is noticed in the equatorial Arabian Sea, whereas the regions north of 15°N continues to gain heat over 175 W.m^{-2} . With the onset of the southwest monsoon, the central Arabian Sea starts

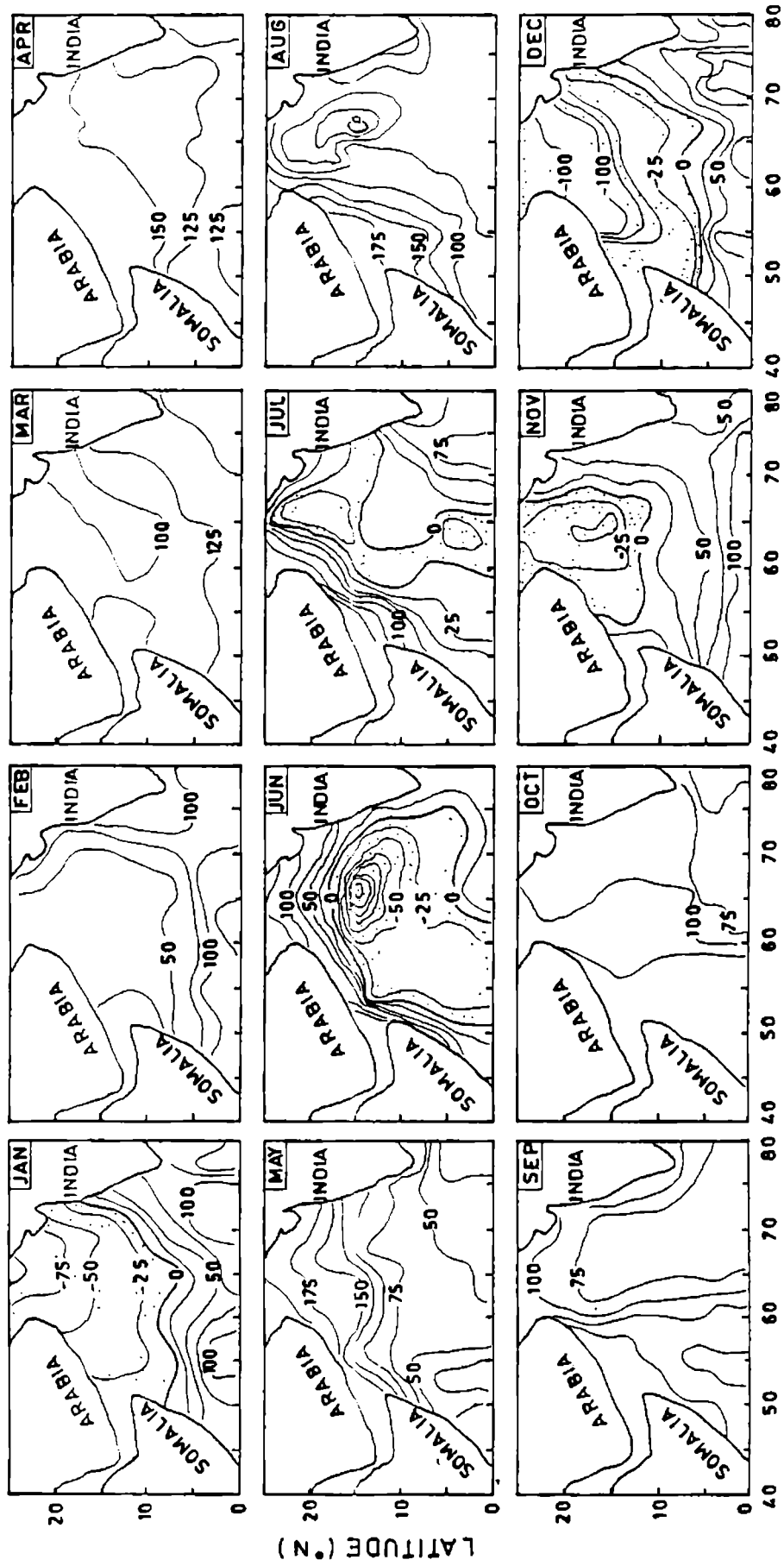


Fig. 3.2 Monthly distribution of the net surface heat flux (Wm^{-2})

losing heat with maximum heat loss (-125 W.m^{-2}) observed in June. The large heat loss in the central Arabian Sea during this period is caused by the combined effect of reduced insolation under overcast skies and larger latent heat flux under to strong winds (Hastenrath and Lamb, 1979a; Krishnamurti, 1981; Hsiung, 1986). The contribution of heat loss in cooling the surface layers of central Arabian Sea has been studied by several authors (Duing and Leetmaa, 1980; Rao, 1986, 87). Contrary to the heat loss in the central Arabian Sea, considerable heat gain is noticed in the upwelling regions, i.e. along eastern and western boundaries of Arabian Sea, where net heat gain exceeds 175 W.m^{-2} . Relatively clear skies in the cold upwelling region (Hastenrath and Lamb, 1979a) leads to higher incoming radiation and suppresses the evaporative heat loss (small $T_s - T_a$) resulting in net heat gain. In general, a negative relationship exists between SST and net heat flux in the upwelling regions. By August, the secondary period of heating starts and maximum values are noticed in the western Arabian Sea in October.

On an annual average, Arabian Sea is characterised by net heat gain with maximum heat flux concentrated in the coastal waters and near the equatorial Arabian Sea (Fig.3.3). A lateral gradient is noticed from the coastal waters towards the central Arabian Sea. The general feature of the net air-sea heat flux agrees well with Hastenrath and Lamb (1979b). However, the differences noticed in some areas could be due to different data processing techniques and the usage of different formulations for the estimation of various air-sea heat fluxes.

The estimates of heat change due to vertical motion were neglected in the earlier heat budget studies due to lack of

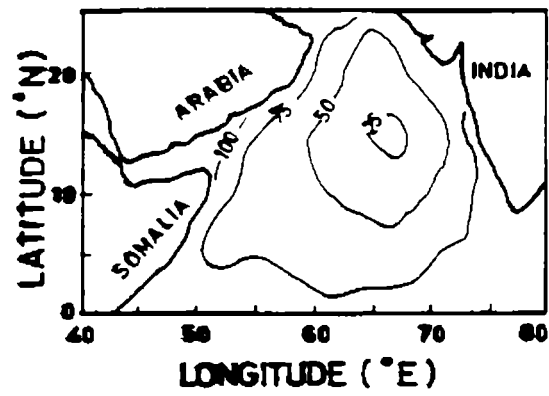


Fig. 3.3 Annual average of net air-sea heat flux($W.m^{-2}$)

sufficient subsurface temperature data sets. However, Rao (1988) made an attempt to study the contribution of this term in the heat budget of the central Arabian Sea. To study the role of vertical motion in the oceanic heat balance, monthly values of the heat change due to vertical motion is presented in Fig.3.4. Positive values denote accumulation of heat and negative values denote depletion of heat from the water column.

In February, a zone of heat loss is evident in southeastern Arabian Sea whereas rest of the Arabian Sea is characterised by accumulation of heat. The depletion of heat noticed in the southeastern Arabian Sea extends northward along the west coast and by May, heat diverges out from the entire Arabian Sea south of 15°N , coastal waters of India, Arabia and Somalia. However, during summer monsoon accumulation of heat is confined to the central and equatorial Arabian Sea (east of 55°E) whereas depletion of heat is noticed in the entire coastal waters which attains maximum in July. The process of coastal upwelling might have caused the depletion of heat in the coastal waters whereas the process of sinking might have increased the heat content in the central Arabian Sea. Just at the time of the withdrawal of the summer monsoon (September), accumulation of heat is noticed in the coastal waters off the southwest coast of India, Arabia and Somalia under the influence of sinking. In October, with the onset of northeast monsoon, the situation is entirely opposite to that in July with accumulation of heat in the coastal waters and depletion of heat in the rest of Arabian Sea. More over as the winter sets in, the northern Arabian Sea experiences depletion of heat and by February the water column starts gaining heat.

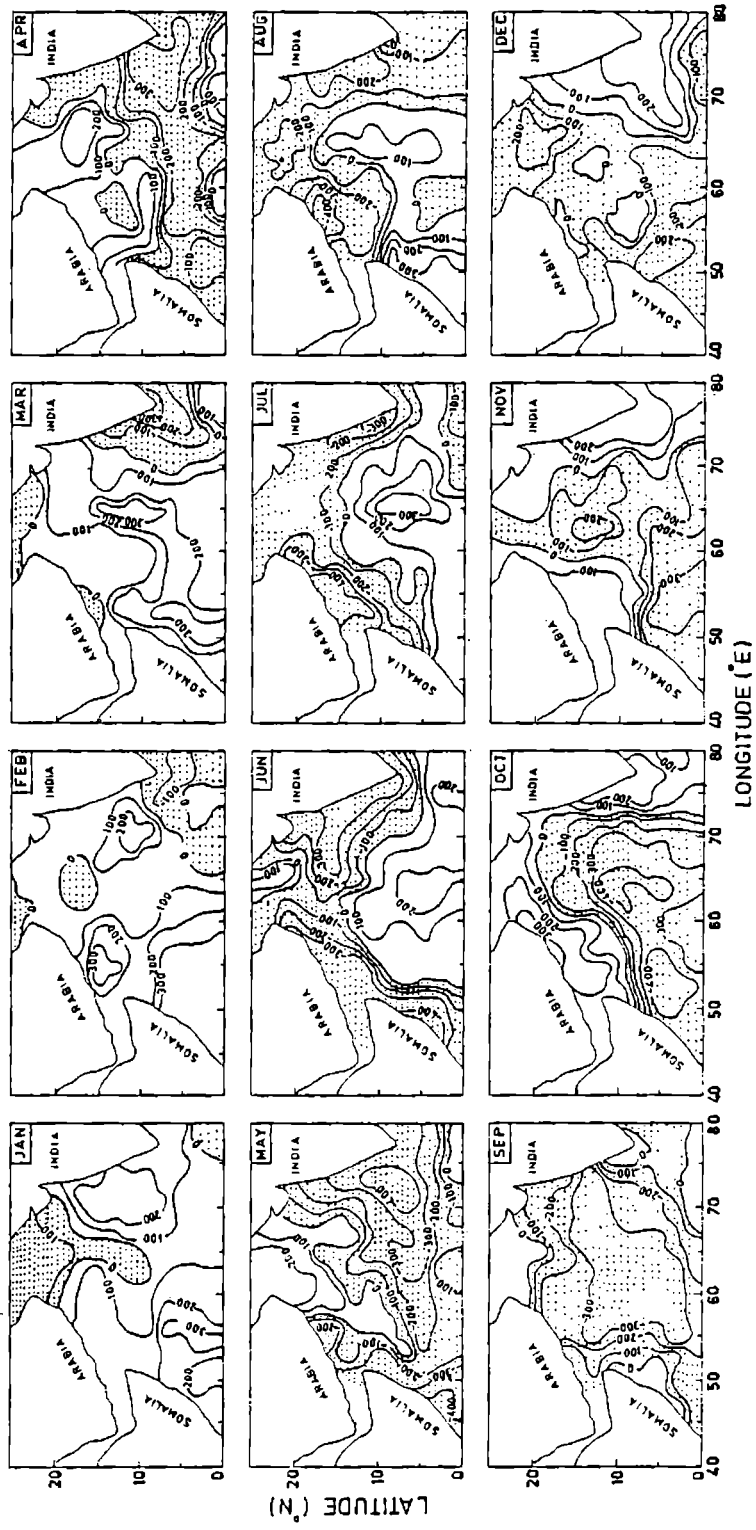


Fig.3.4. Monthly distribution of the heat change due to vertical motion (Wm^{-2})

3.5 Discussion

During winter, the northern Arabian Sea experiences large surface heat loss (approx. -100 W.m^{-2}) whereas heat change due to vertical motion shows an accumulation of 250 W.m^{-2} in the water column. However, the cooling, as indicated by the heat storage, revealed that the effect of heat change due to vertical motion is insignificant in the 200m water column. This implies that the cooling of the water column is mainly governed by the heat exchange across the air-sea interface.

The effect of pre-monsoon heating (February to May) is evident in the entire Arabian Sea though with varying magnitude. The maximum heat input into the ocean is noticed in April when values over 125 W.m^{-2} is evident all over the Arabian Sea. The reduction in heat gain by the ocean in the equatorial belt from May onwards indicates the onset and progress of the monsoon from south. On the otherhand, the northern Arabian Sea continues to gain heat in May. The accumulation of heat at a rate of $125-150 \text{ W.m}^{-2}$ can increase the temperature in the surface layers by $3-4^{\circ}\text{C}$ during pre-monsoon, which is consistent with Rao et al (1991). But the pre-monsoon heating is not reflected in the thermal structure of the 200m water column especially in the eastern Arabian Sea, where cooling is noticed from March onwards suggesting the probable influence of advective processes. The heat change due to vertical motion also suggests removal of heat from the 200m water column.

With the progress of summer monsoon drastic heat loss (-125 W.m^{-2}) was noticed in the central Arabian Sea. It may be noted that the effect of surface heat loss is not reflected in the heat storage rate. Instead, the warming noticed in the heat storage suggests the importance of advective processes in

increasing the temperature of the water column. Corresponding to the net surface heat loss and convergence in the surface layer, the mixed layer in the central Arabian Sea deepens by 50-60m (Fig.2.4). As the entire 200m water column is considered in this study, the heat gain due to convergence (sinking) might have offset the cooling in the SST field. Shetye (1986) proposed that the convergence in the surface layer (sinking) will have negligible effect on the SST variation, but it will increase the temperature of the subsurface levels by pushing down the thermocline.

Contrary to the warming of the 200m water column in the central Arabian Sea, cooling is noticed in the entire coastal waters under the influence of coastal upwelling. However, the net surface heat flux shows gain of heat in the coastal waters due to increased insolation under clear skies and decreased evaporative heat loss due coastal upwelling. The heat change due to vertical motion also suggest removal of heat from the coastal waters. Under the influence of this coastal upwelling the mixed layer shoals in the coastal waters (Fig.2.4). As the upwelled water reaches the surface, its temperature is slightly modified by the heat accumulated in a shallow layer. Even then strong cooling is noticed in the SST field off Somalia ($>5^{\circ}\text{C}$) and off the southwest coast of India ($>3^{\circ}\text{C}$) (Fig.2.3b). Saha (1974) and Duing and Letemaa (1980) stressed the importance of this upwelled water in cooling the Arabian Sea during summer monsoon.

On an annual cycle, the Arabian Sea gains heat at a rate of 68 W.m^{-2} , while the corresponding heat change due to vertical motion is -22 W.m^{-2} . Since the heat storage on an annual cycle is zero, the net heat gain is balanced by horizontal and vertical advection. Due to lack of adequate information on the mass transport, the effect of horizontal

advection is taken as the residual. Hence the heat balance of the Arabian Sea (upper 200m) can be written as (in $W.m^{-2}$)

$$Q_T = Q + Q_{DIV} + Q_{ADV}$$

$$0 = 68 - 22 - 46$$

This suggests that two third of surplus heat gain is compensated by horizontal advection and one third by vertical advection of cold water from interior. Details of these processes are largely unknown due to inadequate knowledge on the mass transport across the equator in the upper as well as in the deeper layers.

3.7 Heat budget components at selected location in the Arabian Sea

The annual march of the heat budget components, viz. net air-sea heat flux, rate of heat storage in the upper 200m water column and the heat change due to vertical motion at selected areas in the Arabian Sea are depicted in Fig.3.5. The regions were selected by considering the factors like upwelling/sinking, winter/summer cooling, net air-sea heat flux etc. The areas chosen are off the Somalia Coast (area I), northern Arabian Sea (area II), southwest coast of India (area III), equatorial Arabian Sea (area IV) and central Arabian Sea (area V).

In all areas, the net air-sea heat flux exhibits a double maxima, with heating during pre- and post- monsoon months. The maximum value of pre- and post monsoon heating is different at these regions indicating a non homogeneous coupling between the ocean and atmosphere. The amplitude of pre-monsoon heating shows an increase towards north and a time lag of one month is noticed in the occurrence of this maxima

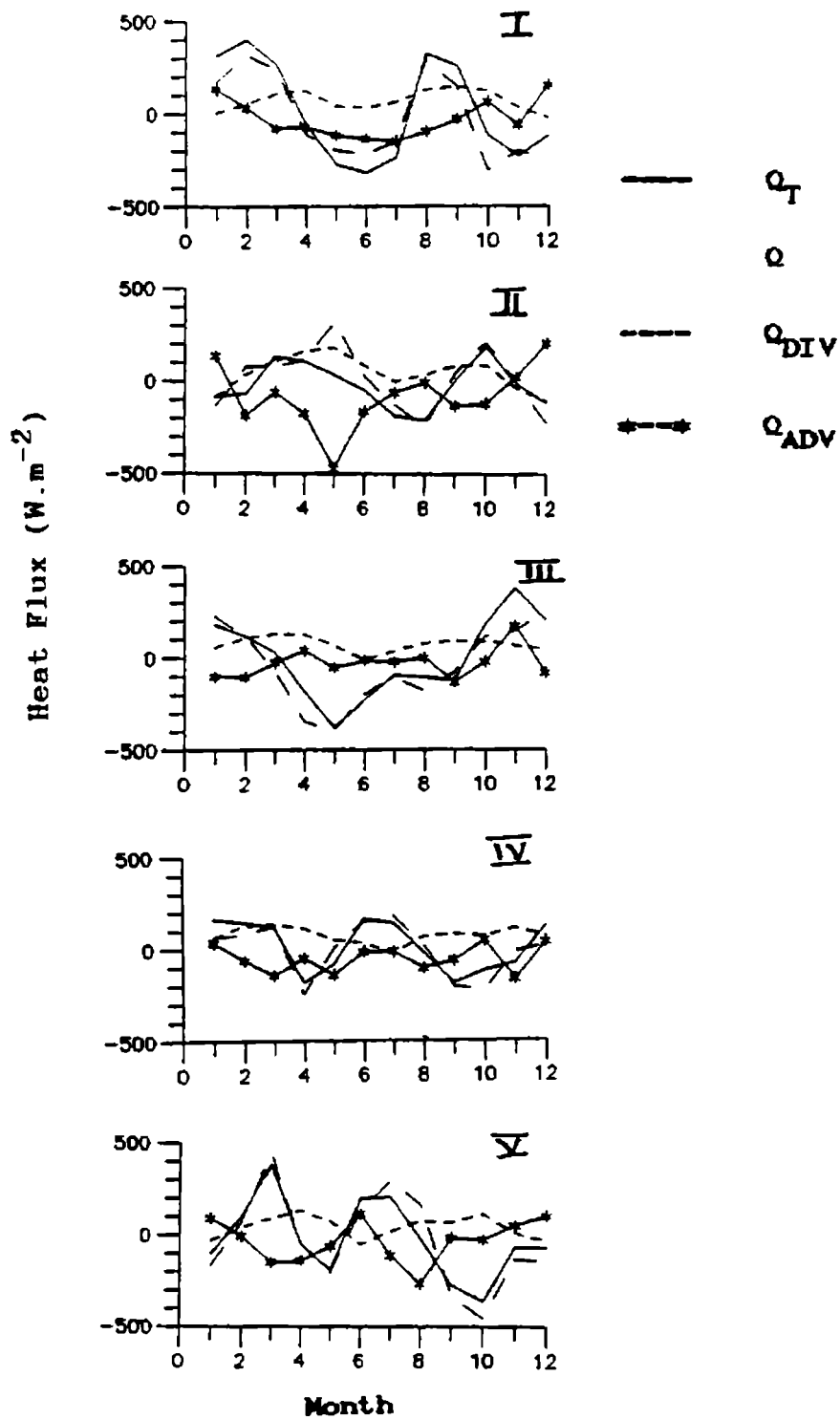


Fig.3.5. Annual march of the heat budget components at selected locations in the Arabian Sea

(125 W.m^{-2} in area IV during March to 200 W.m^{-2} in area II during May). It may be noted that the occurrence of this maxima is more related to the cloud pattern which increases from March to May and from Area II to area IV (Hastenrath and Lamb, 1979a). However, not much difference is noticed in the post-monsoon heating.

With the onset of summer monsoon, area V starts losing heat through intense air-sea exchange processes with maximum heat loss of -60 W.m^{-2} noticed in June. This large heat loss is caused by increased evaporative heat loss under strong winds (Hastenrath and Lamb, 1979a) and the reduction in insolation due to cloudy skies (Hastenrath and Lamb, 1979a; Rao et al, 1991; Hareesh Kumar et al, 1991). However, in the coastal waters (areas I, II, and III), the surface heat loss is insignificant. Clear skies and reduced evaporative heat loss (Hastenrath and Lamb, 1979b) due to cold upwelled water results in an increase in the net heat gain compared to other oceanic regions. Compared to summer cooling, intense winter cooling (-85 W.m^{-2}) is noticed in area II. The effect of winter cooling is also evident in area V though with a lesser magnitude (-25 W.m^{-2}).

In all areas significant changes is noticed in the rate of heat storage in the 200m water column on a seasonal cycle. During winter (December to March/April) all areas, except areas I and II show warming of the water column. In area II, the water column exhibits a cooling tendency in response to the net heat loss across the air-sea interface. A conspicuous feature in the heat storage is the warming of the 200m water column in area V during summer monsoon though surface heat loss is noticed. This warming might have been caused by mixed layer deepening and convergence induced by the negative wind stress curl.

The coastal waters of areas I, II and III start cooling from April, June and March respectively. Compared to all other areas, the cooling of the water column extends over a longer period (March-September) in area III. It may be noted that in coastal waters the removal of heat from the water column is mainly caused by the depletion of heat due to vertical motion. In area I, cooling of the water column is confined to April-July whereas heat change due to vertical motion shows cooling only between May and mid August. A secondary period of cooling is also noticed in area I during September-December. The maximum depletion of heat due to vertical motion (-400 W.m^{-2} in August) is noticed in area III, suggest the significance of vertical motion in maintaining the heat balance if the entire 200m water column is considered. With the reduction in the intensity of cooling due to vertical motion, the water column starts gaining heat. In area II also a cooling phase from June to August and a warming phase from February to June and also from September to December is evident. However, during winter, the greater heat loss at the surface has a substantial role in cooling the water column.

The heat change due to horizontal advection (Q_{ADV}) obtained as the residual in the heat budget equation, exhibits considerable variations both on spatial and temporal scale. In general, Q_{ADV} is negative cooling due to advection on an annual cycle. However, in area III Q_{ADV} is positive between May and July. The horizontal advection is found to be minimum in area III suggesting that the cooling noticed during summer monsoon season is mainly caused by vertical motion. Since Q_{ADV} is derived as the residual, unless some independent estimates of Q_{ADV} is made, only the broad feature can be explained.

3.7 Summer cooling in the Arabian Sea

Arabian Sea is probably the only region in the world ocean which cools during summer. A number of studies have been carried out to understand the importance of atmospheric forcing on the Arabian Sea associated with the onset and progress of the summer monsoon (Tunnel, 1963, Wyrski, 1971; Saha, 1974; Shetye, 1986; Rao, 1988). These studies suggest that the cooling of the Arabian Sea is mainly caused by the surface heat exchange processes and lateral and vertical advection. However, the relative importance of these processes will vary from one region of the Arabian Sea to another. The preliminary heat budget study of Duing and Leetmaa (1980) suggest that coastal upwelling plays a major role in the summer cooling of the Arabian Sea. This conclusion was mainly drawn by neglecting the effect of sinking in the central Arabian Sea and upwelling off the southwest coast of India. Also, the number of temperature profiles for their study was very much limited as only IIOE data was utilised.

The SST variability between May and August (August-May) presented in figure 2.3b revealed cooling in the entire Arabian Sea, with maximum cooling off the Somalia ($>5^{\circ}\text{C}$) and off the southwest coast of India ($>3^{\circ}\text{C}$). The cooling noticed during this period is mainly attributed to the coastal upwelling (Tunnel, 1963; Saha, 1974; Duing and Leetmaa, 1980). The studies by Shetye (1986) and Rao et al (1989) suggested strong convergence (sinking) in the central Arabian Sea in association with the negative wind stress curl. Due to this convergence the temperature at the subsurface level increases and the surface mixed layer deepens (Fig.2.4). However, in the preliminary heat budget studies, Duing and Leetmaa (1980) considers only the effect of upwelling along the coast of Somalia and Arabia. It is felt that the heat change due to

convergence in the central Arabian Sea and coastal upwelling off the southwest coast of India also has to be taken into account while studying the summer cooling of the Arabian Sea.

The heat budget equation of the mixed layer can be written following Duing and Leetmaa (1980) as

$$Q_T = Q + Q_{UP} + Q_{ADV} \quad (3.16)$$

Here Q_T is the heat content change in the entire Arabian Sea between May and August (August-May), Q is the net heat flux from May to August, Q_{UP} is the heat change due to upwelling and Q_{ADV} is the heat change due to horizontal advection which is taken as the residual term in the absence of sufficient information on mass transport. To choose the maximum depth of integration for Q_T and H_{DIV} , the temperature profiles of May and August are compared and the deepest mixed layer of these months (Fig.2.4) for each $2^\circ \times 2^\circ$ grid was taken as the maximum depth (Duing and Leetmaa, 1980).

The difference in the heat content of the mixed layer (August-May) revealed a cooling of the Arabian Sea which was of the order of 3.1×10^{21} J. During this period, the heat accumulated in the surface layer (2.4×10^{21} J) should have resulted in warming of the Arabian Sea if other processes are negligible. This indicate that even during southwest monsoon period, heat gain is much greater than net heat loss across the air-sea interface.

The heat change due to upwelling is computed using the equation (Duing and Leetmaa, 1980)

$$Q_{UP} = \rho \tau_l L \Delta T C_P f^{-1} \quad (3.17)$$

where τ_l is the component of wind stress which induces upwelling between May and August; L is the length of coast line; ΔT is the mean temperature difference between the upwelled water and temperature in the interior of the basin and f is the coriolis parameter. The rate of upwelling along the coast is given by $\tau_l L f^{-1}$. Since mass has to be conserved, the influx of upwelled water is to be compensated by an outflow. This can occur either by a depression of the thermocline in the Arabian Sea or by an outflow across the lateral boundaries. In either case ΔT represents the temperature difference between the outflowing water in the mixed layer and the upwelled water (Duing and Leetmaa, 1980). The length L of the coast line off Somalia and Arabia where pronounced upwelling takes place is 1600km (Duing and Leetma, 1980) and off the southwest coast of India is 700km. The coriolis parameter is evaluated for each 5° grids till the northern limits of the coast line.

The resuting balance thus becomes

$$Q_T = Q + Q_{UP} + Q_{ADV}$$

$$-4.20 \times 10^{14} = 3.10 \times 10^{14} - 4.90 \times 10^{14} - 2.40 \times 10^{14}$$

Obviously Q_{UP} is the largest term in the heat budget equation, while Q_{ADV} is much larger than expected.

It is still not clearly known how the summer cooling which is mainly as a result of upwelling is balanced in the annual heat budget and also how the large quantity of upwelled water replenished at depth. Since Arabian Sea is a region of net heat gain (Q) these are balanced only by horizontal advection and to a certain extent by winter cooling in the

northern Arabian Sea and subsequent sinking and spreading southward. Duing and Leetmaa (1980) points out that heat loss due to winter cooling is -1.9×10^{14} J. Since mass exchange with Red Sea and Persian Gulf are negligible (Duing and Leetmaa, 1980) the balance heat loss of 3×10^{14} J due to upwelling could be replenished by cold water advection across the equator into the Arabian Sea and warm water advection in the surface layers southward from the Arabian Sea. Only few information is available on the exchange of waters at intermediate and deeper layers across the equator in the Indian Ocean. The contribution of surface, intermediate and deep circulation in the Arabian Sea in the summer cooling is far from understood and it needs much detailed knowledge on the intermediate and deep layer mass transport across the equator.

CHAPTER IV

SEASONAL VARIABILITY OF THE THERMOHALINE FIELDS OFF THE WEST COAST OF INDIA

4.1 Introduction

The seasonal variation in the temperature and salinity fields is quite large off the west coast of India where vertical motions are significant. The warmest sea surface temperature (SST) ($>30^{\circ}\text{C}$) generally occurs during April-May (Joseph, 1990) while SST as low as 20° - 22°C is noticed near the coast during July-September (Ramasastri and Myrland, 1959; Pillai et al, 1980) especially off the southwest coast of India due to upwelling. The salinity field in the surface layers is influenced by the inflow of higher saline waters from northern Arabian Sea, low saline waters from Bay of Bengal/Equatorial Indian Ocean and also river discharges (Darbyshire, 1967; Wyrтки, 1971; Johannessen et al, 1981; Pankajakshan and Ramaraju, 1987).

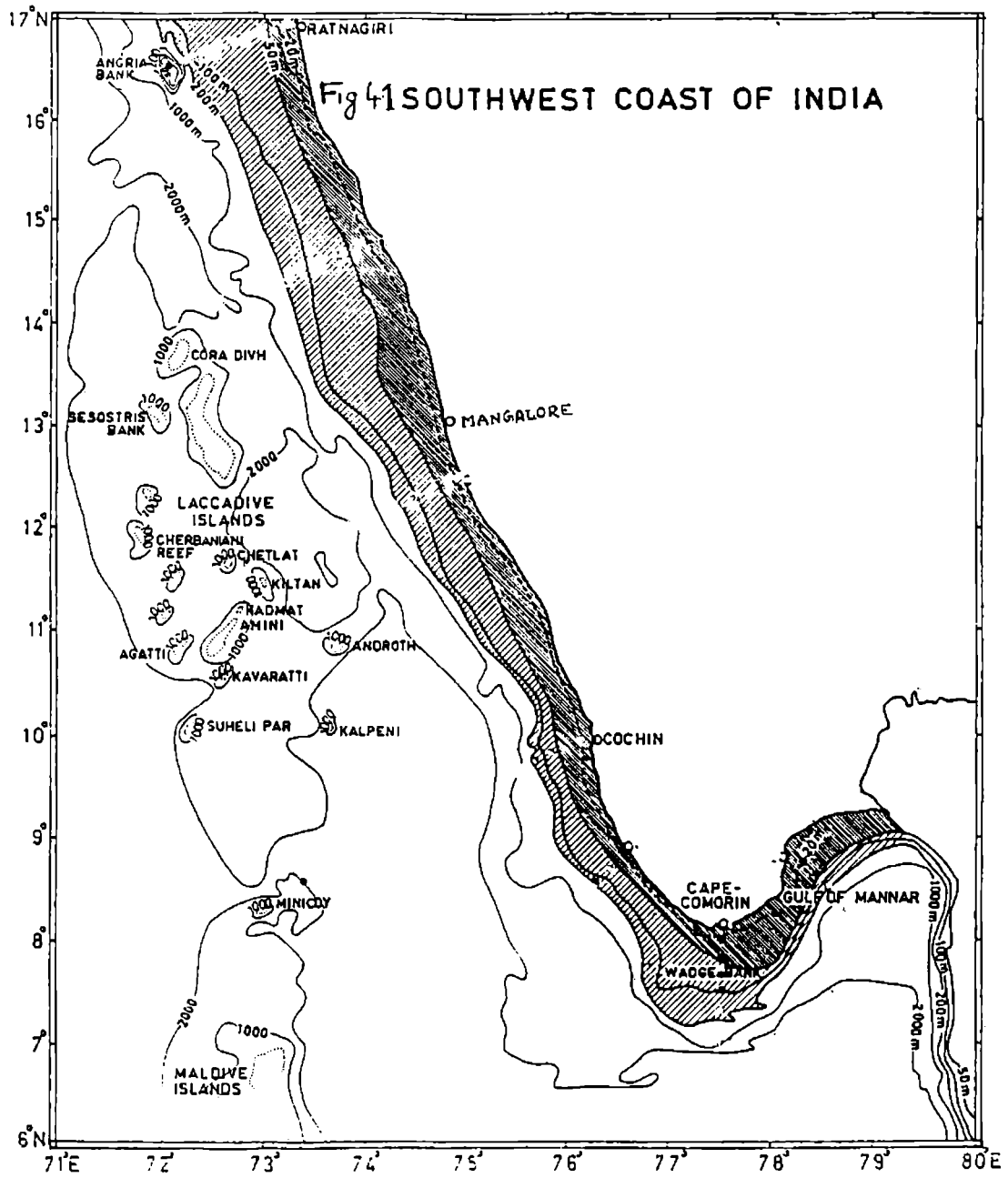
The occurrence of upwelling especially off the southwest coast of India during summer monsoon was reported even before IIOE (Ramasastri and Myrland, 1959; Banse, 1959; Ramamirtham and Jayaramam, 1960). The importance of upwelling on the fishery resources off the west coast of India has been discussed by Banse (1968). The annual cycle of temperature/density fields suggests the occurrence of upwelling from March-August off the southwest coast of India while sinking takes place between November and February (Sharma, 1966, 1968, 1978; Pillai et al, 1980; Mathew, 1983). One of the most striking features in this region is the influx of low saline waters from Bay of Bengal/Equatorial Indian Ocean into the eastern Arabian Sea during winter (Darbyshire, 1967; Wyrтки, 1971; Johannessen et al, 1981; Pankajakshan and Ramaraju, 1987). Certain aspects of coastal upwelling and watermass structure off the west coast of India during southwest monsoon are discussed by Shetye et al (1990). Ramamurthy (1963), Patil et al (1964) and Noble (1966) discussed the thermohaline variability off Karnataka

Coast for selected seasons. All these studies are either limited in time or space and do not describe adequately well the upper layer temperature/salinity field off the west coast of India covering the annual cycle. Hence in this chapter an attempt is made to describe the thermohaline variability in the upper layers off the west coast of India on an annual cycle.

4.2 Surface winds and currents

The seasonal reversing winds and currents in the Arabian Sea exhibit large temporal and spatial variations. In the eastern Arabian Sea northwesterly or northerly winds prevail from December to February, while between May and September southwesterly winds dominate (Fig.1.1). However, a close examination of the wind field reveals a change in direction as the wind approaches the coast (from southwesterly to westerly or northwesterly) off the southwest coast of India during summer monsoon, while the winds continues to be westerly or southwesterly north of 17°N . Moreover, the winds are much stronger in the northeastern Arabian Sea compared to southeastern Arabian Sea during this period. The winds are weak and variable during March - April and October - November. Throughout the year there is always an equatorward component of wind near the coast off the southwest coast of India (Mathew, 1983; Shetye, 1984; Shetye et al, 1990).

One of the striking features of the surface circulation (Fig.1.2) in the eastern Arabian Sea is the reversal of surface current to southerly off the southwest coast of India as early as in February-March (Fig.1.2). However, in the rest of the eastern Arabian Sea the reversal is further delayed. The surface southerly flow is stronger near the coast during southwest monsoon (>1 knot). The surface current changes its



direction to northwesterly off the southwest coast of India as early as August-September which is again much ahead of wind reversal. The surface currents off the west coast of India during December-January flow against the local wind (Fig.1.1 and 1.2) suggesting the importance of internal ocean dynamics in maintaining the flow (Shetye,1984). The surface currents are weak and variable during March - April and October-November.

4.3 Seasonal variability of temperature and salinity of the shelf waters

In order to obtain the broad scale features of the thermohaline variability off the west coast of India, the monthly mean temperature and salinity data on the continental shelf off Cape Comorin, Cochin, Mangalore and Ratnagiri (Fig.4.1) are averaged and presented in Figs.4.2(a-d). The temperature field in the upper 200m water column show significant ascending and descending motion in the annual cycle. The thermoclines shows ascending tendency from March/April onwards and reaches surface layers by June at all locations except off Ratnagiri. The coldest waters in the surface layers are noticed in July off Cape Comorin, in August off Cochin and in September/October of Mangalore. The reverse process of sinking starts by August off Cape Comorin, September off Cochin and by mid-September off Mangalore. However, upward motion continues upto November/December off Ratnagiri and also there is no significant cooling of the surface layers. The pre-monsoon warming is significant at all locations, though a secondary warming is prominent only off Ratnagiri.

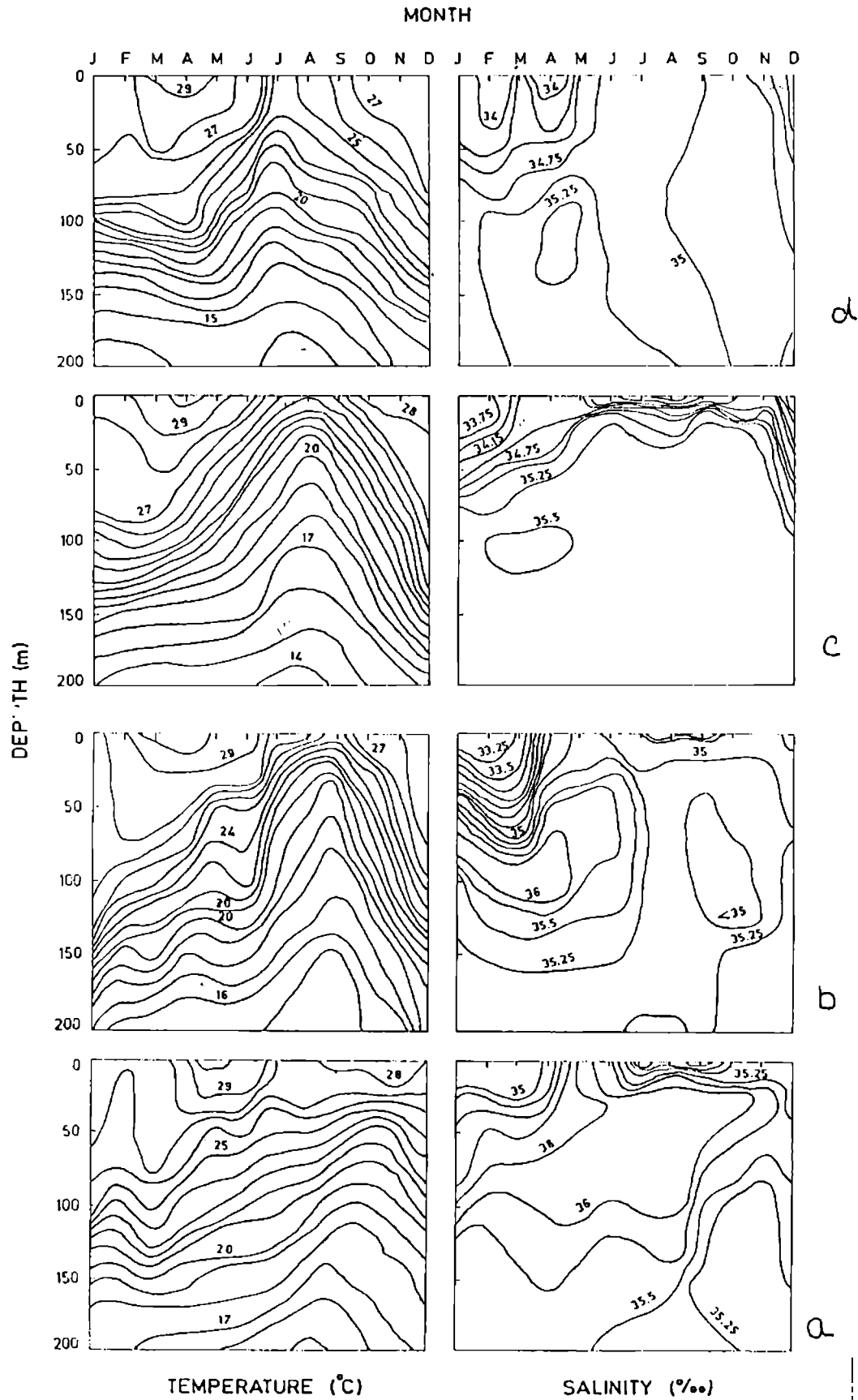


Fig.4.2. Mean monthly distribution of temperature (°C) and salinity (ppt) off (a) Ratnagiri, (b) Mangalore, (c) Cochin and (d) Cape Comorin

The salinity in the surface layers off Cape Comorin are maximum (35%.) during September-October (post monsoon) and minimum during February-March (<34%). However, low saline waters are noticed in the upper layers both in summer and winter at all other three locations. The lowering of salinity during southwest monsoon is mostly confined to the upper 5-10m obviously resulting from monsoonal rain/freshwater discharges. However the low salinity (<34%.) during winter extends at least up to 50m which are of Bay of Bengal/Equatorial Indian Ocean origin (Darbyshire,1967; Wyrтки,1971; Pankajakshan and Ramaraju,1987). The subsurface salinity maxima (>36%.) is more prominent off Ratnagiri and off Mangalore. The haloclines are strong where the effect of low salinity Bay of Bengal/Equatorial Indian Ocean waters and high salinity SHSW are significant, i.e. off Cochin and Mangalore.

4.4 Vertical distribution of temperature and salinity

The monthly cross shelf variation of temperature off Ratnagiri shows deep thermocline (>60m) with surface temperature about 27°C from January to March (Fig.4.3). By April the SST increases to about 30°C near the coast which continues in May. The isotherms show distinct upward sloping towards the coast between May and December indicating a southerly surface flow and upwelling. A mild downward slope of isotherms below 150m is seen only in December probably due to the poleward undercurrent associated with upwelling. The maximum effects of upwelling with coldest surface temperatures (<27°C at the surface near the coast) between October and December.

Near the coast, the surface layer salinity is less than 35%. during January-March which increased with depth (Fig.4.3). The subsurface salinity maxima associated with

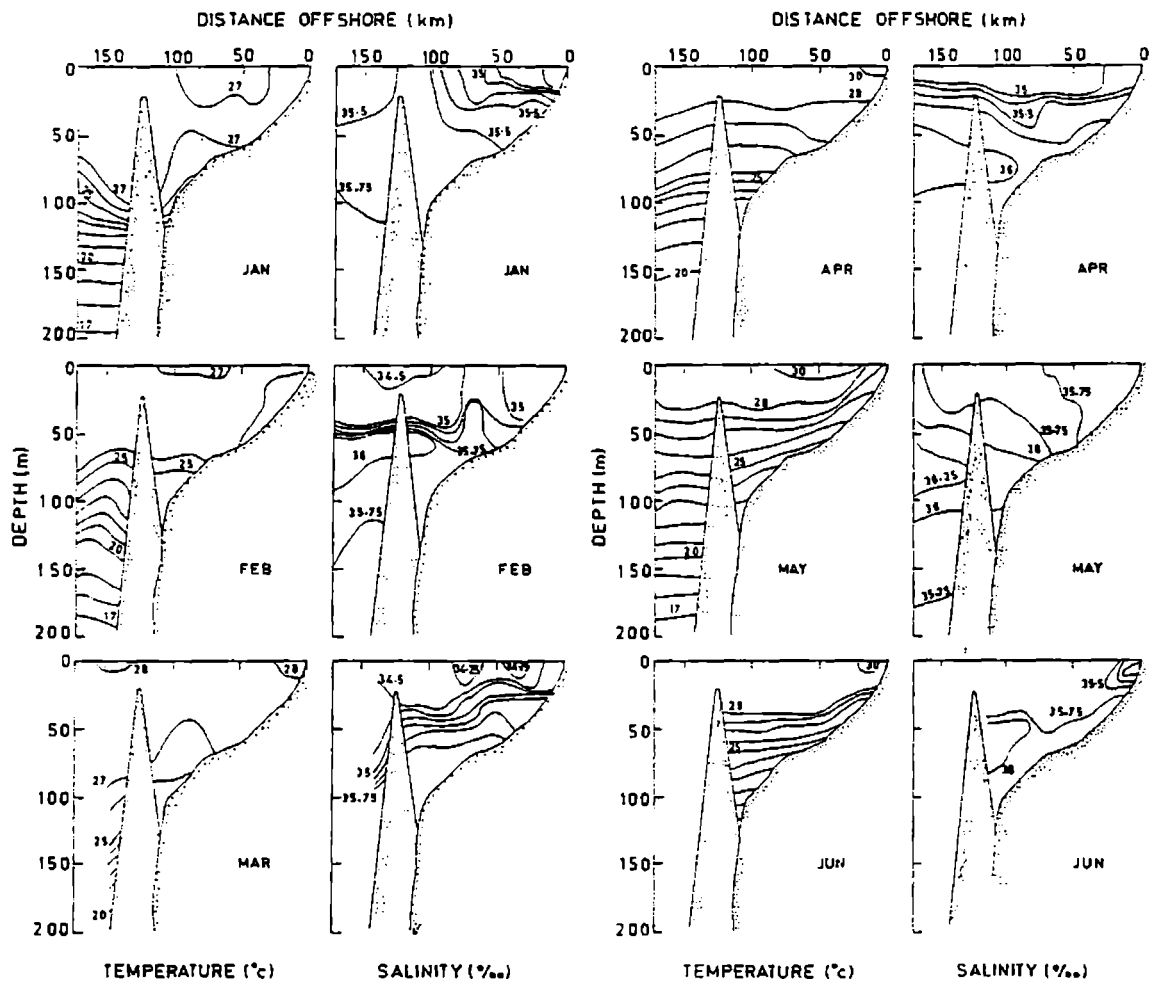


Fig.4.3.a. Vertical sections of temperature ($^{\circ}\text{C}$) and salinity (ppt) off Ratnagiri from January to June

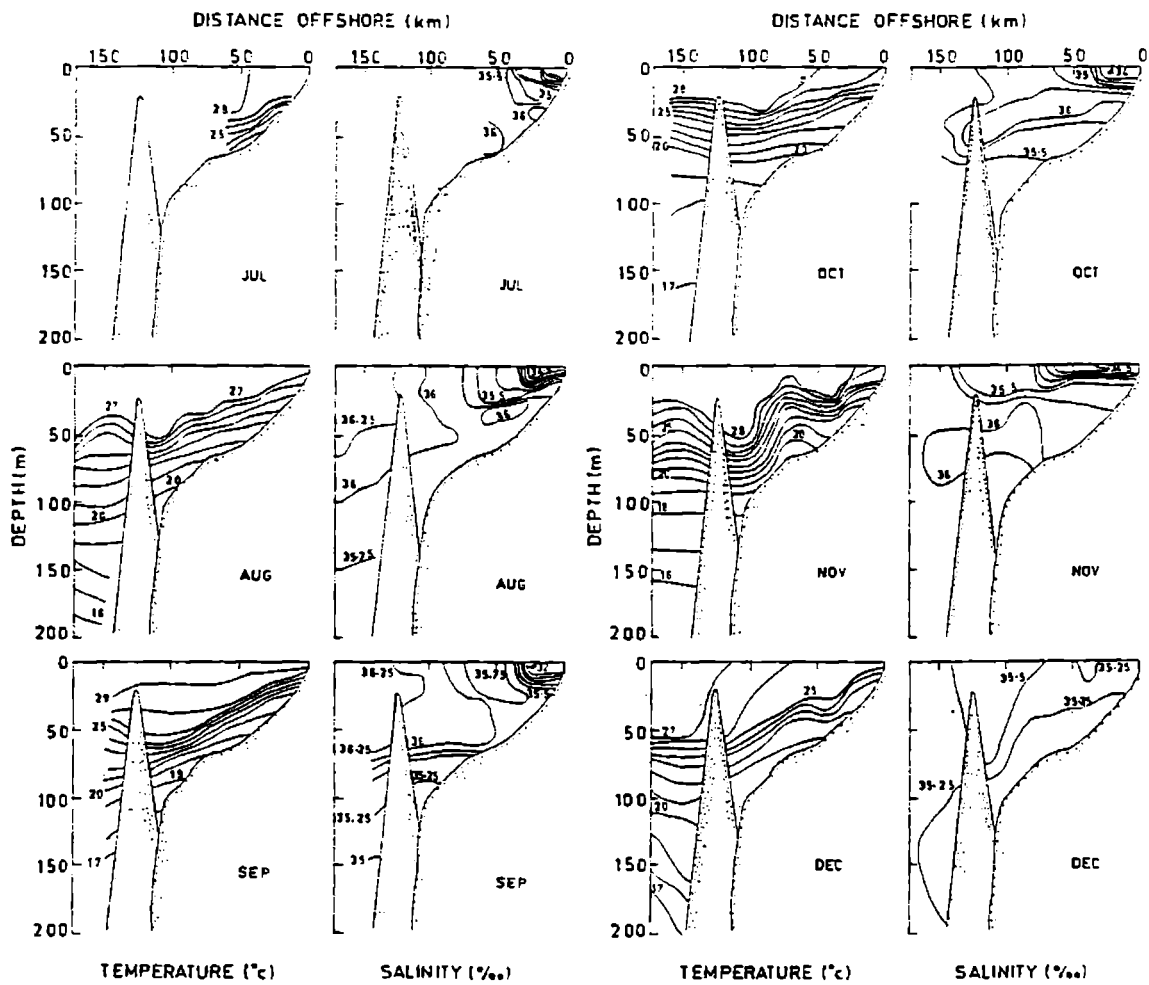


Fig.4.3.b. Vertical sections of temperature ($^{\circ}\text{C}$) and salinity (ppt) off Ratnagiri from July to December

ASHSW is evident in almost all months in the depth range of 50-100m. The maximum surface salinity (>35.5‰) is observed during May-June. The surface salinity drops drastically very near the coast during July-November in association with monsoonal rains and freshwater discharges from rivers.

The vertical sections of temperature off Mangalore (Fig.4.4), Cochin (Fig.4.5) and Cape Comorin (Fig.4.6) follow similar seasonal variations with certain time lags. The thermal field is characterised by deep isothermal layers (>70m) off Mangalore in January and February while similar conditions occur off Cochin during December-January and off Cape Comorin from November-January. The gradual warming of the surface layers and upward movement of isotherms in the lower thermocline (150m) begins by March off the southwest coast of India. The warmest surface temperatures (>30°C) are observed during March-May except off Cape Comorin. The upsloping of isotherms towards the coast in the upper thermocline is evident from April and continues upto November off Mangalore, upto October off Cochin and upto August off Cape Comorin. The coldest surface temperature occur during peak southwest monsoon. The SST drops to as low as 24°C in October off Mangalore, 22°C in August off Cochin and 24°C in July off Cape Comorin. The downsloping of the isotherms towards coast associated with the poleward undercurrent is evident at all locations in the depth range 80-150m with some monthly variations. It is interesting to note that upwelling off the southwest coast of India is a gradual process while sinking is rather rapid and occurs within a month.

The monthly variations of salinity field also shows similar patterns off Mangalore (Fig.4.4), Cochin (Fig.4.5) and Cape Comorin (Fig.4.6). At all locations, the subsurface salinity maxima associated with ASHSW is evident between

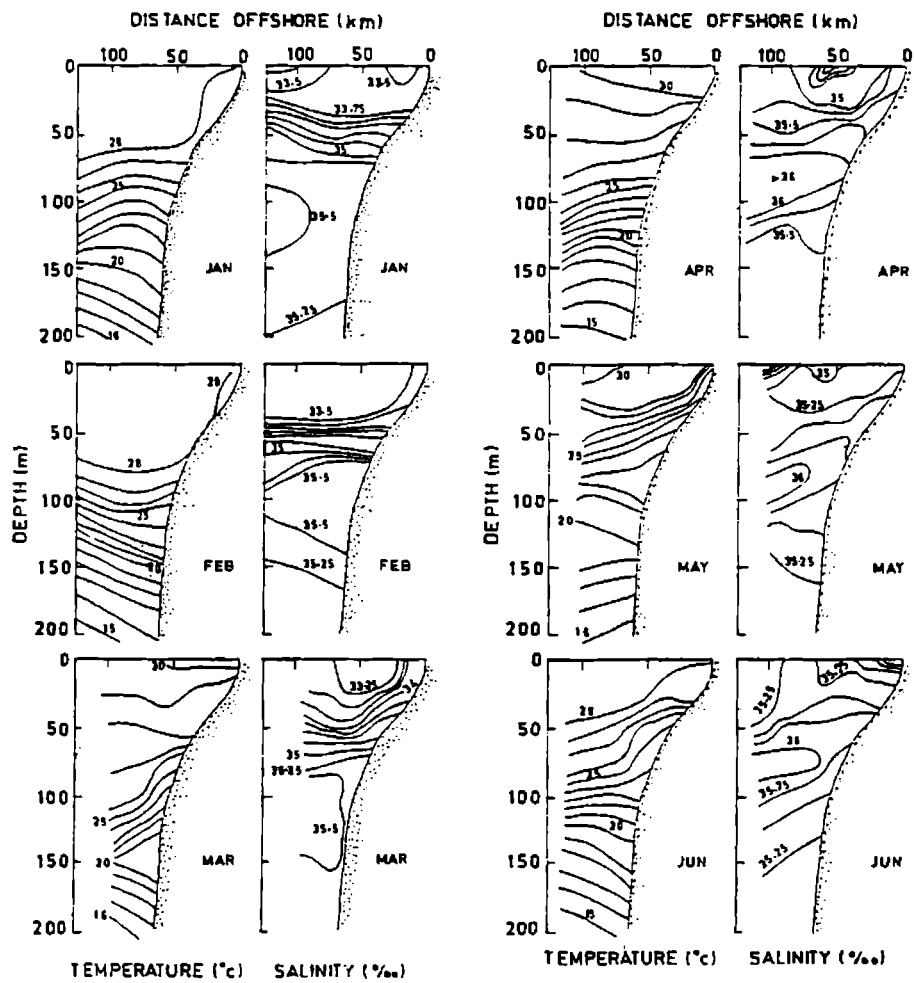


Fig.4.4.a. Vertical sections of temperature ($^{\circ}\text{C}$) and salinity (ppt) off Mangalore from January to June

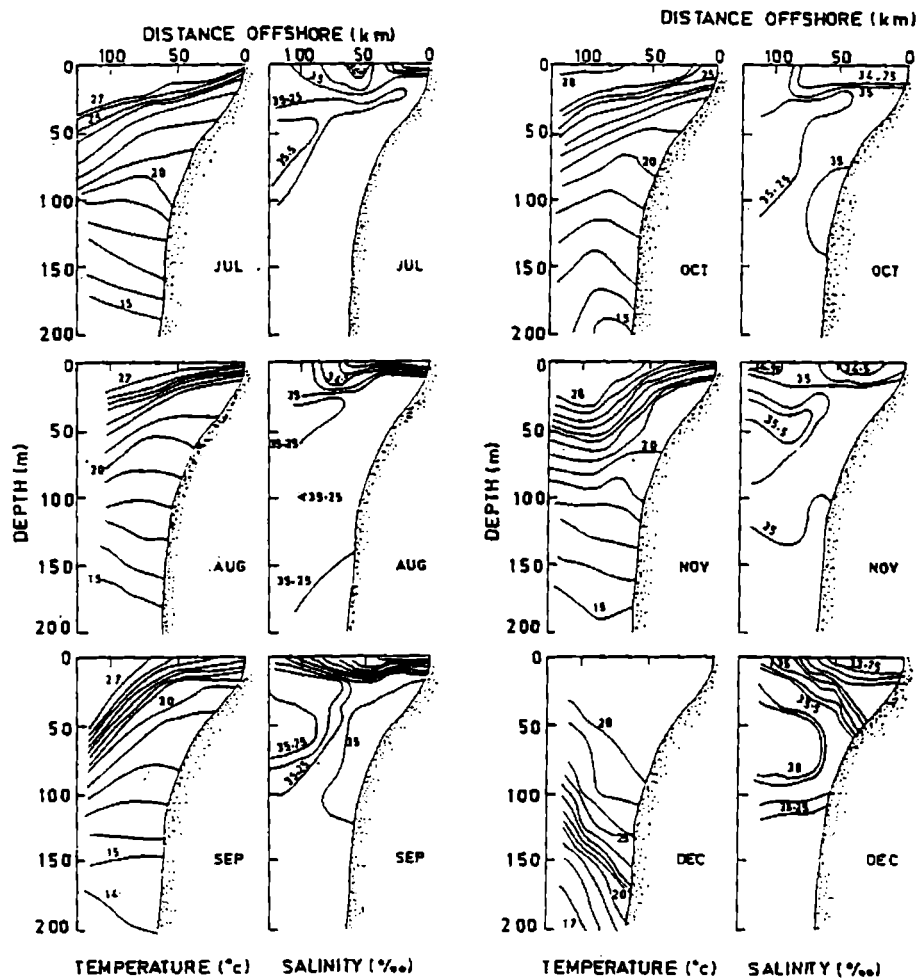


Fig.4.4.b. Vertical sections of temperature ($^{\circ}\text{C}$) and salinity (ppt) off Mangalore from July to December

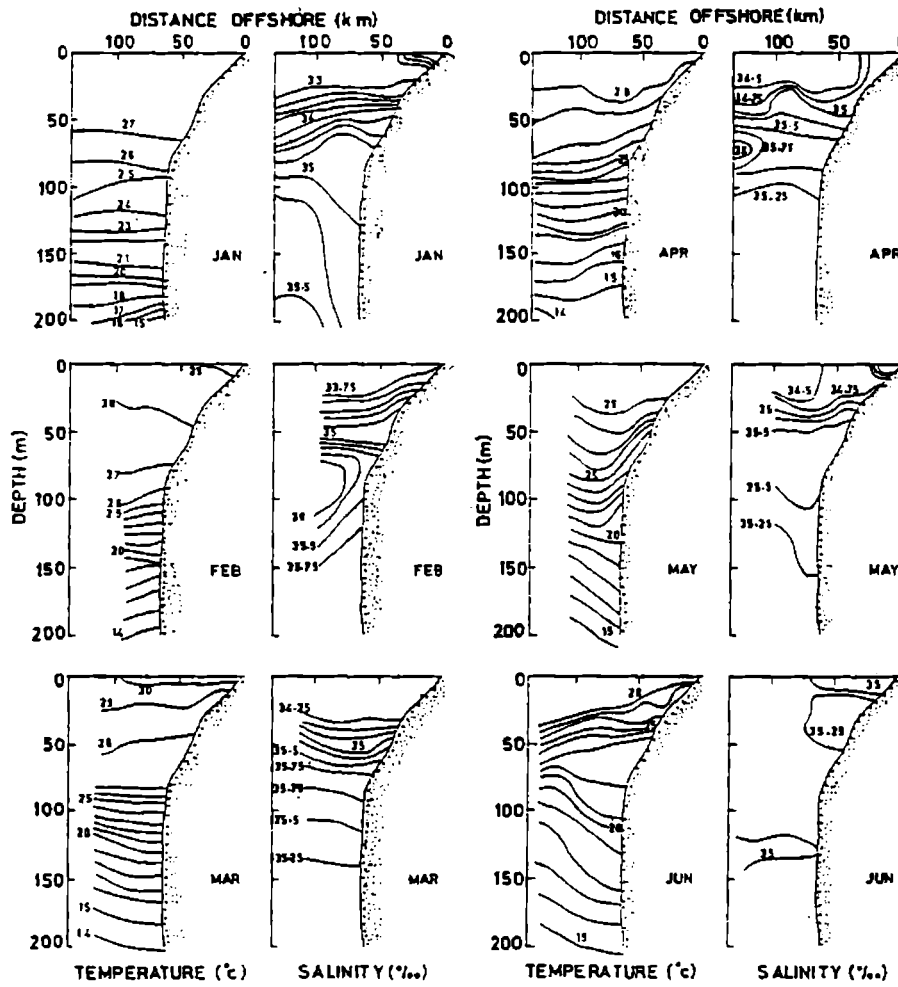


Fig.4.5.a. Vertical sections of temperature ($^{\circ}\text{C}$) and salinity (ppt) off Cochin from January to June

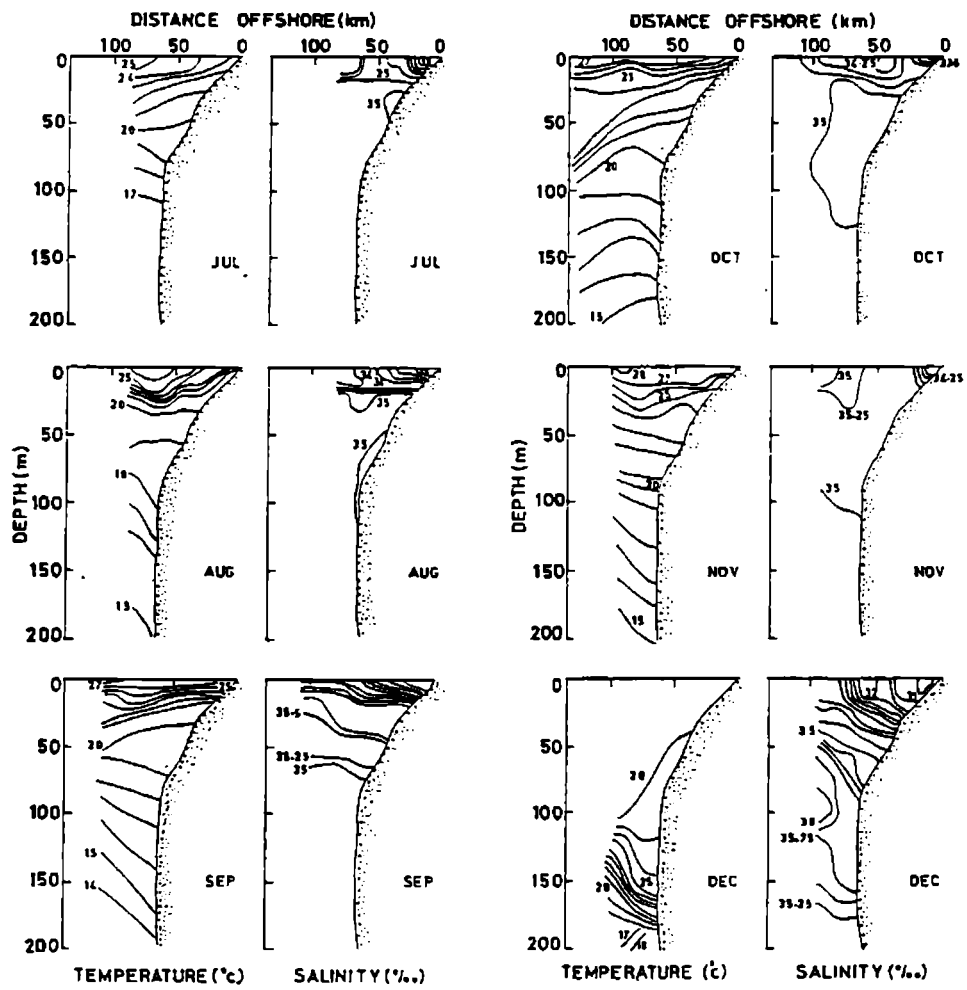


Fig.4.5.b. Vertical sections of temperature ($^{\circ}\text{C}$) and salinity (ppt) off Cochin from July to December

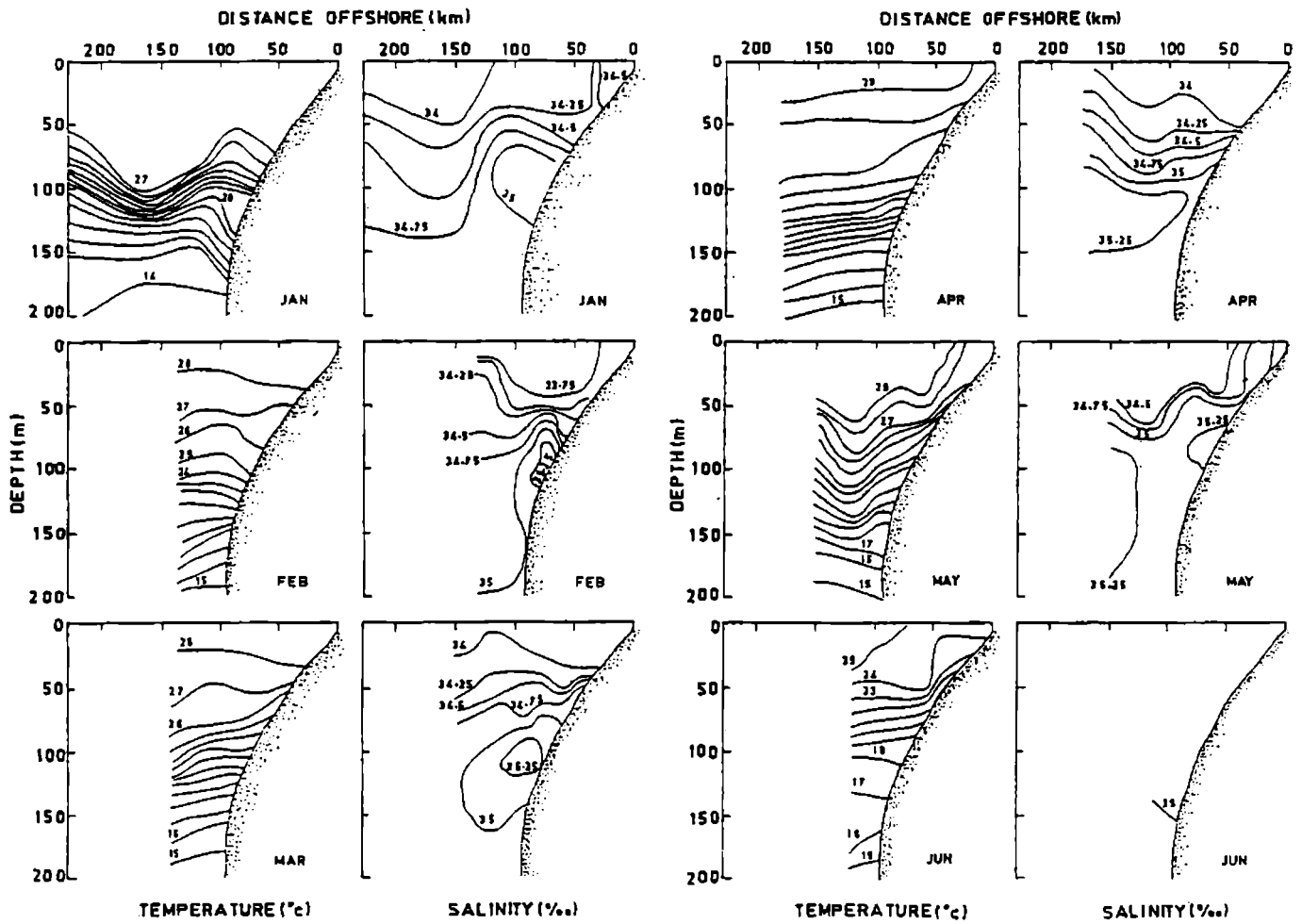


Fig.4.6.a. Vertical sections of temperature ($^{\circ}\text{C}$) and salinity (ppt) off Cape from January to June

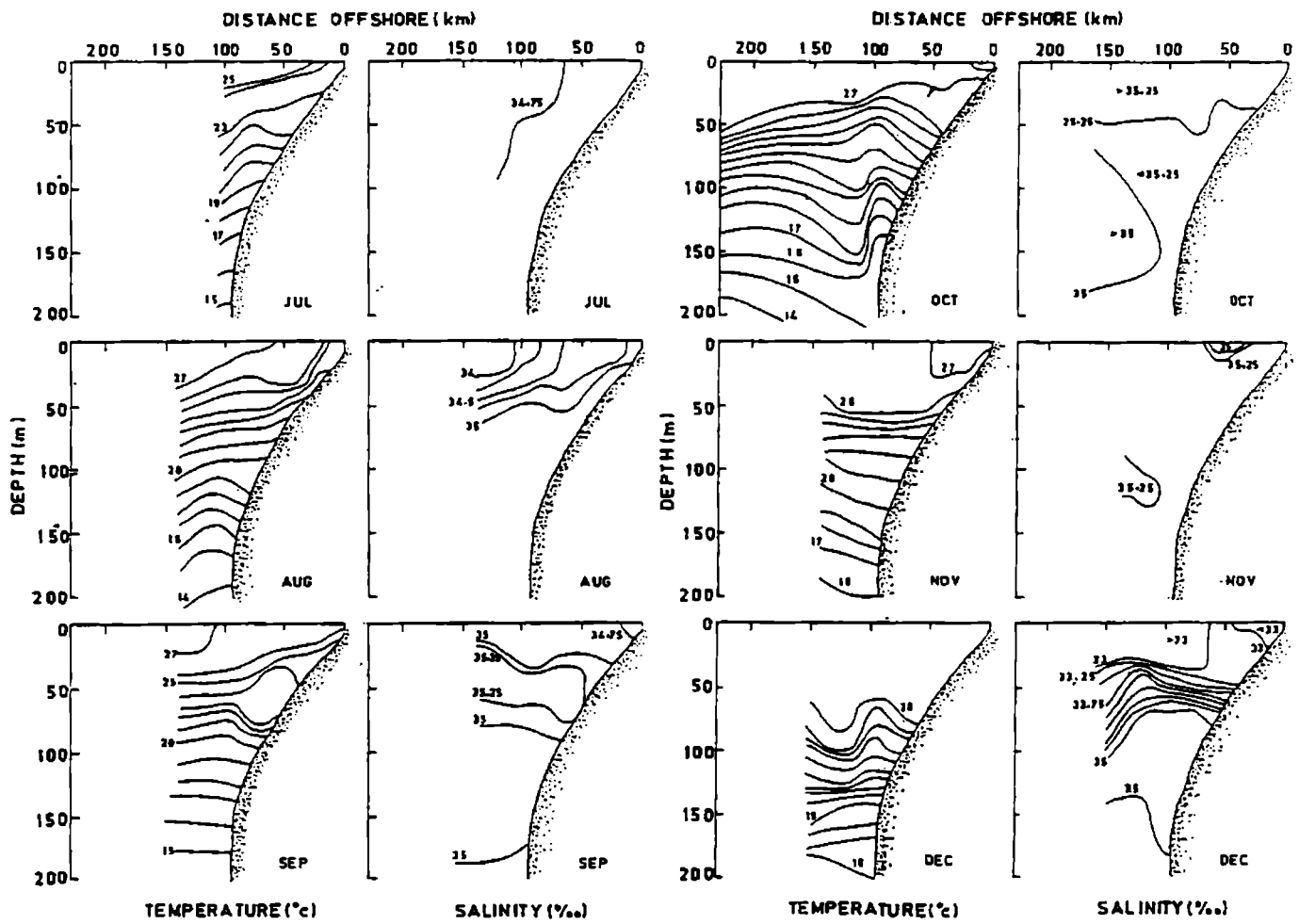


Fig.4.6.b. Vertical sections of temperature ($^{\circ}\text{C}$) and salinity (ppt) off Cape from July to December

50-100m with decreasing core values towards south. The subsurface salinity maxima is not very clear in the Figs. off Cape Comorin because of the contouring interval of 0.25‰, since S_{max} is weak compared to other locations. On an annual cycle the salinity shows least variations off Cape Comorin (2‰) and also with depth. This could be due to the low precipitation rates near the southernmost regions and also due to proximity of Bay of Bengal/equatorial Indian Ocean which are typically low saline and undergo minimum seasonal variation (Wyrtki, 1971). The influx of low saline Bay of Bengal/equatorial Indian Ocean waters is very much evident off Mangalore and Cochin during winter which continues till March. The major differences between the layer distributions is that the summer dilution is limited to the upper 5-10m while the dilution during winter extends at least up to 50m. The subsurface salinity maxima due to ASHSW is evident in all months with minor variations in the core values and core depths. A very conspicuous zone of relatively low salinity is evident at the shelf edge/slope regions during summer at all the locations between 80m and 150m, the region of the poleward undercurrent.

4.5 T-S diagrams for the entire west coast of India

All the monthly hydrographic data available off the west coast of India is utilised to map the T-S diagrams (Fig. 4.7) in order to understand the variability of temperature-salinity characteristics. The T-S plots show maximum scatter during winter and post-monsoon season and minimum scatter during May-June. The large scatter with salinity less than 35‰ during winter is caused by influx of Bay of Bengal/Equatorial Indian Ocean water (above 500 cl/t) into the eastern Arabian Sea (Darbyshire, 1967; Wyrtki, 1971; Pankajakshan and Ramaraju, 1987). The high saline waters centered around 400

cl/t is obvious in all months with maximum salinity (>36%) during summer monsoon. Below the depth of the subsurface high salinity maxima the T-S scatter is maximum from June to November due to large differences in nearshore and offshore stations (below 400 cl/t surface). The minimum scatter of T-S field during May-June is probably resulted from increase of surface layer salinity as the prevailing southerly surface flow brings high saline waters into the southern Arabian Sea. Though the scatter (with low saline waters in the surface layers) is also higher during summer monsoon resulted from rain or river discharge, is rather limited to surface only, which is evident from vertical sections also (Figs.4.3-4.6). Below 300 cl/t the T-S scatter is less heterogeneous with salinities <35.5%.

4.6 T-S characteristics at selected locations off the west coast of India

The monthly composite T-S diagrams off Ratnagiri (Fig.4.8) shows increase of salinity below 400 cl/t thermocline surface. The near surface waters above 400 cl/t with almost uniform temperature (27°C) shows considerable variation in salinity (between 35 and 36%) between January and March. Vertical mixing due to winter convection occurs north of 18°N (Banse, 1968) which is particularly effective on the wide continental shelf off Saurashtra (Shetye et al, 1990). They also suggest that the mixing breaks down the vertical salinity gradient in the equatorial surface water producing a water type defined roughly by temperature 27°C and salinity 36%. After the withdrawal of northeast monsoon, this water is expected to be modified turning warmer and more saline during April-May under intense solar heating and moves southward during summer monsoon which results in the absence of Equatorial surface waters north of 17°N (Shetye et

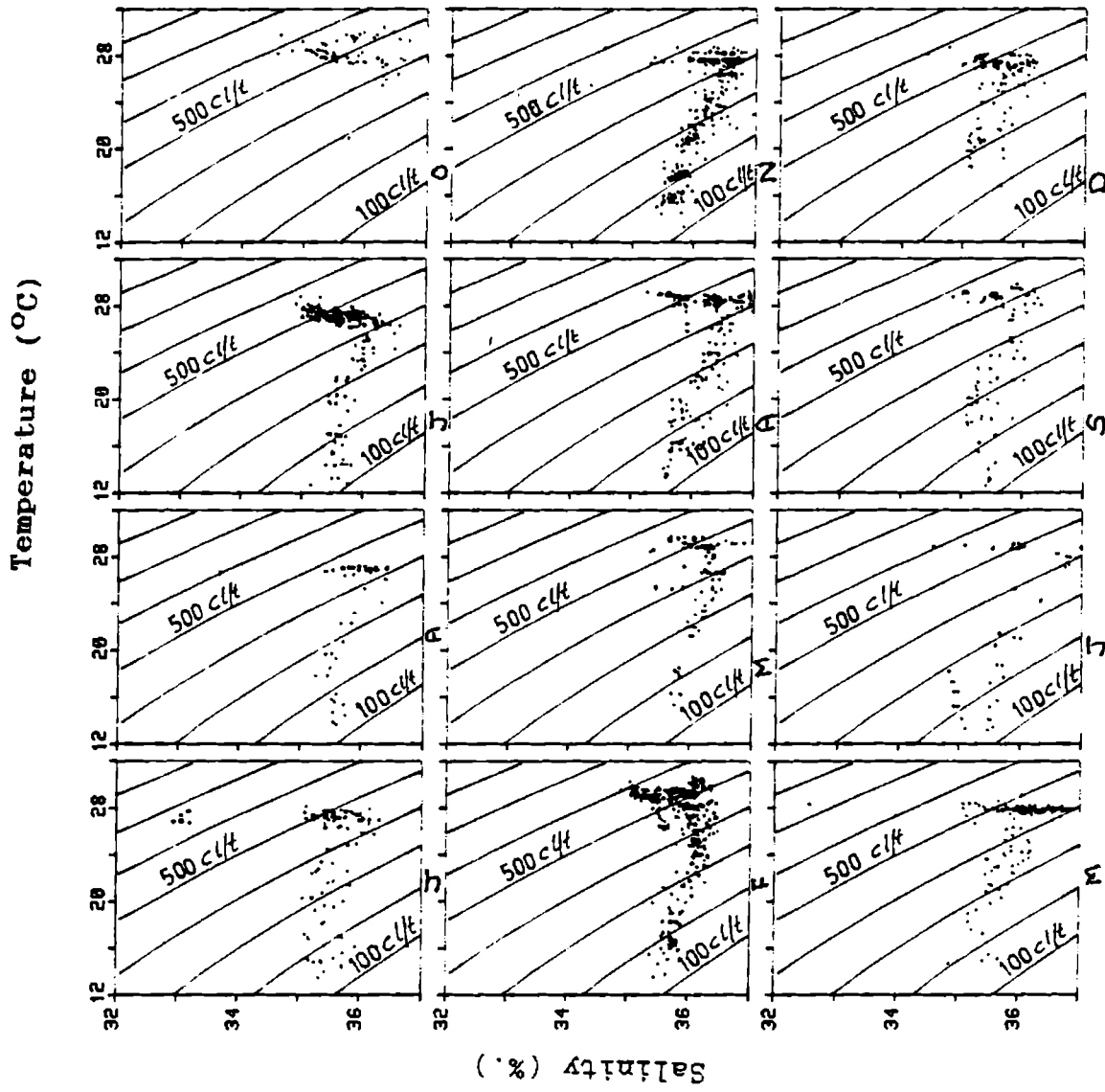


Fig.4.B. Monthly composite T-S diagrams covering all stations off Ratnagiri

al,1990). However, the waters less than 35‰ in the surface layers during March-April is likely to be of Bay of Bengal/Equatorial origin modified (with increase in salinity) as the water moves northwards with the prevailing surface currents.

The T-S scatter is least during May-June-July, when there is summer heating and little influence of freshwater fluxes. The wide scatter during August-September-October especially in the surface layers show importance of freshwater fluxes in the modification of water characteristics. The subsurface salinity maxima is strongest between July and October (37‰) suggesting the importance of high saline waters transported from northern Arabian Sea by the southerly flow during southwest monsoon. Below 300 cl/t the T-S plots shows variation mostly resulted from nearshore and offshore stations. The nearshore stations showed lower salinity while the offshore stations showed relatively higher salinities with depth, particularly during summer as the subsurface undercurrent carries warm less saltier waters northward near the continental slope region.

The T-S characteristics above 500 cl/t is of uniform temperature (28°C) and rapidly changing salinity with depth, during winter at all other three locations. These waters are seen during February-March off Mangalore (Fig.4.9), December-January-February off Cochin (Fig.4.10) and during November-December off Cape (Fig.4.11). This is the period of sinking off the west coast of India (Sharma,1968; Darbyshire,1967). This low salinity water at the surface layers is termed as Equatorial Indian Ocean Water, with the low salinities at the surface due to inflow of Equatorial Water. However, T-S analysis during winter never showed such low salinities in the equatorial region (Eriksen,1979) which

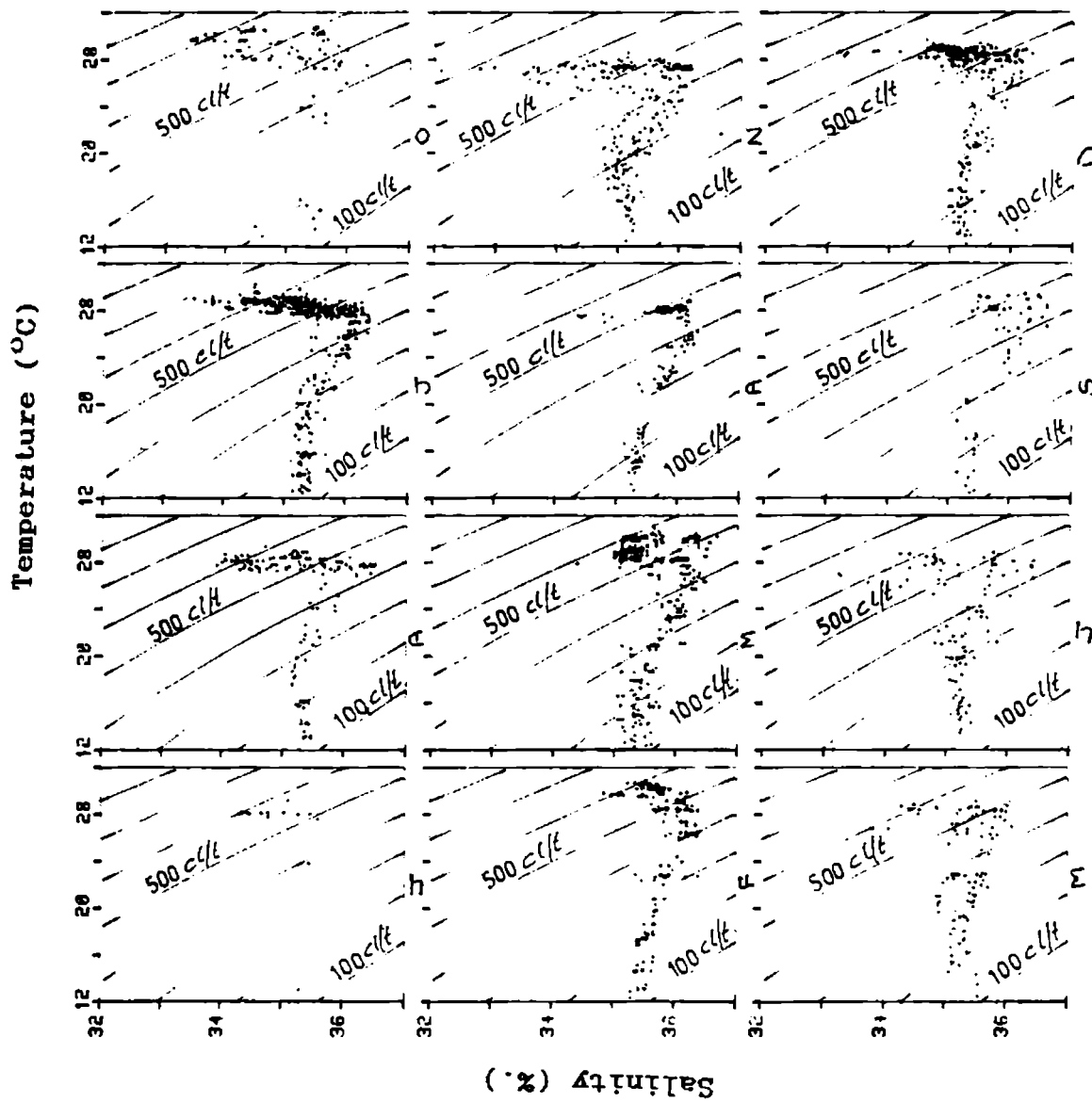


Fig. 4.9. Monthly composite T-S diagrams covering all stations off Mangalore

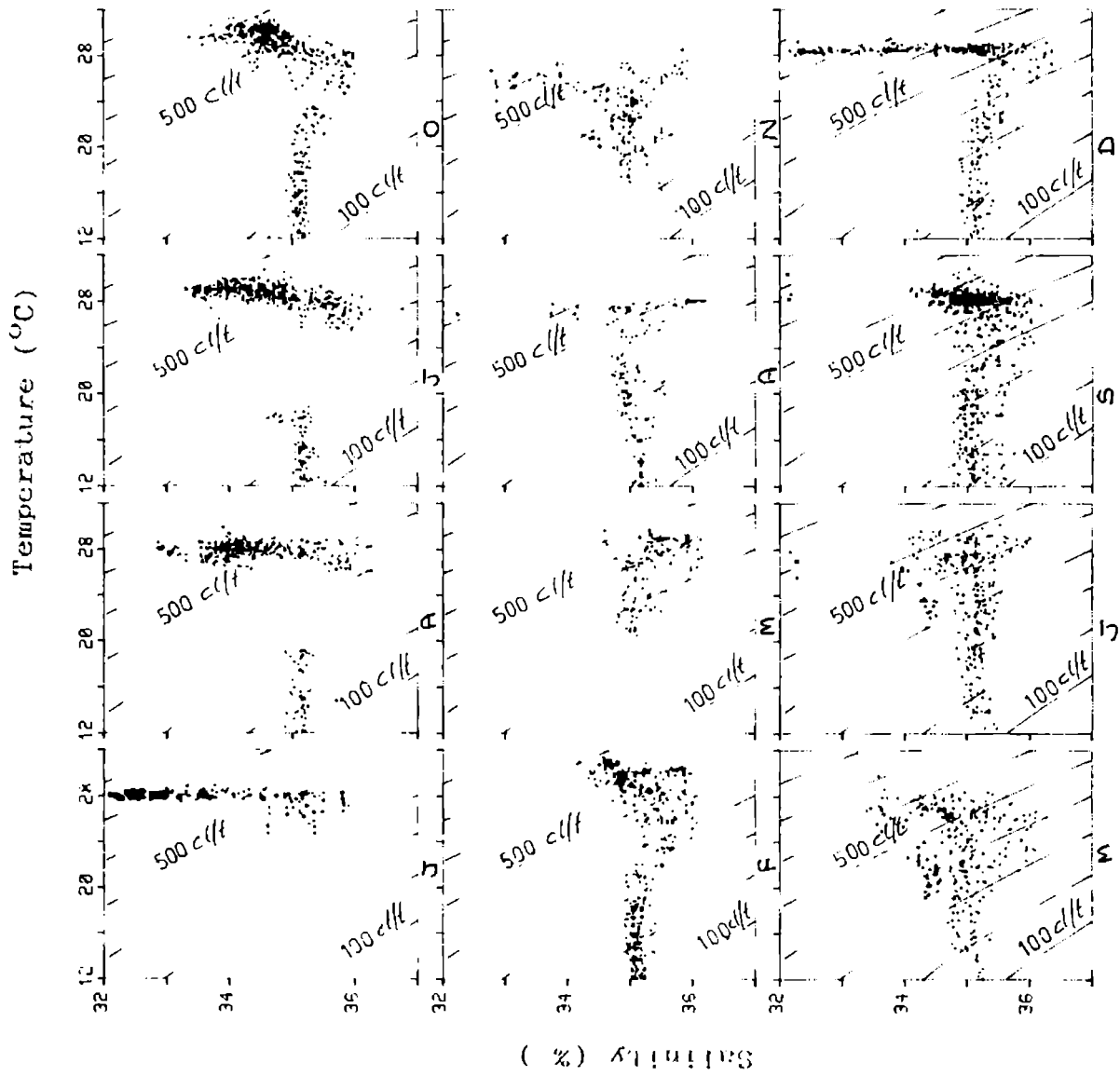


Fig.4.10. Monthly composite T-S diagrams covering all stations off Cochin

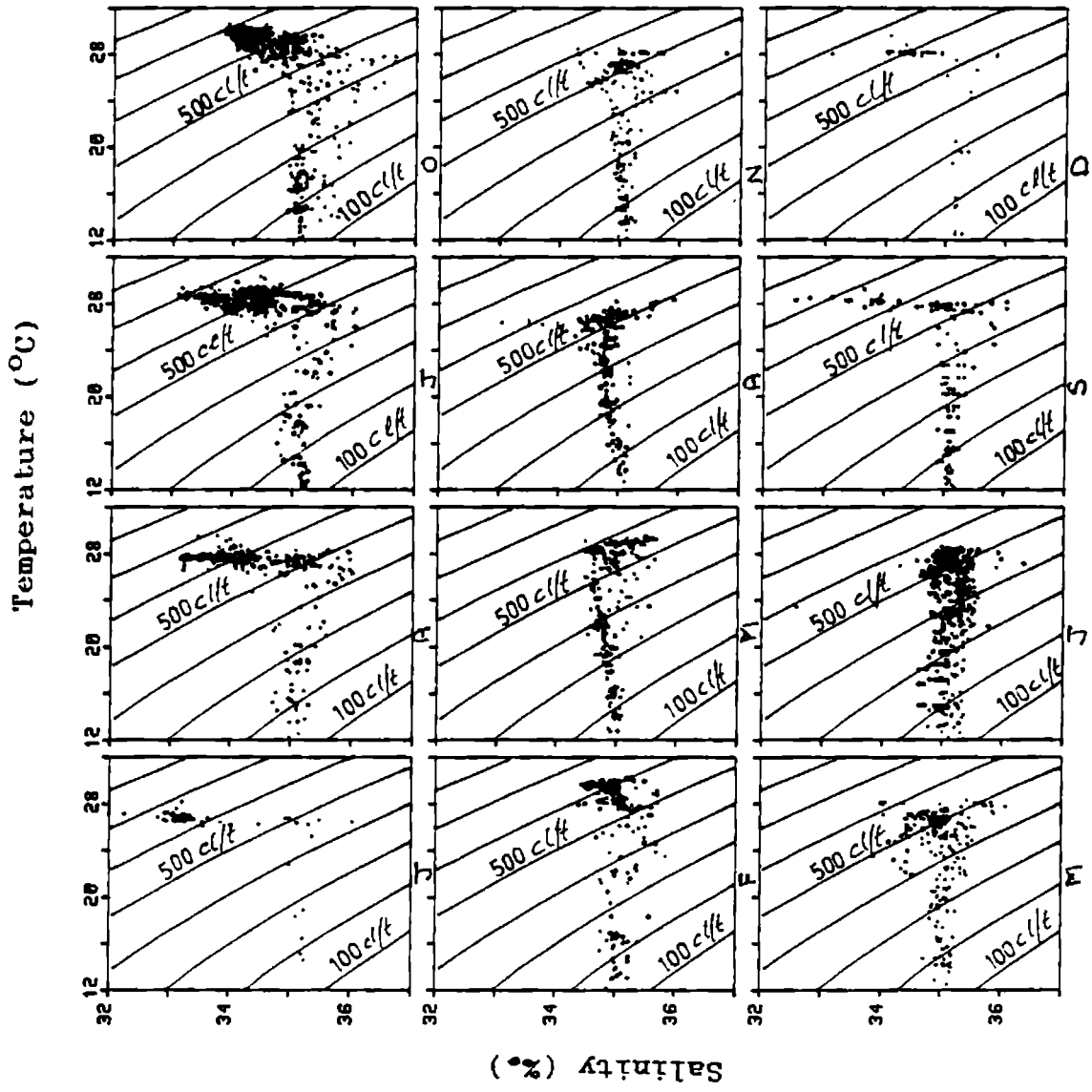


Fig. 4.11. Monthly composite T-S diagrams covering all stations off Cape

exceeded 34%. Observations showed salinities as low as 32-33% during winter especially off Kerala Coast (Darbyshire, 1967; Johannessen et al, 1984). Since such low saline waters are seen only in the Bay of Bengal (Wyrtki, 1971), it is more appropriate to be termed as Bay of Bengal Water (above 500 cl/t). The effect of these waters are observed up to 50m depth. The surface layers also show low saline waters during July-October especially off Mangalore and Cochin due to freshwater inputs confined very close to surface. However, these low salinity waters are absent off Cape due to relatively low rainfall in the southern tip off India. The higher surface layer salinity observed during May-June both off Mangalore and Cochin due to the presence of high saline Arabian Sea Water carried by the southerly flow which results in the retreat of low saline Bay of Bengal waters. The high saline waters slightly above 400 cl/t is obviously related to ASHSW with maximum core value >36% off Mangalore and minimum core value off Cape. Below 400 cl/t the temperature decreases with depth while salinity remain more or less constant upto 200m. It can be noted that the waters are highly heterogeneous off Cochin particularly during August-October. This could be related to large nearshore-offshore difference in thermocline characteristics due to coastal upwelling and presence of different water types, such as ASHSW, freshwater fluxes, Bay of Bengal/Equatorial waters carried by poleward undercurrent etc..

4.7 Northward undercurrent off the west coast of India during upwelling season

Along the eastern boundaries of the oceans a poleward undercurrent has been identified as a component of the coastal circulation system during upwelling (Yoshida and Tsuchiya, 1957). Associated with the offshore Ekman transport

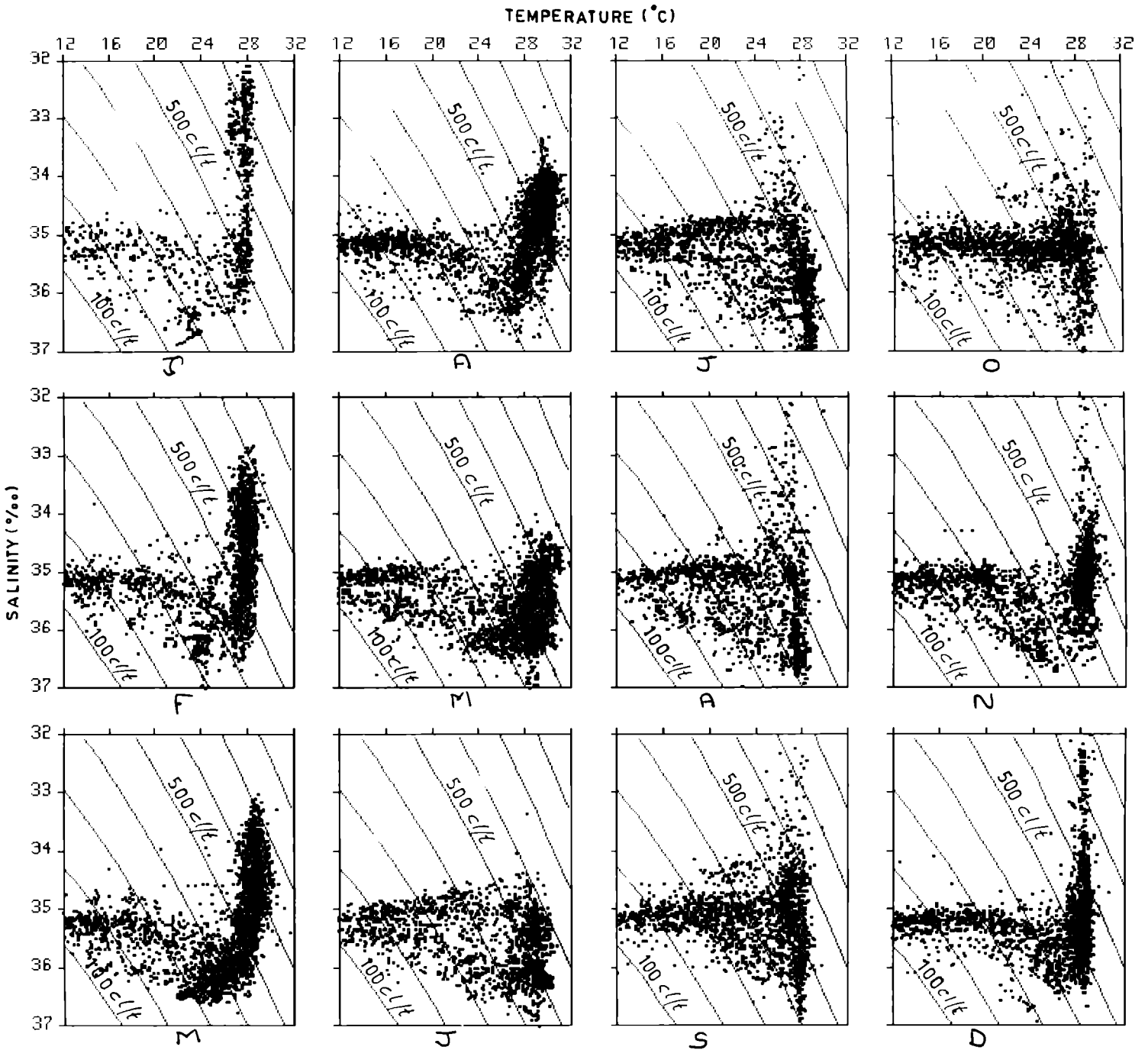


FIG 4.7 MONTHLY COMPOSITE T-S PLOTS COVERING ALL THE STATIONS OFF THE WEST COAST OF INDIA

a surface equatorward flow and poleward undercurrent that decays offshore is noticed. Earlier inferences on the undercurrent was made mainly from the downward slope of isopycnals towards the coast below the surface layers and subsequently direct current measurements confined its presence in all upwelling regions (Hart and Currie, 1960; Wooster and Gilmartin, 1961; Wooster and Reid, 1963; Wooster and Jones, 1970; Huyer and Smith, 1976). As no direct current measurements are available off the west coast of India to identify the northward undercurrent during upwelling, inferences are made from the tilt of isotherms and water characteristics (Mathew, 1983; Antony, 1990; Shetye et al, 1990).

The vertical section of temperature and salinity during the upwelling period does not show any noticeable downward tilt of isotherms towards coast in the subsurface layers off Ratnagiri (below 100m) except in December (Figs.4.3). Probably the Angria bank - a subsurface submerged island may be responsible for modifying the subsurface circulation. However significant downward tilt of isotherms in the subsurface layers is noticed both off Mangalore (Figs.4.4) and Cochin (Figs.4.5) from May to October indicating the presence of a northward undercurrent at the shelf edge/continental slope. The relative position of this undercurrent, though varies slightly from month to month is between 80-150m off both locations. Similar features, though not very conspicuous can also be noticed off Cape Comorin in June and August.

The salinity near the shelf edge at the depth of the subsurface northward flow shows a reduction from offshore to near shore. Near the shelf edge/slope a salinity minima is noticed between 80-150 m at all locations, except off Ratnagiri during summer monsoon (Antony, 1990). However, the core values of this relative salinity minima increased from

south to north. The temperature of water within the undercurrent varies between 18° to 20°C (Antony,1990) while its salinity varies from 34.95‰ off cape Comorin to 35.2‰ off Mangalore in June which also decreased to below 35‰ by October. The waters are in general warmer and less saltier compared to those waters offshore at the same depth. The relatively low salinity of the waters within the undercurrent region is due to its origin near the equatorial region which is typically low saline (Wyrтки,1971). The salinity in the undercurrent region is greater than 35.1‰ during May and June which decreases with the progress of monsoon to about 34.95‰ by September-October both off Cochin and Mangalore suggesting a reduction of salinity in this zone with the progress of monsoon. The vertical sections (Figs.4.3-4.6) shows that the low saline water carried by undercurrent lies below the ASHSW.

The depth of the undercurrent off west coast of India is consistent with those of other upwelling regions such as off California, Peru, southwest Africa etc (Wooster and Gilmartin,1961; Antony,1990). However, the waters carried by the undercurrent in other upwelling regions is characterised by higher salinity where as relatively low salinity waters are carried by the undercurrent off west coast of India. This is attributed to the source of this waters carried by the undercurrent, the Bay of Bengal/equatorial Indian Ocean, which are typically low saline (Wyrтки,1971).waters originate from Bay of Bengal/equatorial Indian Ocean which are typically low saline.

From the tilt of isotherms, it appears that the undercurrent is relatively weak. Due to lack of direct measurements and the limitations of the geostrophic approximation near the coast it is extremely difficult to quantify the speed of the undercurrent. In general the

undercurrent associated with upwelling is relatively weak with speeds ranging from 5-10 cm/s (Wooster and Gilmartin, 1961). As the process of upwelling off west coast of India itself is weaker than those of major upwelling regions the undercurrent also could be weaker (Antony, 1990). The downward tilt of isotherms towards the coast also reduces from Cochin (Fig.4.5) to Ratnagiri (Fig.4.3) which could be due to weakening of undercurrent towards north. Theoretical studies (McCreary and Chao, 1985) have shown that the shelf tends to slow down the undercurrent as the shelf induces a baroclinic component towards equator. The increasing width of shelf towards north also could weaken the undercurrent towards north (Antony, 1990).

4.8 Upwelling and Sinking off the west coast of India

The thermohaline field at different locations off the west coast of India shows significant period of ascending and descending motions (upwelling and sinking). Obviously the duration and intensity of these processes considerably vary from south to north and also in the time domain. The upward motion at subsurface levels (around 150m) starts around March-April off Cape (Fig.4.2d), Cochin (Fig.4.2c) and Mangalore (Fig.4.2b) and by May off Ratnagiri (Fig.4.2a), though heating continues in the surface layers. The thermocline reaches the surface layers by June (Banse, 1968) except off Ratnagiri. The coldest waters at the surface (maximum effect of upwelling) are observed in July off Cape, August off Cochin, September/October off Mangalore. There is not much surface temperature drop off Ratnagiri due to upwelling though the thermocline is very close to surface especially during November-December. Sinking starts by September off Cape, October-November off Cochin and November-December off Mangalore. Compared to upwelling, sinking appears to be a very rapid process and the thermal

structure is characterised by deep mixed layers in November-December off southwest coast of India, while such features are observed only after February off Ratnagiri. This perhaps suggest upwelling and sinking starts early at the south and gradually extends towards north (Sharma,1968;1978).

From the vertical sections it is obvious that from about 100m in February the 24°C isotherm reaches the surface off Cape Comorin in July, while the corresponding change off Mangalore is about 110m (between February and October). The 22°C isotherm shows a upward movement of about 130m between February and August off Cochin, while the 25°C isotherm exhibits upward movement of 100m between March and December. This suggest an average vertical movement of about 20m per month off the southwest coast of India, while it is of the order of about 10-12m per month off Ratnagiri. However, the upward movement of isotherms could be of the order of 30m per month off the southwest coast of India especially between May and June (Mathew,1983). Compared to upwelling, sinking is rapid with downward movement of 24°C isotherms by over 40m and 100m between November and December off Cape and Cochin respectively. The corresponding change is about 150m off Mangalore between November and December near the coast and about 100m off Ratnagiri during the same period. This suggest that the speed of sinking is about 3 to 5 times higher than that of upwelling off the southwest coast of India.

There has been considerable difference of opinion regarding the mechanism which induces upwelling and sinking off the west coast of India. Darbyshire (1967), Banse (1968) and Sharma (1968;1978) considered the upwelling off the southwest coast of India as current induced as it occur during southwest monsoon. However, Ramamirtham and Jayaramam (1960) pointed out the possible role of wind induced upwelling off

the southwest coast of India as they noticed westerly or northwesterly winds near the coast during summer monsoon. The possible occurrence of wind induced upwelling during summer monsoon off the southwest coast of India (as in any other eastern boundary upwelling system) has been discussed by Mathew (1983), Shetye (1984), Shetye et al (1990).

It is the equatorial component of wind stress along the eastern boundaries which produces offshore Ekman transport and hence upwelling (Pickard and Emery, 1982). The monthly mean equatorward and shoreward component of wind stress for the 1° latitude/longitude off Cape, Cochin, Mangalore and Ratnagiri are computed (Fig.4.12) to understand the possible relationship of wind and vertical motion in these regions.

4.9 Role of surface winds

In order to understand the possible role of winds on the process of upwelling and sinking at different parts of the west coast of India, the surface wind stress parallel and perpendicular to the coast for each month is computed (Figs.4.12). The monthly wind data averaged over each 1° latitude/longitude off Cape Comorin, Cochin, Mangalore and Ratnagiri are utilised for this study. It is well known that equatorward component of wind stress induces upwelling along the eastern boundaries of the oceans while poleward component of wind stress induces sinking.

The wind stress parallel to the coast shows an equatorward component throughout the year of Cape, Cochin and Mangalore while it is poleward off Ratanagiri during July/August (Fig.4.12). Theoretically (McCreary, 1981) the local wind field is conducive to upwelling during all months along the southwest coast of India. However, the magnitude of

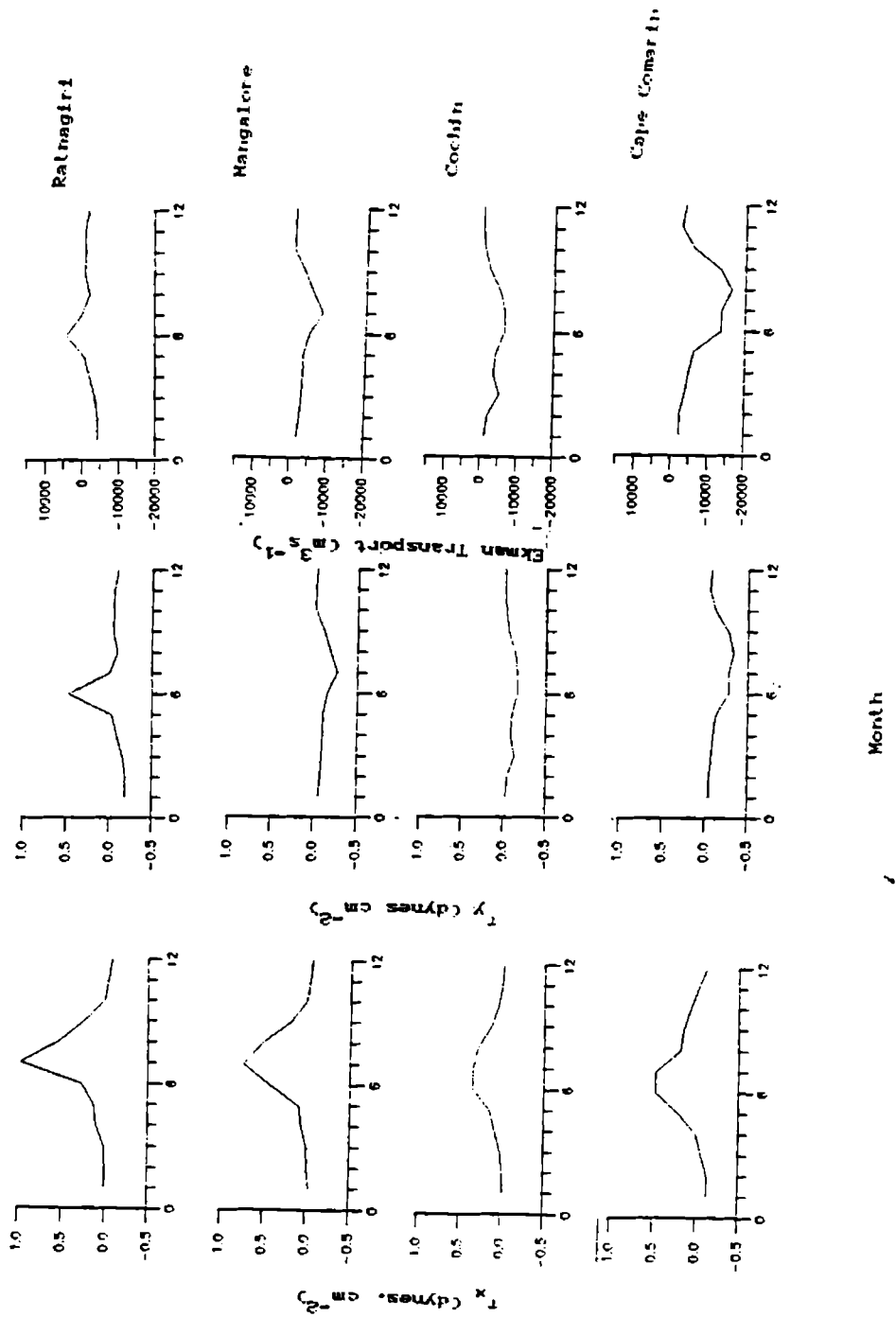


Fig 4.12. Mean monthly variation of wind stress (a) perpendicular
 (b) parallel to the coast and (c) Ekman transport

this wind stress is too small except during southwest monsoon, when it exceeded -0.3 off Cape, -0.16 off Cochin and -0.17 ^{dynes/cm²} off Mangalore.

Theoretical studies of wind driven eastern boundary currents have shown that the intensity of upwelling and surface transport are proportional to the offshore Ekman transport (τ_l/f , where τ_l is wind stress component parallel to the coast and f is the coriolis parameter). Even for the same τ_l the Ekman transport is much higher near the equator compared to higher latitude. The Ekman transport is maximum off Cape Comorin especially during June-July-August with values exceeding 2.5×10^4 m³/s. The maximum offshore Ekman transport occurs during summer monsoon off Cochin and Mangalore with values of the order of 1.5×10^4 m³/s and 2.4×10^4 m³/s respectively. However, the Ekman transport is onshore during July-August off Ratnagiri.

It is well known that the monsoonal winds blow in pulses, with high wind speed ($>10\text{m.s}^{-1}$) for few days followed by few days of weak winds. The strong winds of short durations can produce 'upwelling events' (Huyer,1976), when the offshore transport can be at least five to ten times higher than the monthly mean values. During the summer monsoon of 1987, the average wind speed off the west coast of India was of the order of 8 m.s^{-1} (Shetye et al,1990) which is also much higher than the monthly mean values. The possible occurrence of 'upwelling events' associated with periods of strong winds ($>10 \text{ m.s}^{-1}$) during summer monsoon need to be investigated. The northward decrease of offshore Ekman transport and even onshore Ekman transport off Ratnagiri during summer monsoon explains the relative decrease of upwelling intensity towards north (Mathew,1983).

Though there is offshore Ekman transport off the west coast of India in all months, it is too weak to induce significant vertical motion except during summer monsoon. However, surprisingly sinking occurs in this region during November-February, with the surface flow turns towards north (Wyrtki, 1971; Rao et al, 1991). This northerly flow is opposite to wind direction and is driven by nearshore-offshore density gradient (Sheye^u, 1984). The reasons for the onshore-offshore density gradient (Mathew, 1983) is not clearly known and could be related to the large scale general circulation in the northern Indian Ocean. Perhaps the northerly flow in winter off the west coast of India and the Leeuwin Current off the west coast of Australia (Godfrey and Ridgway, 1985) are unique in many respects since both currents are against the local winds.

From the vertical sections it is obvious that upward motion in deeper layers start by March-April off southwest coast of India, eventhough the offshore Ekman transport is weak. It is interesting to note that the surface currents in this regions reverse to southerly in February-March (Fig.1.2). The upward motion in deeper layers (150m) is difficult to explain, since the winds are weak and variable during this period. It appears that the surface current reversal during February-March is related to the large scale circulation system and the thermal response in the deeper layers could be forced by internal ocean dynamics rather than by local winds. Similarly the process of sinking occur when offshore Ekman transport continues and occur very rapidly with the reversal in surface flow. It needs a very detailed study^u to identify the causes of surface current reversal in this region as it appears that they are not related to the local wind system.

4.10 Role of surface currents

Besides wind, coastal currents can also be forced by a longshore density gradient imposed at the surface. In the northern hemisphere if the surface density increases (decreases) towards north the resulting current is northward (southward). The wind driven and thermohaline driven components of the current at the surface can be made by comparing

$$F_w = \frac{1}{2} \tau_l \quad \text{with} \quad F_T = \frac{g}{\rho} H^2 \Delta$$

where F_w represents the wind-driven component and F_T the thermohaline driven contribution of current (Pedlosky, 1974), τ_l, g, H and Δ are longshore wind stress, acceleration due to gravity, mean depth of the shelf and longshore surface density gradient respectively.

Between November-March τ_l is weak though equatorward while the the surface flow is northward. The data sets shows mean surface density gradient along the west coast of India is $2.2 \times 10^{-11} \text{ gm.cm}^{-3}$ during this period, while it is $-0.8 \times 10^{-11} \text{ gm.cm}^{-3}$ during May-October. Obviously the flow during November-March is driven by thermohaline gradients. while during summer monsoon the effects of both wind and thermohaline field supports a southward flow. During August F_w represents wind forcing of $0.25 \text{ dynes.cm}^{-2}$ (Shetye, 1984). This suggests that the surface current also may have some influence on the upwelling off the west coast of India particularly north of Mangalore. However, south of Mangalore upwelling during southwest monsoon is mostly wind driven as in all classical upwelling systems during summer monsoons.

The analysis suggest few important inferences. During summer monsoon, the upwelling off the southwest coast of India is mainly wind-driven as in any other eastern boundary upwelling system with a poleward undercurrent between 80-150m depth. The surface current also is favourable for upwelling though its influence could be limited. However, north of about 15°N , the upwelling during southwest monsoon is current driven as the wind is not favourable to produce offshore Ekman transport. Wind driven upwelling occur off Ratnagiri during November-December, though the intensity of upwelling is much less compared to that off the southwest coast of India. Against the local southerly winds, the surface flow turns northerly during winter obviously driven by the thermohaline field. During this period, sinking is noticed off the west coast of India. Upwelling and sinking starts early in the south and extends towards north which is consistent with the local wind and current field. It is not clear why the surface current turns to southerly off the southwest coast of India as early as in February-March. However, this seems to have a profound influence on the subsurface thermal structure as upward movement of isotherms in the deeper layers starts during this period, though the wind field is very weak. Hence it is inferred that the onset of upwelling is related to the reversal of current off the west coast of India. However, the upwelling off the southwest coast of India during summer monsoon is mainly wind driven, while it is current driven off Ratnagiri. Wind driven upwelling is noticed off Ratnagiri during November-December with evidence of a poleward undercurrent in the subsurface layers.

CHAPTER V

NUMERICAL SIMULATION OF MIXED LAYER CHARACTERISTICS DURING
PRE- AND POST- ONSET REGIMES OF SUMMER MONSOON

5.1 Introduction

Advance knowledge on the upper ocean thermal structure has immense application on various activities like ocean thermal energy conversion, long range weather and climate prediction, fisheries exploitation, anti-submarine warfare operation etc. The work of Bryan (1969) on long range weather prediction indicate that the climate and its fluctuations are profoundly influenced by the interaction between the ocean and atmosphere on a variety of space-time scales. However, most of the atmospheric processes are found to occur over a time scale of 1-5 days (Denman, 1973) and hence an accurate and reliable knowledge of the upper ocean thermal structure is very much required on a synoptic scale. Even on a diurnal scale, the temperature of the ocean shows marked variability over a few hundred of kilometers. With the advent of satellites, the sea surface temperature (SST) can be routinely monitored over a large area. But the corresponding information on the variability of the subsurface thermal structure is quite meagre, as the satellites provide information mainly on surface features only. In the absence of adequate in situ measurements, numerical models can provide valuable information on the subsurface thermal structure derived from routine measurements of atmospheric parameters (in conjunction with SST).

Several attempts on one-dimensional numerical modeling of the mixed layer characteristics are available in the literature with time scales ranging from diurnal to seasonal scales (Kraus and Turner, 1967; Denman, 1973; Pollard et al, 1973; Mellor and Durbin, 1975; Miller, 1976; Thompson, 1976, Niiler and Kraus, 1977, Price et al, 1986). However, most of these studies are limited to Pacific and Atlantic Oceans where

long time series measurements of temperature profiles and surface meteorological elements are made from weather ship stations.

The simulation of mixed layer characteristics on short time scale in the Arabian Sea during pre-onset and active phase of the monsoon are limited due to lack of adequate data. Rao (1986) and Rao and Mathew (1990) evaluated Miller's (1976) model - a modified version of Kraus and Turner (1967) and Denman (1973) models - to simulate the cooling and deepening of the mixed layer at selected locations in the central Arabian Sea during the onset phase of the monsoon. The simulation of mixed layer temperature (MLT) and depth (MLD) at a station in the western equatorial Arabian Sea by Joseph et al (1990) utilising the model of Miller (1976) showed reasonably good agreement with the observations when the effect of lateral advection is included. In these studies model simulations were carried out by tuning the coefficients γ (extinction coefficient) and m (fraction of wind energy used for mixing) to get the best result. Studies of Denman and Miyake (1973), Rao and Mathew (1990) and Rao et al (1991) revealed that the model of Miller (1976) is in general suitable for the simulation of the mixed layer characteristics on a synoptic scale when one dimensional processes are dominant. Hence in this chapter the one-dimensional numerical model of Miller (1976), the modified version of Kraus and Turner (1967) and Denman (1973) is used to simulate the mixed layer characteristics at selected locations in the Arabian Sea for short durations corresponding to pre- and active phases of the summer monsoon utilising the extinction coefficient, γ derived from secchi disc measurements.

5.2 Observations

The major part of the data sets utilised in this study correspond to open ocean conditions of the Arabian Sea during MONSOON-77 and MONEK-79 field experimental programmes (April/May and June/July). In addition, data sets collected in the coastal waters off Bombay and off Karwar during June/July (occupied by RV Gaveshani) are also utilised. The first period, April/May, represents pre-onset regime of the southwest monsoon and the second period, June/July, represents active regime of the southwest monsoon. The station locations shown in Fig.5.1 are designated as N77, E77, S77, W77, N79, E79, S79 and W79 corresponding to the four corners of the USSR polygon during 1977 and 1979 respectively and DK79 and DP79 corresponding to Indian ship locations during MONEK-79 and B88 and K89 corresponding to the coastal stations off Bombay and off Karwar respectively. The station locations, observational periods and the station symbols used are presented in Table 5.1. Hourly surface marine meteorological data (solar radiation, albedo, wind speed and direction, visually observed cloud, atmospheric pressure, air temperature, wet bulb/dew point temperature) and vertical profiles of temperature and salinity were collected from these locations. Wherever direct solar radiation measurements are not available, hourly incoming radiation is computed following Lumb (1964). Details of the computational procedures of effective back radiation, sensible and latent heat flux are already discussed in chapter 3.

5.2.1 Surface meteorology and heat budget

The pre-monsoon season is generally characterised by fair weather conditions resulting in net heat gain to the ocean causing shallow and warm mixed layer. However, the

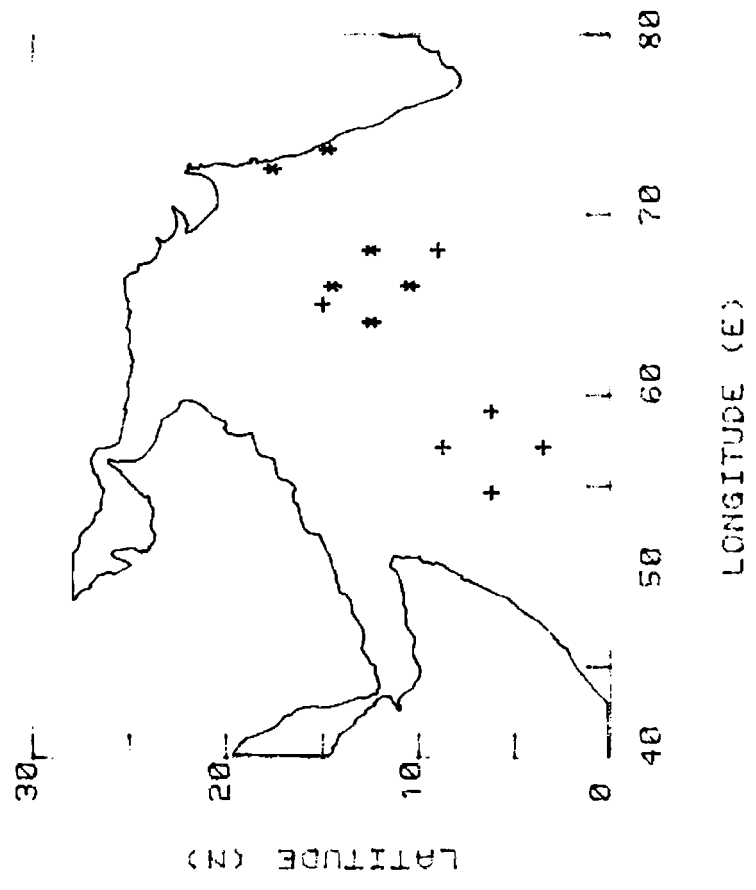


FIG.5.1. Station Location Map

- + Pre-onset phase
- * Active phase

surface meteorological conditions at different locations during this period considerably varied in space and time (Fig.5.2). In general, all the locations experienced high atmospheric pressure (PR), low wind speed (FF) and low cloud amount (CL). Barring few days all the locations received surplus of heat (Q). However, on days when the wind speed exceeded 8 m.s^{-1} , net heat loss was noticed at N79, E79, S79 and W79. At DK79 and DP79, the wind speed was less than 5 m.s^{-1} throughout the observational period and substantial heat gain was noticed on all days. During this period there was an average heat gain of 120.2, 67.5, 76.5, 100.9, 57.3, 125.6 and 169.2 W.m^{-2} at N79, E79, S79, W79, DK79 and DP79 respectively. In contrast to the pre- monsoon period, active monsoon period is characterised by higher wind speed (in general $>10 \text{ m.s}^{-1}$), overcast skies and low atmospheric pressure especially in the central Arabian Sea (N77, E77, S77 and W77) (Fig.5.3a&b). Except on days when the wind speed was less than 8 m.s^{-1} , the ocean lost heat to the atmosphere which was much larger during the onset regimes (7-20 June, 1977) with the average heat loss at N77, E77, S77 and W77 was -229.4, -262.3, -222.4 and -285.3 W.m^{-2} (Fig.5.3a&b) and SST dropped by 1.3°C , 1.32°C , 0.98°C and 1.14°C (Fig.5.3a&b) respectively. However, during active phase (30 June-15 July, 1977), at all locations the net heat loss by the ocean was not comparable to the onset phase. During this period the average rate of heat loss at N77, E77, S77 and W77 was of the order of -149.6, -152.6, -56.8 and -132.7 W.m^{-2} and the corresponding change in SST was 0.36°C , 0.22°C , 0.6°C and 0.5°C .

Contrary to the drastic heat loss in the central Arabian Sea, the coastal waters off Bombay and Karwar shows an average heat gain of 11.8 and 41.3 W.m^{-2} and a SST change of 0.08°C and 0.18°C .

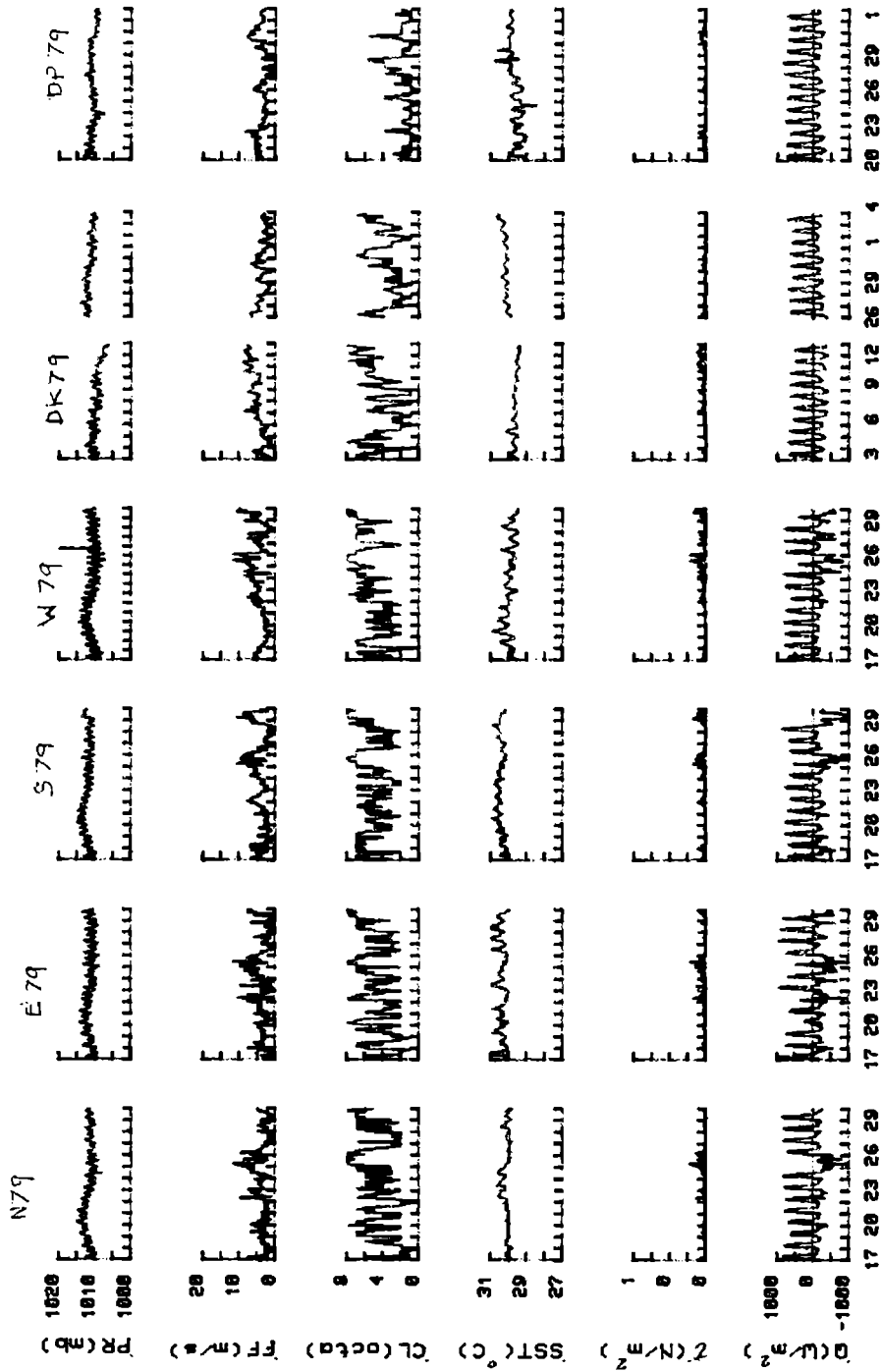


Fig-5.2. Atmospheric pressure (PR), wind speed (FF), cloud cover (CL), sea surface temperature (SST), wind stress (τ) and net surface heat flux (Q) for the pre-onset phase at selected locations in the Arabian Sea

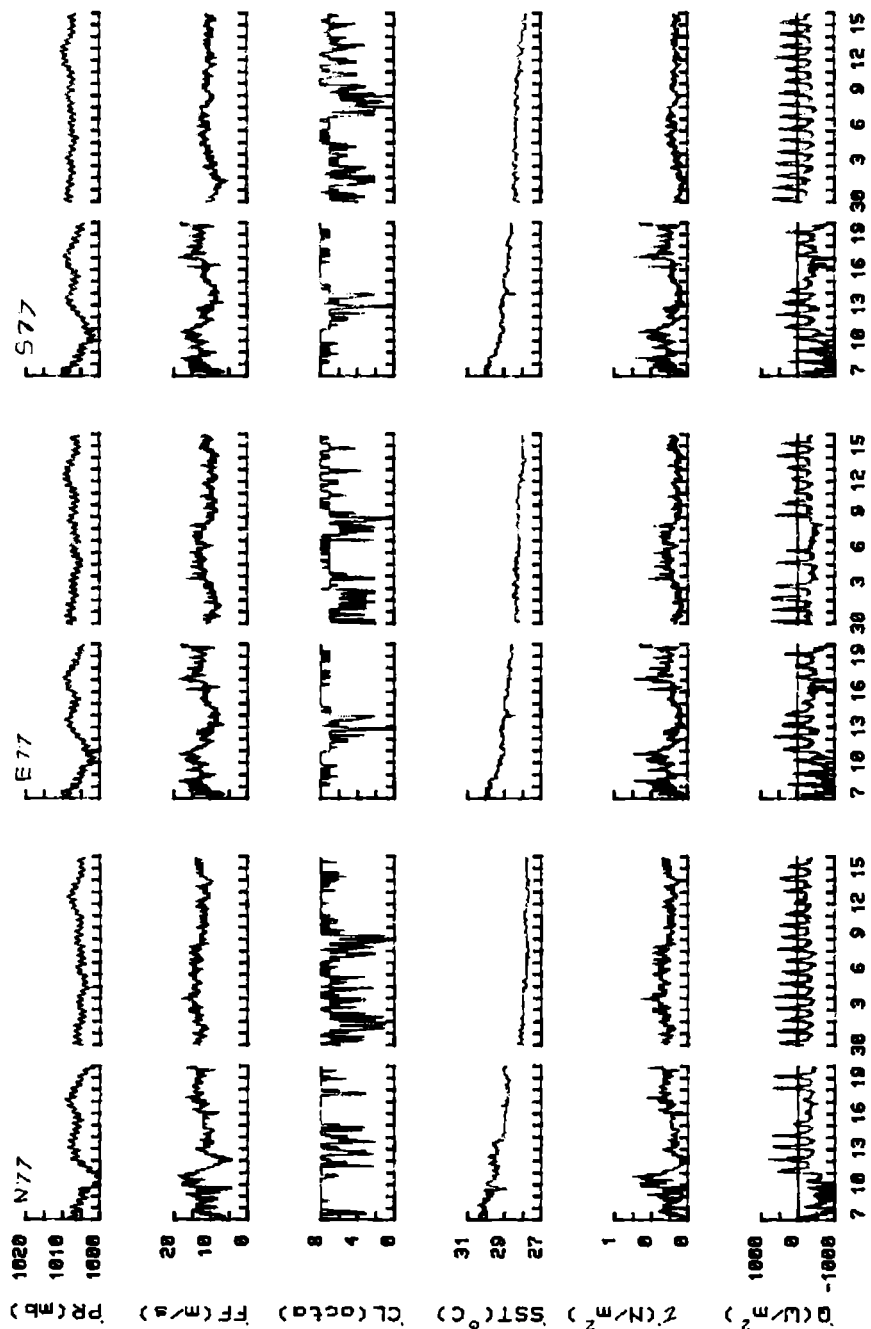


Fig.5.3 Atmospheric pressure (PR), wind speed (FF), cloud cover (CL), sea surface temperature (SST), wind stress (τ) and net surface heat flux (Q) for the active phase at selected locations in the Arabian sea

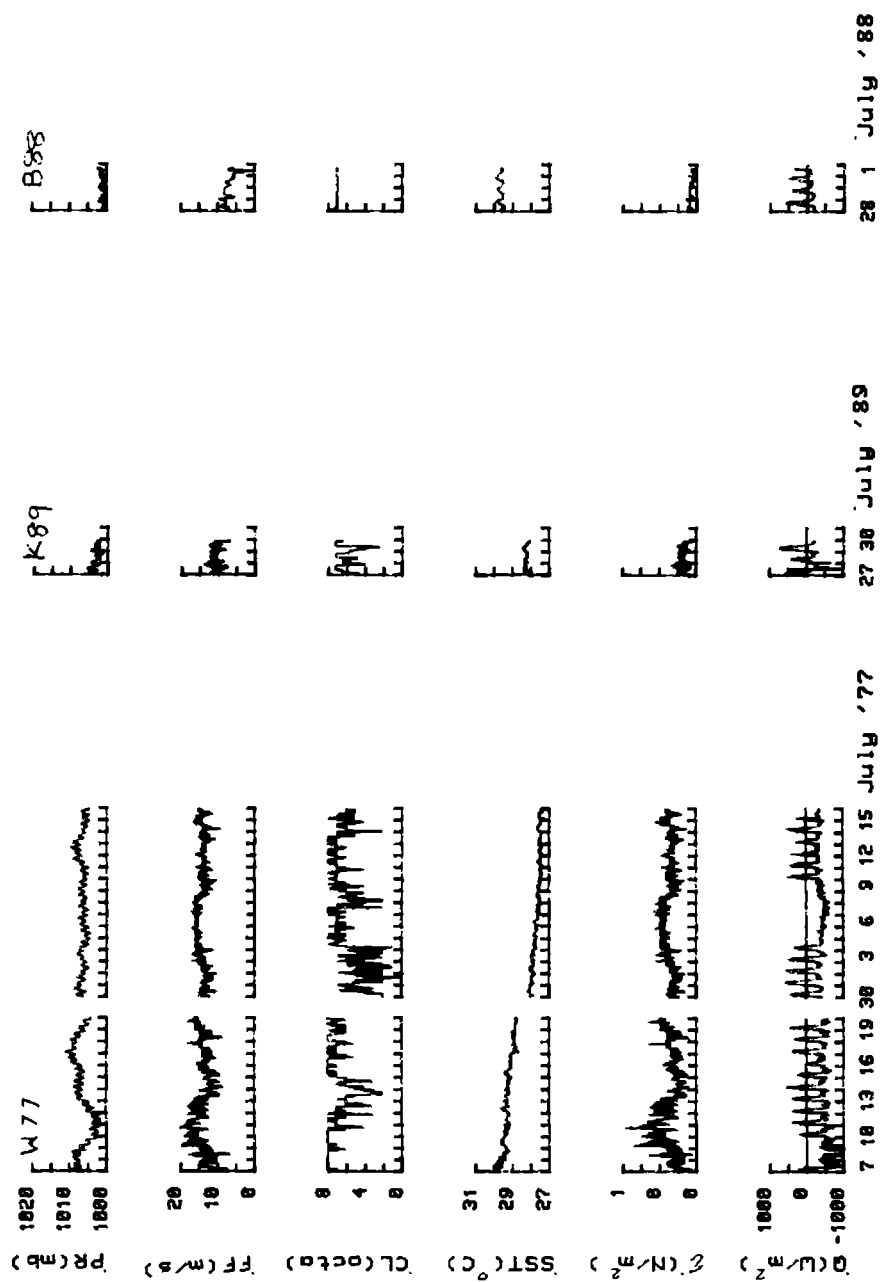


Fig.5.36 Atmospheric pressure (PR), wind speed (ff), cloud cover (CL), sea surface temperature (SST), wind stress (Z) and net heat flux (Q) for the active phase at selected locations in the Arabian Sea

5.3 Modelling of the mixed layer characteristics

It is well known that during surface heating and under light wind conditions, the mixed layer shoals and its temperature increases. Under strong winds, even if there is net heating, the surface layer thickness increases and its temperature decreases. These changes are caused by the turbulent entrainment of colder and denser water into the mixed layer from below. The net surface cooling can also deepen the mixed layer through convective overturning.

5.3.1 Assumptions

The ocean is assumed to be horizontally homogeneous, incompressible and stably stratified fluid (Boussinesq approximation). The 'wave' like dynamical effects such as gravitational, inertial and Rossby waves are ignored. The surface mixed layer is considered to be vertically homogeneous down to a level 'h' with a density discontinuity at the base (Fig.5.4). All the heat and momentum are uniformly distributed throughout this layer by turbulent diffusion. The time scales for the distribution of these properties are small compared to the times over which the processes of interest are assumed to occur. Below the surface layer, a stable density profile is specified at $z=-h$.

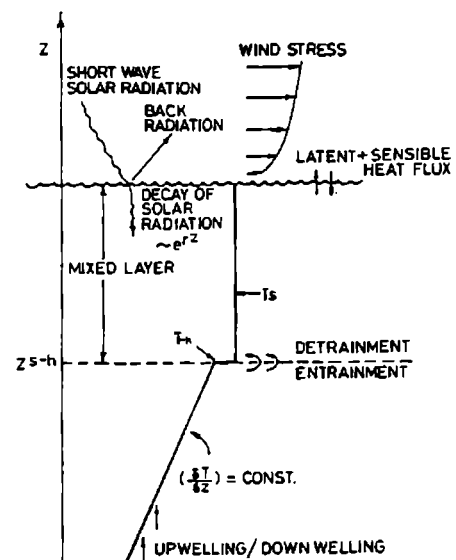


Fig. 5.4

The time dependent behaviour of the mixed layer at a stationary position is formulated from a set of differential equations derived based on conservation equations of thermal energy, salinity and mechanical energy with appropriate boundary conditions. In the final equations, time derivatives of h (mixed layer depth), T (mixed layer temperature), S (mixed layer salinity), T_{-h} (temperature immediately below the mixed layer) and S_{-h} (salinity immediately below the mixed layer) are expressed in terms of the time-dependant boundary inputs, like wind stress, incoming solar radiation, net heat loss at the surface and the temperature and salinity (or density) gradient below the mixed layer.

5.3.2 Boundary conditions

i) At the upper boundary

At the top of the surface layer, the turbulent heat flux must be equal to the net heat transfer through the ocean surface and that of salinity is equal to the fresh water times the surface salinity.

ii) At the mixed layer base

The effect of diffusion across the stable interface at the bottom of the mixed layer is neglected and all the mixing processes are associated with the entrainment of the denser water into the mixed layer.

iii) At the lower boundary

In order to specify the system completely, the temperature gradient below the mixed layer should be known. The assumptions made here are (a) no turbulent energy

penetrates below $z=-h$ and (b) the local surface influence acting on the ocean at $z < -h$ is a small fraction of solar radiation which penetrates to that depth.

5.3.3 Integral equations of the mixed layer

To obtain explicit expressions for the characteristics of the mixed layer, the equations for the conservation of thermal energy, salinity and mechanical energy have to be integrated over the mixed layer depth. The simplified one dimensional equations used in the mixed layer simulations are (Miller, 1976)

$$\frac{dh}{dt} \frac{2[G-D + \gamma^{-1} Q_I (1-e^{-\gamma h})] - h[Q_B + Q_E + Q_H + Q_I (1+e^{-\gamma h}) + \frac{\lambda}{\alpha} S(P-E)]}{h[T-T_h + \frac{\lambda}{\alpha} (S-S_h)]} \quad (5.1)$$

$$\frac{dT}{dt} = \frac{1}{h} \left[- \frac{dh}{dt} (T-T_h) + Q_B + Q_E + Q_H + Q_I (1-e^{-\gamma h}) \right] \quad (5.2)$$

$$\frac{dS}{dt} = \frac{1}{h} \left[- \frac{dh}{dt} (S-S_h) + S(P-E) \right] \quad (5.3)$$

$$\frac{dT_{-h}}{dt} = \gamma Q_I e^{-\gamma h} - \frac{dh}{dt} \left(\frac{\partial T}{\partial z} \right)_{-h} \quad (5.4)$$

$$\frac{dS_{-h}}{dt} = - \frac{dh}{dt} \left(\frac{\partial S}{\partial z} \right)_{-h} \quad (5.5)$$

where dh/dt is the rate of mixed layer deepening; $G-D$, fraction of the turbulent energy derived from wind ($-m\tau U/\alpha\rho g$); m , fraction of energy transferred from wind; τ , wind stress; g , acceleration due to gravity; ρ , mean density of mixed

layer; γ , extinction coefficient; Q_I , solar radiation incident on the sea surface; h , depth of mixed layer; Q_B , effective back radiation; Q_E , latent heat flux, Q_H , sensible heat flux; λ , coefficient of thermal expansion; α , coefficient of saline contraction; P , precipitation and E , evaporation.

For the wind dominated regime ($dh/dt > 0$), the cold water from below the mixed layer is entrained into the mixed layer as a result of work done by the turbulent eddies against the buoyancy forces. Then the layer deepens and its temperature decreases. In such cases, the equations 5.1-5.5 were solved using the Runge-kutta numerical integration scheme with a time step of 5 minutes.

For the heat dominated regime ($dh/dt < 0$), the entrainment mixing at the base of the mixed layer does not appear in the equations. Hence, all the available turbulent kinetic energy is used in mixing the lighter water near the surface uniformly and leaves the mixed layer unchanged or a shallow layer will develop under light winds. In such cases, terms involving the below layer density gradient loses its significance and 'h' is determined using Newton's iterative technique.

$$h = \frac{2(G-D + Q_I \gamma e^{-\gamma h})}{(Q_I (1 + e^{-\gamma h}) + Q_B + Q_E + Q_H)} \quad (5.6)$$

$$\Delta T_s = \frac{\Delta t}{h} [Q_I (1 - e^{-\gamma h}) + Q_B + Q_E + Q_H] \quad (5.7)$$

The two unknowns or uncertain parameters used in this model are the fraction of wind mixing energy (m) which is used to increase the potential energy of the upper layer and the extinction coefficient for solar radiation (γ) in sea water.

The momentum imparted by the wind into the ocean is used to generate surface waves. A part of this wave energy is utilised to increase the turbulence through wave breaking which in turn increases the potential energy of the system. Turner (1969) suggested that only a fraction of the energy transferred from wind is used to increase the potential energy. In the absence of any information about the time variation of 'm', the model calculations are made on the assumption that the rate of increase of potential energy due to mechanical mixing is constant. The laboratory experiments of Kato and Phillips (1969) suggested a value of 0.0015 for 'm' while Denman (1973) used $m=0.0012$ on an idealised case of wind mixing and diurnal heating which are much lower than the values of 0.01 obtained by Turner (1969). However, in the present numerical simulation $m=0.0009$ was found to give best results.

Solar radiation reaching the ocean surface consists mainly of visible and infra-red part of the spectrum. However, the radiation mainly in the wave length range $0.3-1\mu\text{m}$ only penetrates to deeper levels. So, an average extinction coefficient γ is defined for these wave lengths, such that the solar radiation available at a depth $z=-h$ is

$$I(-h) = I_0 e^{-\gamma h} \quad (5.8)$$

Usually in the open ocean γ varies between $0.001.\text{cm}^{-1}$ and $0.003.\text{cm}^{-1}$ (Jerlov, 1968). Utilising all the available Secchi disk values (D) in the Arabian Sea, a seasonal average is computed on a $2^\circ \times 2^\circ$ grid (Fig.5.5). The extinction coefficient, γ is computed from this Secchi disc values using the relationship $\gamma=1.7/D$. In the present numerical simulation, the values of γ obtained from the above relation for the appropriate locations are used.

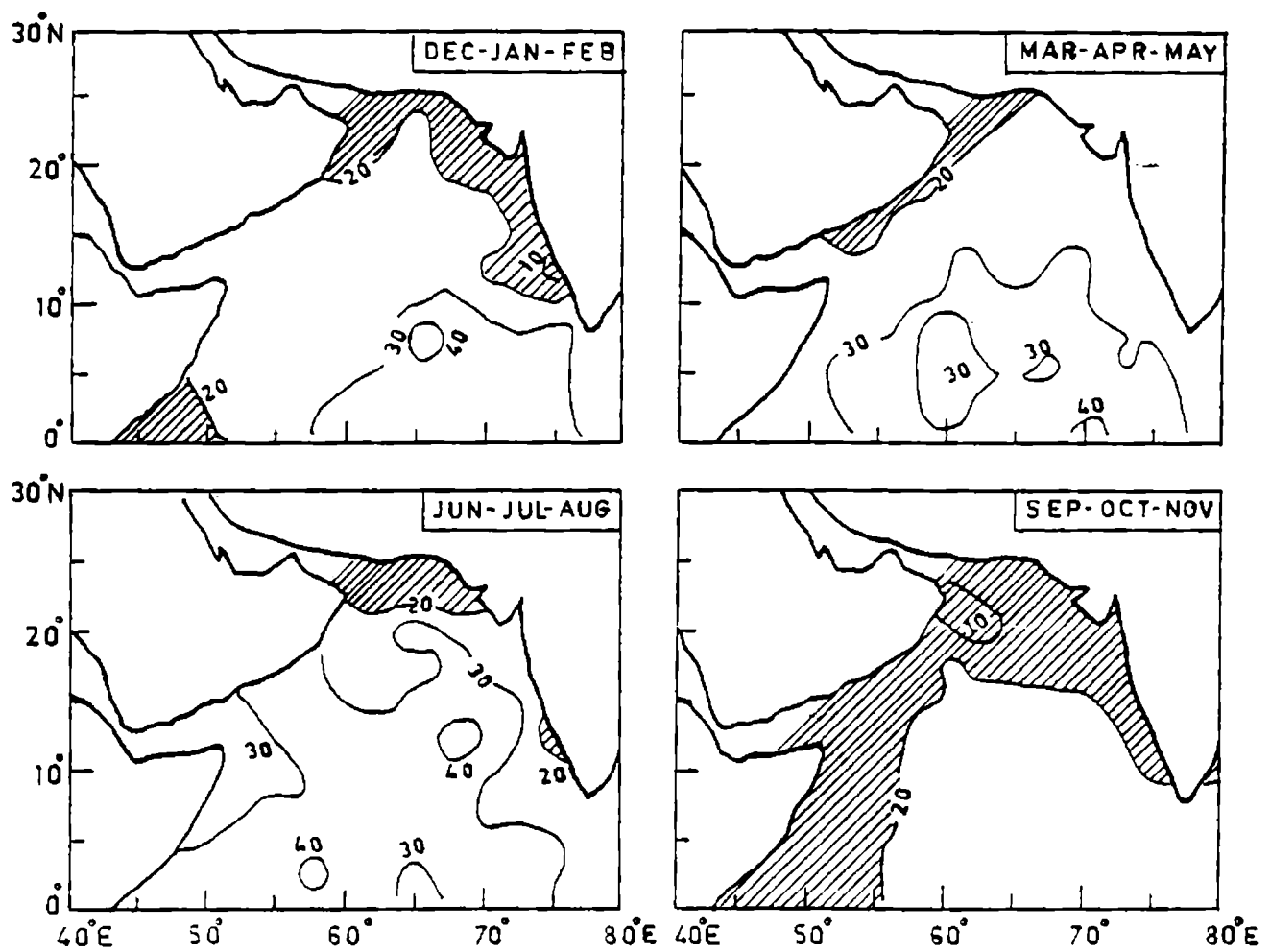


Fig. 5.5 Three month averages of Secchi disc depth (m)

5.4 Simulation

The model of Miller (1976) is used to simulate MLT and MLD at selected locations in the Arabian sea during pre-onset regimes and active regimes of the southwest monsoon for short time scales (few days to few weeks). The extinction coefficient used to run the model and the Root Mean Square error (R.M.S. error) for MLT and MLD are presented in Table 5.1.

6.4.1 Pre-monsoon

The mixed layer simulations are carried out for four stations in the western equatorial Arabian Sea (N79, E79, S79 and W79) and at two stations in the eastern Arabian Sea (DP79 and DK79). The results of the simulation along with the observed values are presented in Fig.5.6.

The progressive warming of the surface layers was clearly evident from the two stations (DP79 and DK79) in the eastern Arabian Sea and the initial few days (up to 22 May) at the four locations (N79, E79, S79 and W79) in the western equatorial Arabian Sea. The observed MLD was in general less than 50m in the Arabian Sea and is characterised by large amplitude vertical displacements. In the western equatorial Arabian Sea, except at E79, all the other three stations showed cooling of the mixed layer with different dates of onset of cooling. But such a cooling was not noticed at DP79 and DK79 in the eastern Arabian Sea. The cooling started earlier at W79 (22 May) and at a later date at S79 (24 May) and at N79 (25 May). From the detailed measurements of the flow pattern in the western equatorial Indian ocean, Leetmaa et al (1979) and Swallow et al (1983) found that the northward flowing western boundary current, which brings cold and low

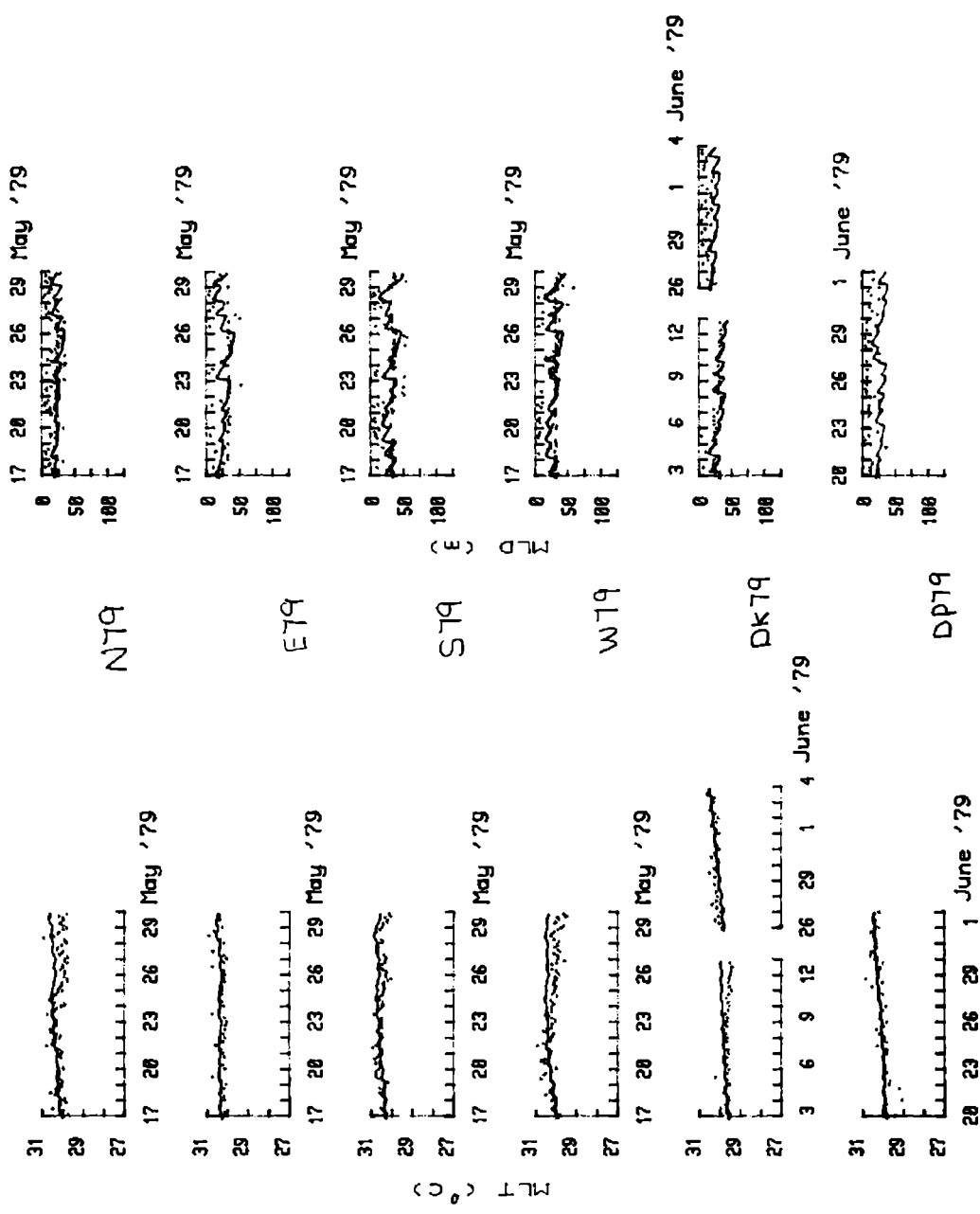


Fig.5.6 Observed (.....) and Simulated (—) Mixed Layer Temperature (MLT)

and Mixed Layer Depth (MLD) for the pre-onset phase at selected

locations in the Arabian Sea

saline water, turned offshore near 2-3°N after 20 May and intruded into the observational site causing a drop in the observed MLT in 1979.

The comparison between the observed and simulated MLT is good at E79 (minimum R.M.S. error of 0.17°C), during the later part (after 26 May) at DK79 (R.M.S. error of 0.18°C) and during the initial few days at N79, S79, W79. After 24 May, the model simulated a slightly warmer layer at N79, S79 and W79. This may be due to the non-inclusion of the advective correction for cold water intrusion. Eventhough, the model simulates the diurnal oscillation in MLT, the magnitude of these oscillations is small when compared to the observed. The MLD simulation shows a fairly good agreement with the observed at E79, S79 and W79 (R.M.S. errors of 9.7, 9.7 and 8.3m respectively), whereas at N79 and in the eastern Arabian Sea (except during the intial period at DK79), the model simulated deeper mixed layer (R.M.S. error >10m).

5.4.2 Active Monsoon

During this period, the simulations are carried out at four stations in the central Arabian Sea (N77, E77, S77 and W77) and at two stations in the coastal waters off the west coast of India (B88 and K89). In the central Arabian Sea, the model simulations are carried out corresponding to onset (7-19 June, 1977) and active regimes (30 June-15 July, 1977) of southwest monsoon. The observed and simulated values are presented in Fig.5.7.

The surface waters at N77 was warmer by 0.5°C than the other three locations during the intial days of the onset regime. But by the end of this regime, N77 and E77 experienced a dramatic cooling of 2°C and 1.5°C respectively,

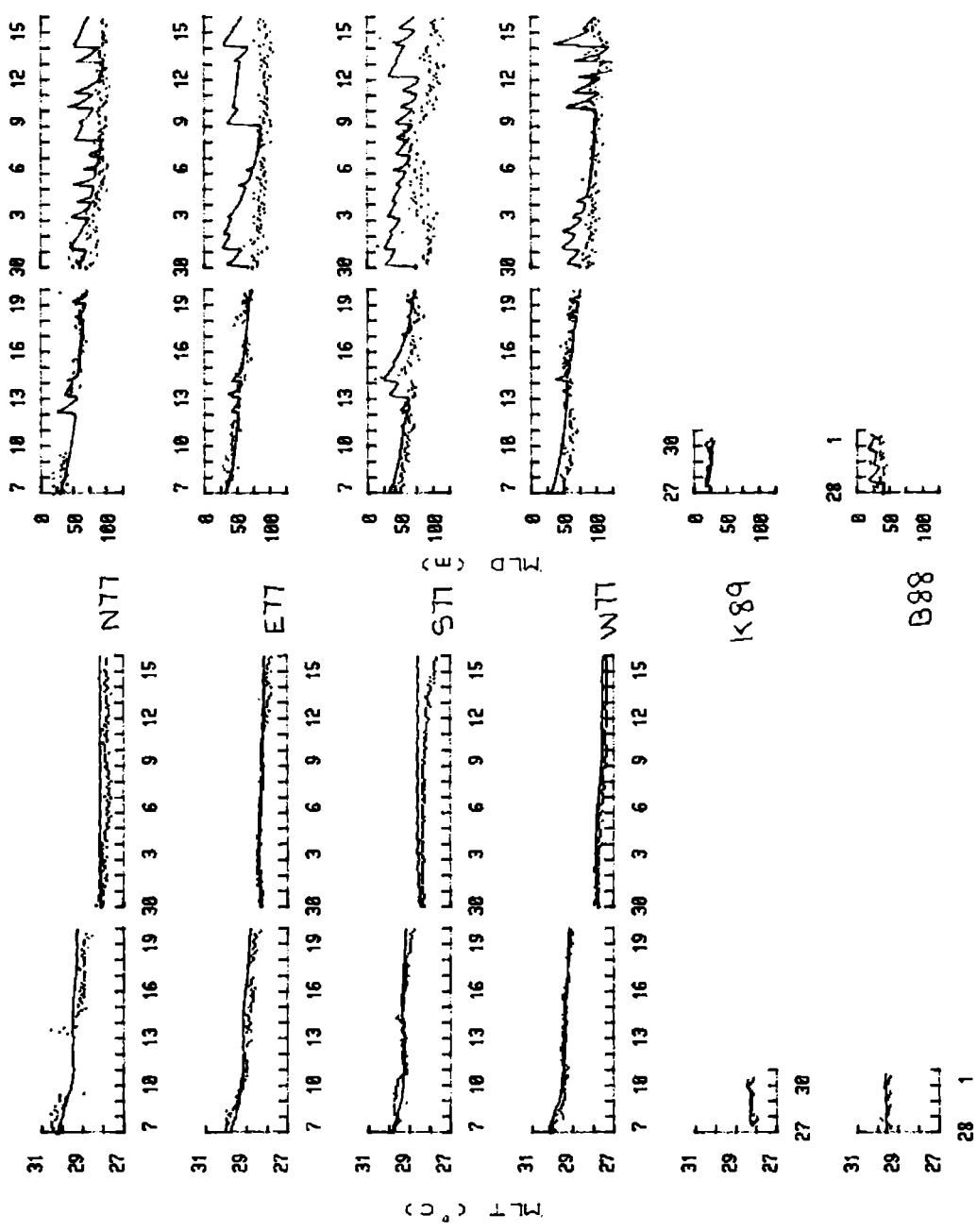


Fig. 5.7. Observed (.....) and Simulated (—) Mixed Layer Temperature (MLT)

and Mixed Layer Depth (MLD) for the onset phase at selected

locations in the Arabian Sea

whereas at S77 and W77 only a cooling of only $< 1^{\circ}\text{C}$ was noticed. Correspondingly, mixed layer deepening was maximum at N77 (55m) and E77 (50m) whereas at S77 and W77 the deepening was less than 25 m. During the active phase, mixed layer deepening was evident at all the stations. It is also noticed that the magnitude of the diurnal variation in the observed MLT and MLD was very weak during both the regimes. The deeper mixed layer and the greater turbulence induced by the wind and buoyant mixing might have reduced the diurnal amplitude in the temperature field.

In general, the model simulated the cooling and deepening rates in the central Arabian Sea reasonably well during the onset phase. The agreement between simulated and observed MLT is good at all the stations, except after 15 June at N77 and after 9 July at S77. Out of the four stations in the central Arabian Sea, the maximum agreement between the observed and simulated MLT in both the phases was obtained at E77 (R.M.S. errors of 0.22°C and 0.11°C) and at W77 (0.14°C and 0.17°C). This implies that at E77 and at W77 the MLT changes can be reasonably well accounted by the 1-D forcing functions of surface wind stress and net air-sea heat flux, as entrainment is not included in the model simulation. The MLD simulation also shows good agreement with observations during the onset phase at all the locations (R.M.S. errors less than 10m), whereas during the active phase the model simulated shallow layers at N77, E77 and S77 (R.M.S. errors greater than 20m). The amplitude of this simulated MLD is also quite large compared to the observed.

Studies by Sastry and Ramesh Babu (1979), Bruce (1982) revealed that the negative wind stress curl at the surface (convergence) causes deepening of the mixed layer in the central Arabian Sea. However, Shetye (1986) found that

convergence has only marginal effect on the SST variation, but it influences the temperature distribution in the subsurface levels by pushing down the thermocline. So, the unrealistic simulation of the shallow MLD during active regime may be caused by the non inclusion of convergence in the model. During this period, the horizontal advection of cold water from the coastal upwelling regions to the central Arabian Sea, which is not incorporated in the model, also could be important in the mixed layer variation (Duing and Leetmaa, 1980).

In the coastal waters, the simulations are carried out at one station each off Karwar (K89) and off Bombay (B88) and the results are presented in Fig.5.7. At K89, the observed MLT was around 28°C with MLD showing a slight deepening trend. But at B88, the MLT was around 29.5°C and the MLD was around 40m. The simulation of MLT and MLD at K89 (R.M.S. errors of 0.15°C and 4.2m respectively) and B88 (R.M.S. errors of 0.14°C and 10.2 respectively) shows good agreement with the observations during the onset regime. The success of the simulation during the onset period can be due to the dominance of 1-D processes over other processes like vertical and lateral advection from coastal boundaries during this period. Denman & Miyake (1973) also reported that the advection of heat by horizontal/vertical motion may not significantly influence the mixed layer variability on short time scales.

Table 5.1

A. Pre-onset Regime

Location	Symbol	Period	γ (cm ⁻¹)	R.M.S. Error	
				MLT (°C)	MLD (m)
8°48 N, 57°03 E	N79	17-30 May 79	0.0005	0.28	10.9
6°15 N, 59°08 E	E79	17-30 May 79	0.0005	0.17	9.7
3°56 N, 57°10 E	S79	17-30 May 79	0.0005	0.23	9.7
6°25 N, 54°38 E	W79	17-30 May 79	0.0005	0.33	8.3
15°00 N, 65°00 E	DP79	20 May-8 June 79	0.0005	0.52	15.4
		3-13 May 79	0.0005	0.26	7.1
9°00 N, 68°00 E	DK79	26 May-6 June 79	0.0005	0.18	12.1

B. Active Regime

Location	Symbol	Period	γ (cm ⁻¹)	R.M.S. Error	
				MLT (°C)	MLD (m)
14°30 N, 66°00 E	N77	7-19 June 77	0.0005	0.38	8.7
		30 June-15 July 77	0.0005	0.22	21.0
12°30 N, 68°00 E	E77	7-20 June 77	0.0005	0.22	7.7
		30 June-15 July 77	0.0005	0.11	37.5
10°30 N, 66°00 E	S77	7-20 June 77	0.0005	0.14	10.6
		30 June-15 July 77	0.0005	0.17	20.4
12°30 N, 64°00 E	W77	7-20 June 77	0.0005	0.10	6.5
		30 June-15 July 77	0.0005	0.12	9.4
18°15 N, 71°35 E	B88	28 June-1 July 88	0.0007	0.14	10.2
14°45 N, 73°35 E	K89	27 June-1 July 89	0.0007	0.15	4.2

CHAPTER VI

INTRA-DIURNAL VARIABILITY IN THE UPPER OCEAN OBSERVATIONS AND SIMULATIONS

6.1 Introduction

Knowledge on the diurnal scale variability of the ocean thermal structure is essential for underwater acoustic surveillance operations, fisheries exploration, monitoring pollutant dispersion etc. Several attempts are made to document and explain the diurnal scale variability of the ocean thermal structure (Stommel and Woodcock, 1951; Kraus and Rooth, 1962; Shonting, 1964; Howe and Tait, 1969; Ostapoff and Worthem, 1974). The results of these studies revealed that the diurnal variation of wind stress and surface heating play a significant role in the diurnal variability of the upper ocean dynamics. The solar heating, which attains maximum near mid day, tends to stratify the upper layer and inhibits vertical mixing, whereas the winds enhance the vertical mixing through mechanical turbulence. The balance between these two processes creates a diurnal cycle in the upper ocean. Hence, to understand the diurnal cycle of the upper ocean, it is required to study how the surface mixed layer is maintained by the balance between the stabilisation caused by incoming short wave radiation and the destabilisation caused by buoyancy flux and wind stress. Lukas (1991) noticed that the heating/cooling cycle in the upper ocean produces a diurnal cycle of non-sinusoidal nature in the sea surface temperature (SST) with SST skewed towards higher values. The amplitude of this diurnal scale variation is quite small in the open ocean but may be large in sheltered and coastal areas (Pickard and Emery, 1982) due to the shallow water column with high turbidity. However, in the Arabian Sea, information on the diurnal scale variability of the thermal structure is meagre due to the non-availability of the systematic time series measurements with short sampling interval.

Several theoretical one dimensional models are available in the literature to simulate the temperature and the thickness of the upper homogeneous layer on a synoptic time scale. These models assume a surface homogeneous layer having a density jump at its base. The field observations revealed that instead of a sharp jump, there is a smooth and thick transition layer beneath the mixed layer base. This aspect is considered in the simulation of the diurnal cycle in the upper ocean by Price et al (1986).

In this chapter, the observed diurnal cycle at a station off Cochin, southwest coast of India is studied for a one week period and the one-dimensional model of Price et al (1986) is utilised to simulate the observed diurnal cycle. The parameterisation of the convective and wind mixing processes were also tested with this data set.

6.2 Data

FORV Sagar Sampada occupied a stationary position (Fig.6.1) in the coastal waters off Cochin ($9^{\circ}45'N$ $75^{\circ}44'E$) for a seven day period (0600 hrs on 10 to 0600 hrs on 17 April, 1991). Surface marine meteorological elements and vertical profiles of temperature and salinity (using STD; accuracy $\pm 0.05^{\circ}C$) were collected at three hourly interval up to 16 April (0600 hrs) and at hourly interval from 16 April (0600 hrs) to 17 April (0600 hrs). The subsurface currents are also measured at 1, 20, 40, 60 and 80m depths at 2 minute sampling interval from a mooring of Aanderaa RCM4 and RCM7 current meters.

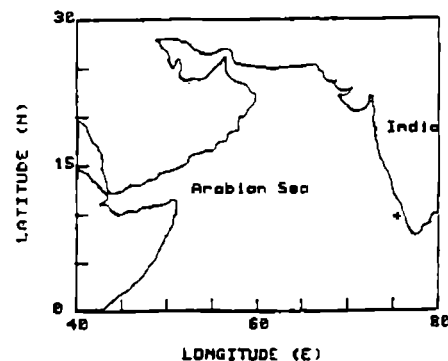


Fig 6.1. Station Location Map

6.3 Surface meteorology and thermal structure

The surface meteorological forcings play a significant role in producing variation in the upper ocean. In order to gain a better understanding of the variability in the thermal structure due to the atmospheric forcing functions, incoming shortwave radiation Q_I , total heat loss Q_L , net air-sea heat flux Q , surface wind stress τ and the temperature at selected depth levels are presented in Fig.6.2. The net air-sea flux Q , is the sum of incoming short wave radiation (Q_I) and the net heat loss (Q_L) which include effective back radiation, latent heat and sensible heat fluxes. Since, the direct solar radiation measurements are not available, Q_I is estimated following Lumb (1964). The details of the estimation procedures of other heat budget components are described in chapter III. On most of the days, solar heating was strong (peak value of $Q_I \approx 720 \text{ W.m}^{-2}$) but Q_L varied from -100 to -247 W.m^{-2} with maximum heat loss occurring during night (Fig.6.2). Correspondingly, the net oceanic heat gain (Q) showed an accumulation of heat during day time and release of heat during night time, thus producing a diurnal thermal cycle in the upper ocean.

The time series of temperature shows the dominance of high frequency oscillation below 15m. In the upper 10m a well defined diurnal thermal cycle was evident in the time series of temperature on all days with different amplitudes. It is interesting to note that the amplitude of the diurnal thermal cycle has a strong dependence on the net air-sea heat flux and wind stress. The largest response in the thermal structure was noticed on 13 and 15 April in association with near zero wind stress ($\tau < 0.003 \text{ N.m}^{-2}$) and large net heat gain ($Q > 600 \text{ W.m}^{-2}$). Under these conditions wind mixing may become

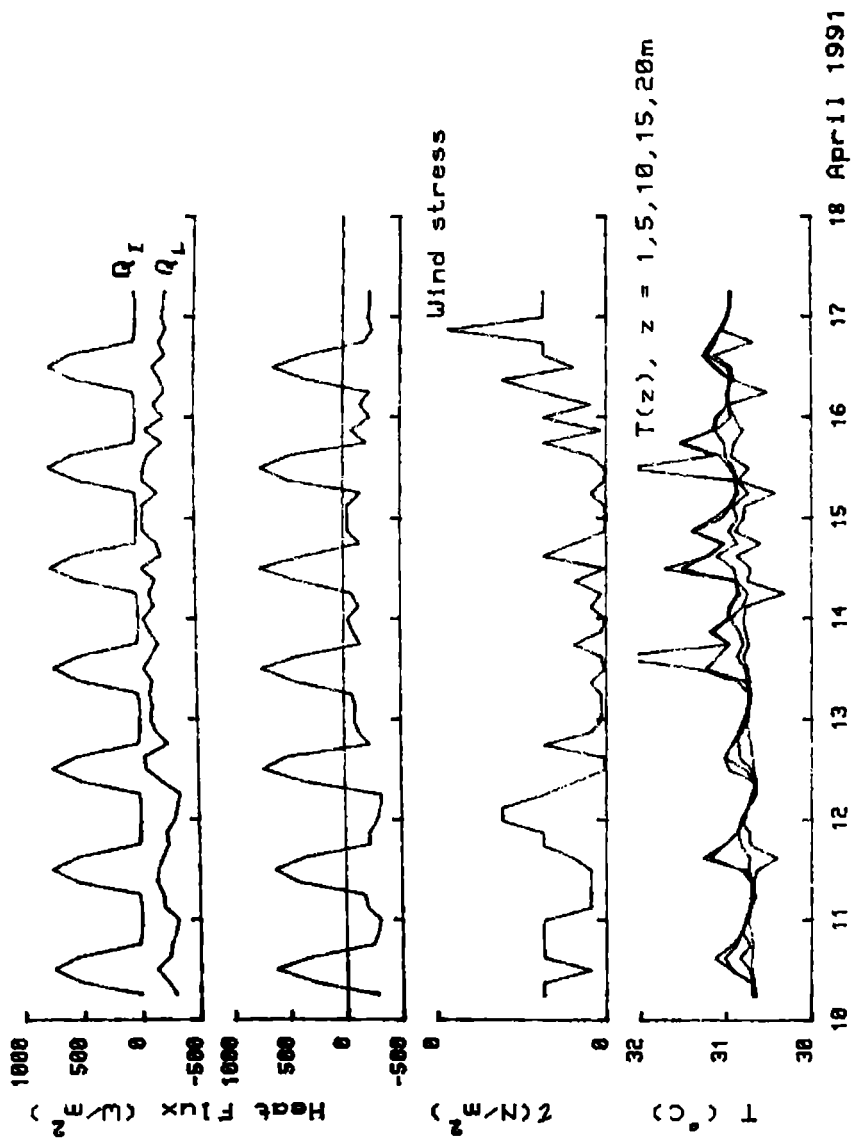


Fig. 6.2 Air-sea fluxes and temperature at selected depths

Insolation (Q_I), net heat loss (Q_L), net surface flux (Q)

insignificant. However, the maximum response in the thermal structure was confined to the 1m depth level, below which the diurnal amplitude became weak indicating that the depth of convection to be less than 5m. Bruce and Firing (1974) also reported a shallow layer of 1-2m thickness that was warmer than the main mixed layer under light winds. The comparatively higher wind stress ($\tau > 0.015 \text{ N.m}^{-2}$) and the greater nocturnal heat loss from the ocean ($Q_L > -240 \text{ W.m}^{-2}$) on 10 and 16 April, distributed the accumulated heat to deeper levels through mechanical and convective mixing, thus reducing the diurnal amplitude of SST ($< 0.5^\circ\text{C}$). The minimum heat gain (457 W.m^{-2}) and maximum wind stress (0.02 N.m^{-2}) was noticed on 16 April. As a result, the surface isothermal layer is quite deep compared to other days caused by both mechanical and buoyancy mixing and thus reduced the diurnal amplitude in SST. So the days that produce largest diurnal warming in the upper layers are characterised by light winds and increase in the wind stress and the net reduction in heat gain from the ocean reduces the diurnal warming.

6.4 Upper Ocean Modeling

The simplified 1-D prognostic equations for temperature, salinity and momentum for the mixed layer (Niiler and Kraus, 1977) in the conventional cartesian co-ordinate system (z positive downward) are given below.

$$\frac{\partial T}{\partial t} = \frac{1}{h} \left(\frac{Q}{\rho C_p} - \frac{dh}{dt} (T - T_h) \right) \quad (6.1)$$

$$\frac{\partial S}{\partial t} = \frac{1}{h} (S(E-P) - \frac{dh}{dt} (S - S_h)) \quad (6.2)$$

$$\frac{\partial V}{\partial t} = -f \times V + \frac{1}{h} \left(\frac{\tau}{\rho} - \frac{dh}{dt} (V - V_h) \right) \quad (6.3)$$

were Q , net surface heat flux; ρ , mean density of the mixed layer; C_p , specific heat at constant pressure; T , mixed layer temperature; T_h , temperature just below the mixed layer; S , mixed layer salinity; S_h , salinity just below the mixed layer; $E-P$, evaporation minus precipitation; f , coriolis parameter; V , mixed layer velocity; V_h , velocity just below the mixed layer and τ , surface wind stress.

Price et al (1986) assumed that the diurnal cycle rides passively and non-interactively on the top of the ambient oceanic variability. Here, the diurnal warming is viewed as a local ocean response to solar radiation, net heat flux and wind stress at the surface. Under this assumption, the simplified one dimensional heat budget equations for the diurnal cycle are

$$\frac{\partial T}{\partial t} = - \frac{1}{\rho C_p} \frac{\partial F}{\partial z} \quad (6.4)$$

$$\frac{\partial S}{\partial t} = - \frac{\partial E}{\partial z} \quad (6.5)$$

$$\frac{\partial V}{\partial t} = -f \times V - \frac{1}{\rho} \frac{\partial G}{\partial z} \quad (6.6)$$

Simpson and Dickey (1981) emphasized the importance of parameterising the penetration of solar radiation accurately in the studies of diurnal cycle in the upper ocean and concluded that the double exponential data fit of Paulson and Simpson (1977) give a reasonably good estimate of the downward irradiance.

$$F(z) = Q_1 (I_1 e^{-z/\gamma_1} + I_2 e^{-z/\gamma_2}) \quad (6.7)$$

where $F(z)$, heat flux profile; γ_1, γ_2 are the absorption coefficients for short wavelength (1.5m) and long wavelengths (14m) of insolation; I_1, I_2 are the short wavelength (0.77) and long wavelength (1- I_1) fraction of insolation.

The absorbed heat is mixed deeper by wind mixing, which is parameterised as an adjustment to shear flow stability and by free mixing, which occur whenever there is net heat loss at the surface. The stability criteria for these mixing processes are given by

$$\frac{\partial \rho}{\partial z} \geq 0 \quad \text{for static stability} \quad (6.8)$$

$$R_B = \frac{g \Delta \rho h}{\rho (\Delta V)^2} \geq 0.65 \quad \text{for mixed layer stability} \quad (6.9)$$

$$R_G = \frac{g \partial \rho / \partial z}{\rho (\partial V / \partial z)^2} \geq 0.25 \quad \text{for shear flow stability} \quad (6.10)$$

In the ocean, vertical motion can occur depending on the variation of density with depth. Hence one should examine the vertical density gradient to understand the stability of the fluid. If $\partial \rho / \partial z > 0$, the fluid will be stable and vice versa. The absorption of heat from the sun stratifies the surface layers during day time, whereas during night time, the loss of heat increases the density of the surface layers which sets instability in the vertical. So, equation 6.8 accounts for free convection, which occurs as a result of instability created by the surface cooling. The resulting free convection will mix all the properties down to the convection depth.

Equation 6.9 controls the mixed layer entrainment by the relaxation of the bulk Richardson number (R_B), which is a function of the current shear and stratification at the base of the mixed layer. Pollard et al (1973) suggested this R_B as the stability criteria for the mixed layer. When the current shear becomes sufficiently large to violate the stability resulting from density stratification (i.e. $R_B \geq R_{Bcrit}$), the mixed layer deepens by turbulent mixing. The laboratory experiment of Ellison and Turner (1959) revealed that when R_B increased from 0.4 to 0.8, the entrainment tendency decreased by an order, suggesting approximate limit of R_{Bcrit} . It is this cut off limit that determines the thickness of the surface mixed layer. Pollard et al (1973) assumed R_{Bcrit} as unity, whereas Price et al (1978) and Price et al (1986) suggested R_{Bcrit} as 0.65.

Equation 6.10 simulates the effect of shear flow instability by the relaxation of the gradient Richardson number (R_G). As a result of the entrainment mixing, a surface mixed layer with a sharp density difference across the base of the mixed layer will develop. Buoyancy and horizontal velocity considerably vary across this interface. When the interface is highly stratified, the vertical mixing will be inhibited. If there is sufficient shear to disturb the stratification, as given by the stability criteria $R_G < R_{Gcrit}$, dynamic instability may occur and the resulting internal mixing can overturn the density distribution over a given depth range (Thorpe, 1971). Similarly, when $R_G \geq R_{Gcrit}$, the turbulent vertical transport of heat and momentum will stop. Miles (1961) showed that a stratified shear flow is stable only when $R_G \geq 0.25$ everywhere in the flow. For a rain formed mixed layer, Price (1979) estimated R_{Gcrit} as 0.26. Piat and

Hopfinger (1981) obtained the value of R_{ocrit} as 0.33 from the laboratory experiments whereas Price et al (1986) suggested the value of R_{ocrit} as 0.25.

6.5 Boundary conditions

i) At the upper boundary

At the surface, the turbulent heat flux is equal to the net air-sea heat flux (Q), salinity is equal to the fresh water ($P-E$) times the surface salinity and the magnitude of the momentum flux to the surface wind stress (τ). i.e. at $z=0$

$$F(0) = Q \quad (6.11)$$

$$E(0) = S(P-E) \quad (6.12)$$

$$G(0) = \tau \quad (6.13)$$

ii) Interior of the mixed layer

The diffusion across the stable interface is neglected. All mixing processes are associated with the entrainment of cold and denser water from below the mixed layer. All the turbulent heat fluxes are assumed to vanish below this surface layer. Then the temperature of the interior can increase only by the absorption of the small fraction of penetrating solar radiation. The equations describing the interior are

$$\frac{\partial T}{\partial t} = \frac{\partial F(z)}{\partial z} \quad (6.14)$$

$$\frac{\partial S}{\partial t} = 0 \quad (6.15)$$

$$\frac{\partial V}{\partial t} = -f \times V \quad (6.16)$$

6.6 Implementation

The simulation is carried out on a vertical grid of 1m resolution (Δz) and a time step of 900s (Δt). At each time step Q_I is absorbed in the water column (according to equation 6.7) and the net heat loss Q_L and the freshwater flux E-P are computed at the surface. Since there was no rain during the observational period P is considered as zero.

Then the density profile is calculated from the equation of state of sea water

$$\rho(z) = \rho_o + \alpha (T_z - T_o) + \beta (S_z - S_o) \quad (6.17)$$

Here, ρ_o , T_o and S_o are the reference density, temperature and salinity respectively and α and β are the coefficients of thermal expansion and saline contraction.

$$\alpha = \frac{1}{\rho_o} \frac{\partial \rho}{\partial T} \quad (6.18)$$

$$\beta = \frac{1}{\rho_o} \frac{\partial \rho}{\partial S} \quad (6.19)$$

The static stability of the water column is then checked by the stability criteria $\partial\rho/\partial z \geq 0$ and if found unstable, the water column was made statically stable by mixing all the properties downward.

The wind stress is then distributed throughout the mixed layer and momentum balance was stepped forward and R_B was computed. If $R_B < 0.65$, the mixed layer entrains successively deeper until $R_B \geq 0.65$.

R_σ is then computed between two successive depth levels over the stratified portion of the profile. If $R_\sigma < 0.25$, then all the properties at these two depth levels are partially mixed according to

$$\rho_j' = \rho_j \left(1 - \frac{R_\sigma}{R_\sigma}\right) (\rho_j - \rho_{j+1}) / 2 \quad (6.20)$$

$$\rho_{j+1}' = \rho_{j+1} \left(1 - \frac{R_\sigma}{R_\sigma}\right) (\rho_j - \rho_{j+1}) / 2 \quad (6.21)$$

where $(\rho_{j+1})'$ represents the value after mixing.

R_σ is again computed from $i-1$ to $i+2$ levels and the mixing process continued until $R_\sigma \geq 0.25$ throughout the stratified region of the profile.

6.7 Simulations

The integration was begun from an initial condition estimated from the data at 0600 hrs on 16 April, 1991 and continued with a 15 minutes time step until 0500 hrs 17 April, 1991. All timings reported here are in IST.

The results of the model simulation for 16-17 April, 1991 are presented in Fig.6.3. Since the thickness of the surface mixed layer was less than 20m, only the upper 20m of the observed and simulated vertical temperature profiles are presented. The simulation of the diurnal thermal cycle using Price et al (1986) is encouraging. When the incoming radiation is maximum (around noon time), the model simulated a shallow (<5m) and slightly warmer surface layer compared to the observed. The departures noticed between the observed and simulated profiles in the thermocline region at certain hours are attributed to the influence of internal waves and tides.

To study more about the effect of wind stress and heating/cooling on the diurnal thermal cycle hourly net air-sea heat flux (Q), wind stress (τ), time series of temperature at selected depth levels, trapping depth (D_T) and penetration depth (D_p) computed from both the observed and simulated temperature profiles are presented in Fig.6.4.

The trapping depth (D_T) is defined as the mean depth value of the temperature anomaly profile (Price et al, 1986).

$$D_T = \frac{1}{T_s} \int_{Z_r}^{Z_s} T'_z dz \quad (6.22)$$

$$T'_{(z,t)} = T_{(z,t)} - T_{(z_r,t)} \quad (6.23)$$

The reference level Z_r is chosen in such a way that (i) it should be within the vertically homogeneous layer and (ii) it should be deep enough that the diurnal amplitude at Z_r is negligible. In this study Z_r is taken as 15 m and Z_s as 1m.

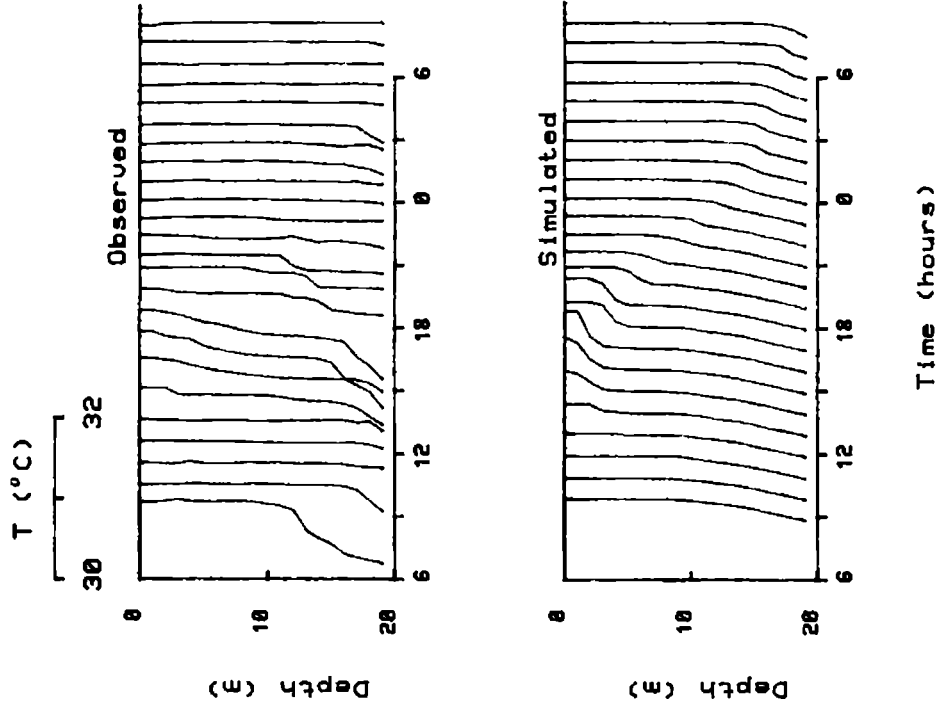


Fig. 6.3. Observed and simulated vertical temperature profiles for 16 April 1991

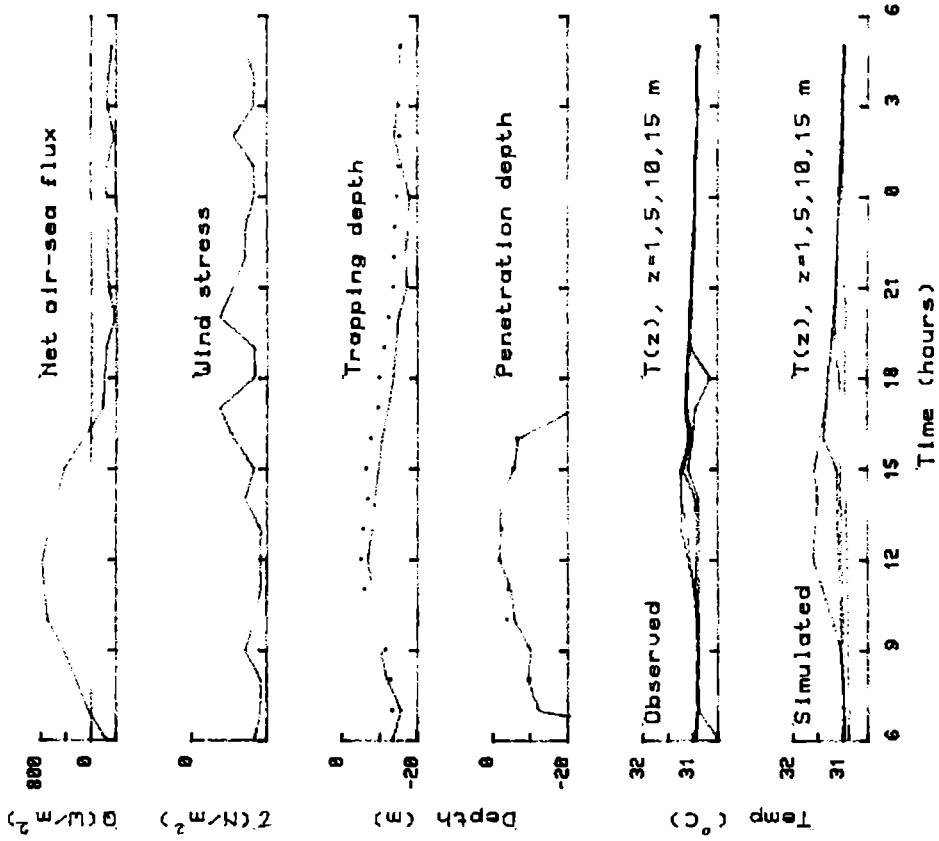


Fig.6.4. Net air-sea flux (Q), Wind stress (τ), Trapping depth computed from the STD (—) and simulated (---) profiles, Penetration depth computed from the STD (—) and simulated (---) profiles and the temperature at selected depth from the STD and simulated profiles

The penetration depth (D_p), defined as the length scale $(\partial/\partial z)^{-1}$ of the 1-D heat equation is (Price et al, 1986)

$$D_p = \frac{Q}{\rho C_p (\partial T_s / \partial t)} \quad (6.24)$$

The advantages of these two length scales are that they are (i) model independent (ii) parameter free and (iii) can be estimated from the observed and simulated data. The trapping depth gives the depth of surface trapping of solar radiation. During day time, when heat accumulates in the surface layer, D_p is a direct measure of the wind mixing.

From the sunrise till noon, the accumulation of heat, as indicated by the increase of temperature at 1 and 5m, is noticed in the surface layers (Fig.6.4). With the increase in net surface heat flux, D_T and D_p showed a shoaling tendency and reached the minimum values (6m and 2m respectively for D_T and D_p) by 1200 hrs, coinciding with the time of maximum heat input into the ocean. The time series of temperature at selected depths obtained from both the observed and simulated temperature profiles also revealed that the minimum D_T is less than 5m. Since D_T is less than 5m, all the accumulated heat might have been trapped within this level. Starting within few hours from noon, wind and convective mixing began to mix the accumulated heat in the surface layer to deeper levels. Correspondingly D_T and D_p showed a deepening trend.

An attempt is also made here to study the importance of the three mixing processes in the coastal waters off Cochin (Fig.6.5). In all the four cases, the shoaling/deepening of the surface mixed layer is clearly evident.

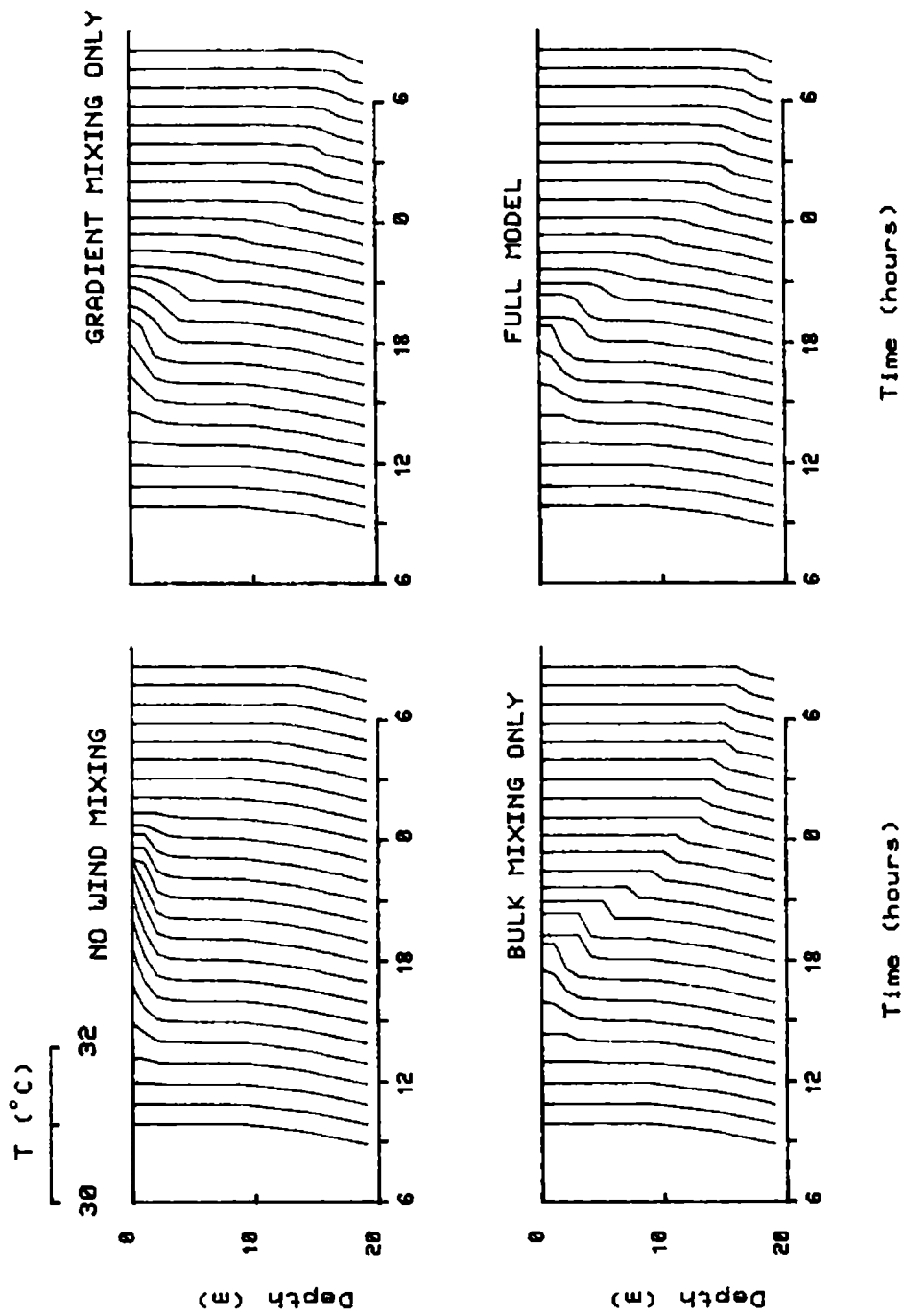


Fig. 6.5. Mixing experiments run using the numerical model

a. Free mixing only

The effect of wind mixing was stopped in the model by specifying $R_B = R_G = 0$. In this case the vertical mixing will occur only to the convection depth by free convection. During day time, incoming radiation was much greater than the heat loss due to evaporation and effective back radiation (Fig.6.4). Since there is no wind mixing, all the absorbed heat was trapped in a shallow layer ($D_T = 3.6\text{m}$) which increased the temperature of this layer abruptly ($\bar{T}_S = 0.78^\circ\text{C}$). Below 4m, the corresponding temperature rise was not evident. However, such an unrealistic situation was not noticed in the observed profiles. With the dominance of heat loss in the afternoon hours, the increased heat loss mixes the stored heat to deeper levels thereby destroying the abrupt temperature rise in the surface layers. So from this simulation, the importance of wind mixing processes in distributing the accumulated heat to deeper levels that cannot be reached by the convective process is clearly evident.

b. Bulk mixing only

By specifying $R_G = 0$, the model becomes the Dynamic Instability Model (Pollard et al, 1973; Price et al, 1978). In this case, the model simulated a good account of the vertical mixing processes in the surface layer, as indicated by the D_T (4.8m) and \bar{T}_S (0.53°C). But the simulated vertical temperature profiles shows a surface mixed layer with a sharp temperature at the base, which was quite unrealistic when compared with the observed profiles. The temperature gradient across this mixed layer was found to be maximum around local noon and decreases with the increase in the mechanical and

buoyant mixing and the associated deepening of the surface mixed layer.

c. Gradient mixing only

When $R_b = 0$ also a reasonable good account of the mixing process in the surface layer is evident ($D_T=4.0m$ and $\bar{T}_S=0.65^\circ C$). From the sunrise to noon, when the convective mixing is weak, the accumulated heat is trapped in a shallow layer and increased the surface temperature. However, with the dominance of the convective mixing from late afternoon hours, the accumulated heat is mixed to a deeper level (15m).

d. Full model

With all the mixing processes acting, the model simulated the vertical temperature profiles nearly as observed in the coastal waters off Cochin during April, 1991 ($D_T=5.4m$ and $\bar{T}_S=0.45^\circ C$). The surface mixed layer shoaled from sunrise to noon and deepened from late afternoon hours. At noon, the mixed layer was quite shallow (< 5m) followed by a smooth transition layer of 10m thickness below.

6.8 Scale analysis

Most of the day to day variability in the temperature and velocity field is caused by the variation in the net air-sea flux and wind stress. Price et al (1986) studied the response of these parameters on a diurnal scale in the upper ocean and developed new scale estimates for trapping depth (D_T), temperature (δT) and velocity (δV) anomalies based on heat budget and wind stress.

$$D_T = \frac{\tau}{Q^{0.5}} \frac{P_a}{P_\tau^{0.5}} \left(\frac{C_p}{-ag} \right) \quad (6.25)$$

$$\partial T = \frac{Q^{1.5}}{\tau} \frac{P_a^{1.5}}{P_\tau} \frac{(-ag)^{0.5}}{\rho C_p^{1.5}} \quad (6.26)$$

$$\partial V = Q^{0.5} \frac{P_a^{0.5}}{\rho} \left(\frac{-ag^{0.5}}{C_p} \right) \quad (6.27)$$

Here, P_a , the time scale of heating is half the interval during which $Q_T + Q_L > 0$ and P_τ , the acceleration time scale.

The effect of the variation in Q could be seen by comparing the days 13 and 15 April, when the wind stress, τ was roughly equal ($\tau = 0.002 \text{ N.m}^{-2}$). The estimated D_T was nearly equal on both the days even though the magnitude of Q was different. But ∂T was slightly larger on 15 April, corresponding to large Q , indicating a direct relationship of ∂T and ∂V with Q . The observed D_T and ∂T also showed similar variation, but with different magnitudes. It might be noted that the scale analysis showed a broad agreement in the general trend of the observed values, but differed in their absolute magnitudes.

Similarly, the effect of the variation of τ could be seen by comparing the days 13 and 14 April when Q was roughly equal (600 W.m^{-2}). On these days the estimated D_T and ∂T was almost equal whereas ∂V showed larger values on 14 April. The observed D_T and ∂V also showed similar variation with the scale estimates.

Table 6.1. Diurnal cycle parameters and scale for 10 to 16 April 91

	10	11	12	13	14	15	16
τ N.m ⁻²	0.016	0.010	0.014	0.002	0.005	0.003	0.02
Q_I W.m ⁻²	701	715	715	704	715	722	704
Q_L W.m ⁻²	-243	-205	-202	-103	-115	-102	-247
Q W.m ⁻²	468	510	513	601	600	620	457
Estimated							
∂T C	0.34	0.64	0.48	1.40	1.39	1.52	0.30
D_T m	4.4	2.54	3.48	1.58	1.60	1.42	5.38
∂V m.s ⁻¹	0.09	0.10	0.10	0.07	0.17	0.11	0.10
Observed							
∂T C	0.48	0.60	0.36	1.70	0.90	1.32	0.34
D_T m	3.9	5.0	4.4	2.9	6.0	2.8	6.0
∂V m.s ⁻¹	0.09	0.08	0.17	0.04	0.08	0.14	0.14

CHAPTER VII

SUMMARY AND CONCLUSIONS

A comprehensive documentation of the annual march of the heat budget components, viz. net air-sea heat flux, rate of oceanic heat storage and heat change due to vertical motion is presented. In the Arabian Sea, the cooling of the water column starts by March off the southwest coast of India which coincides with the commencement of upwelling. During southwest monsoon season, the entire coastal waters exhibits depletion of heat due to coastal upwelling whereas in the central and equatorial Arabian Sea accumulation of heat, caused by mixed layer deepening and convergence in the surface layer, is noticed. The rate of oceanic heat storage and the net air-sea heat flux shows an inverse relationship during summer monsoon season in the central Arabian Sea. The heat change due to vertical motion also revealed the release of heat by the coastal water and gain of heat in the central Arabian Sea during summer monsoon season. However, with the commencement of northeast monsoon season, the central Arabian Sea experience depletion of heat while in the coastal water accumulation of heat is evident.

Arabian Sea is probably the only region of the world ocean which cools during summer. An attempt has been made to parameterise the cooling in the Arabian Sea during this period. The analysis revealed that the cooling in the Arabian Sea is mainly caused by upwelling ($-4.9 \times 10^{14} \text{ W.m}^{-2}$) and the effect of horizontal advection ($-2.4 \times 10^{14} \text{ W.m}^{-2}$) in cooling the Arabian Sea is much larger than expected.

The distribution of the mixed layer in the Arabian Sea shows considerable variations on an annual cycle. When the net heat input into the ocean is maximum (April-May), Arabian Sea is characterised by shallow mixed layers (<50m) with marginal changes. With the onset and progress of the summer monsoon, increased mechanical and buoyant mixing along with sinking deepens the mixed layer in the central Arabian Sea by

more than 120m. However, in the coastal waters, the process of coastal upwelling inhibits the deepening rate and shoals the mixed layer. In the Arabian Sea, the deepest mixed layer (>140m) is noticed during winter and is confined to the coastal regions of northern Arabian Sea.

The salinity maxima in the upper 200m water column lies around 400 cl/t which corresponds to the Arabian Sea High Salinity Watermass. The shallow core depth (<25m) and higher core values (>36.6‰) during summer/winter months suggests the northeastern Arabian Sea as the origin of this watermass. As this high saline water traverse southwards/southeastwards, it occupies deeper levels with decrease of salinity.

The difference between the subsurface salinity maxima and surface salinity ($\Delta S = S_{\max} - S_0$) is maximum in the eastern Arabian Sea whereas rest of the Arabian Sea is characterised by ΔS less than 0.1‰. Since not much difference is noticed in the core salinity values, the larger ΔS (>1.4‰) off the west coast of India was caused by the dilution in the surface layers due to precipitation and river discharges during summer monsoon season and the intrusion of low saline Bay of Bengal/Equatorial Indian Ocean water during northeast monsoon season. However, in the central Arabian Sea increased evaporation and strong vertical mixing of surface waters with subsurface high saline waters increase the surface salinity and thus reduce ΔS during southwest monsoon.

Even on a synoptic scale (few days to few weeks) significant variations are noticed in the surface layer thermohaline characteristics of the Arabian Sea during pre- and active regimes of the summer monsoon season. With the onset and progress of the summer monsoon maximum cooling and deepening of the surface mixed layer is noticed in the central Arabian Sea. The cooling is mainly caused by the increased

heat loss due to strong winds, decreased insolation under cloudy atmosphere and advection of cold upwelled water from the coastal boundaries. The strong wind and buoyancy mixing along with convergence induced by the clockwise wind stress curl deepens the mixed layer in the central Arabian Sea. Interestingly the cooling in the central Arabian Sea is confined only to the surface layers, while significant warming is noticed in the thermocline region. The mixed layer deepening along with convergence in the surface layers might have produced this warming in the thermocline region. However, due to the process of upwelling, waters in the coastal regions exhibit cooling down to entire 200m.

Contrary to the surface temperature in the central Arabian Sea, surface salinity increases with the progress of the summer monsoon. The increase in the surface salinity decreases towards the eastern boundary due to mixing with freshwater. The depth of occurrence of the subsurface salinity maxima shoaled towards the coast due to coastal upwelling.

The upper layers off the west coast of India show significant thermohaline variability during the annual cycle. The maximum SST ($>30^{\circ}\text{C}$) is noticed in April-May off the southwest coast of India while SST as low as 22°C is noticed off Cochin near the coast in August. The surface salinity shows variation due to influx of high saline Arabian Sea waters, low saline Bay of Bengal/Equatorial Indian Ocean water and freshwater discharges during summer monsoon.

The T-S plots show the presence of waters with temperature about 28°C but salinity rapidly increases with depth (from 33 to 35‰) off the southwest coast of India during winter, termed the Bay of Bengal water mass. These waters could be traced even off Ratnagiri and occupies in the

upper 50m. Below this the Arabian Sea High Salinity Watermass is noticed and found throughout the year around 400-500 cl/t. The waters are less heterogeneous during May-June when the Bay of Bengal water retreats under the prevailing southerly flow which brings high saline water (>35‰) from northern Arabian Sea and when the dilution due to freshwater fluxes is also less. The upper 5-10m are characterised by very low salinity during summer monsoon due to freshwater inputs off the west coast of India. During summer monsoon relatively low salinity waters (35 ‰) are transported northward by the poleward undercurrent which is clearly noticeable off Cochin and Mangalore.

The thermal structure clearly shows evidence of upwelling and sinking off the west coast of India during different part of the year. The upwelling off the southwest coast of India starts by March-April and continues upto August-September while upwelling continues upto December off Ratnagiri. Sinking starts by October-November off Cochin and between November and December off Mangalore and after December off Ratnagiri. The thermal field also suggest early onset and cessation of upwelling in the south while upwelling continues for a longer period off Ratnagiri. From the vertical displacements of isotherms it appears that upwelling is a rather slow process while sinking occur rapidly off the west coast of India. The average speed of upwelling is of the order of about 20m per month while the speed of sinking is about 3-5 times higher than that of upwelling. The analysis further suggest that during summer monsoon the upwelling off the southwest coast of India is mainly wind driven while it is current driven north of 15°N. However, during November - December, upwelling is wind driven off Ratnagiri.

The downward sloping of isotherms and low saline water close to the slope regions suggest the presence of a poleward

undercurrent in the depth range of 80-150m during summer monsoon off the southwest coast of India. This poleward flow is prominent off Cochin and Mangalore where the core salinity in the slope regions also show a decrease. With the progress of monsoon it seems that the speed of the undercurrent decreases as it moves northward.

During pre-onset and active regimes of the summer monsoon an attempt is made to simulate the changes in the mixed layer characteristics with the time series data sets collected from selected locations in the Arabian Sea using the one dimensional model of Miller (1976). Eventhough the model simulated the diurnal variations in MLT, the magnitude of these variations are found to be small compared to observed. The simulation of a warmer surface layer in the western equatorial Arabian Sea during pre-monsoon suggest importance of cold water intrusion into the observational site. However, the MLD simulation reveals fairly good agreement with observations.

During the onset phase (7-19 June,1977) the model simulated the cooling and deepening of the mixed layer in the central Arabian Sea very well, indicating the predominance of one dimensional process in controlling the mixed layer variability. However, during active phase (30 June-15 July,1977) the model simulated shallow mixed layers with larger amplitudes whereas the MLT simulation reveals very good agreement with observations. The excellent agreement obtained between the observed and simulated MLD and MLT in the coastal waters during active phase suggests the dominance of one dimensional processes over vertical/lateral advection in controlling the mixed layer variability on short time scales.

In general it can concluded that the one dimensional mixed layer model of Miller (1976) simulated MLT and MLD

fairly well during the onset phase of the southwest monsoon. However, during active phase, internal ocean dynamics have to be included in the model physics to obtain a good simulation of MLT and MLD.

STD and surface marine meteorological measurements made from FORV Sagar Sampada during April 1991 was utilised to study the diurnal scale variability in the upper layers of the coastal waters of Cochin. The diurnal variation of temperature in the upper layers revealed a strong dependence on net air-sea heat flux and surface wind stress. The days that produced maximum diurnal amplitude in SST ($>1.5^{\circ}\text{C}$) was characterised by weak wind stress ($\tau < 0.003 \text{ N.m}^{-2}$) and large heat input into the ocean ($>600 \text{ W.m}^{-2}$). During these days, the penetration of diurnal heating was limited to shallower depths ($<5\text{m}$). However, under strong winds ($\tau > 0.02 \text{ N.m}^{-2}$) and weak heat input ($<450 \text{ W.m}^{-2}$), the diurnal amplitude in SST reduced to 0.5°C .

An attempt is made to simulate the intra-diurnal variation in the thermal structure on 16/17 April, 1991 using the one dimensional model of Price et al (1986). The model gives a good simulation of the overall structure of the temperature profiles. However, around noon time warmer surface layer was noticed in the simulated temperature profile compared to the observed.

The mixing experiments run with the numerical model revealed the importance of wind mixing (in terms of R_b and R_g) and buoyant mixing (in terms of Q) in the simulation of the vertical temperature profiles. When only the effect of buoyant mixing is included, an abrupt rise in surface temperature is noticed (0.78°C) around noon time. Similar situations are also noticed when R_b and R_g was included (0.53°C and 0.65°C respectively in SST). Also the shape of

the temperature profiles is quite unrealistic when the effect of only the individual processes are included. However, when all the mixing processes are acting, the diurnal thermal response in the SST (0.45°C) is found to be quite nearer to the observed changes in SST (0.34°C).

The depth of surface trapping of heat and momentum (Trapping Depth, D_T), penetration depth (D_P) and the scale analysis for trapping depth, temperature and velocity anomalies were also estimated. The minimum value of D_T (6m) and D_P (2m) was noticed around noon time when the net heat flux is maximum and vice versa. This suggests an inverse relationship of D_T and D_P with net surface heat flux, whereas the temperature and velocity anomalies show a direct relationship with the net surface heat flux. The scale analysis revealed a broad agreement in the general trend but differ in the absolute magnitudes.

7.1 Future outlook

The evaluation of the mixed layer models suggest that the one dimensional processes does not adequately give a better picture of the mixed layer characteristics in the Arabian Sea during active summer monsoon season. In this light it is felt that the use of three dimensional models, where more physics describing the internal ocean dynamics are included, may give a better simulation of the mixed layer variability.

The study revealed that the cooling noticed in the Arabian Sea during summer monsoon is mainly due to upwelling. The contribution of surface, intermediate and deep circulation to the summer cooling in the Arabian Sea requires a better understanding of the intermediate and deep layer mass transport across the equator.

- G 5155 -

The strong monsoon winds blowing in pulses can produce upwelling events in the coastal regions of the Arabian Sea, the knowledge of which is fragmentary. Some case studies have to be carried out to enhance the present understanding of 'upwelling events'.

The results of the present study could be utilised to understand the acoustic propagation characteristics in the Arabian Sea about which only fragmentary informations are available.



REFERENCES

- Antony M K (1990) Northward undercurrent along the west coast of India during upwelling - Some inferences. *Indian Journal of Marine Sciences*, 19, 95-101
- Banse K (1968) Hydrography of the Arabian Sea shelf of India and Pakistan and effects on demersal fishes. *Deep-Sea Research*, 15, 45-79.
- Brockmann C, E Fahrback, A Huyer and R L Smith (1980) The poleward undercurrent along the Peru coast 5 to 15°S. *Deep-Sea Research*, 27, 847-856.
- Bruce J G (1973) Large scale variations of the Somali Current during the southwest monsoon 1970. *Deep-Sea Research*, 20, 837-846.
- Bruce J G (1974) Some details of upwelling off the Somali and Arabian coasts. *Journal of Marine Research*, 32, 419-423.
- Bruce J G and E Firing (1974) Temperature measurements in the upper 10m with modified expendable bathythermograph probes. *Journal of Geophysical Research*, 79, 4110-4111.
- Bruce J G (1982) Variations in the thermal structure and wind field occurring in the western Indian Ocean during the monsoons (Naval Oceanographic Office, Technical Report 272, USA)
- Bryan K (1969) Climate and the ocean circulation : III The ocean model. *Monthly Weather Review*, 97, 806-827.
- Budyko M I (1963) *Atlas of the Heat Balance of the Earth* (Gidrometeorozdat, Moscow) pp 69.
- Colborn J G (1975) *The thermal structure of the Indian Ocean*. (University Press of Hawaii, Honolulu) pp 173.
- Colon J A (1964) An interaction between the southwest monsoon current and the sea surface over the Arabian Sea. *Indian Journal of Meteorology and Geophysics*, 15, 183-200.
- Currie R I, A E Fisher and P M Hargreaves (1973) Arabian Sea upwelling. In *The biology of the Indian Ocean*, B Zeitzchel and S A Gerlach (Ed.), Springer-Verlag, 37-53.
- Cutler A and J Swallow (1984) *Surface currents of the Indian Ocean (to 25°S, 100°E)* (Compiled from Archived historical data). (UK Institute of Oceanographic Sciences, Bracknell) pp 8 and charts 36.

- Darbyshire M (1967) The surface waters off the coast of Kerala, southwest India. *Deep-Sea Research*, 14, 295-320.
- Denman K L (1973) A time-dependant model of the upper ocean. *Journal of Physical Oceanography*, 3, 173-184.
- Denman K L and M Miyake (1973) Upper layer modifications at Ocean Station Papa Observations and simulation. *Journal of Physical Oceanography*, 3, 185-196.
- Duing W (1970) **The monsoon regime of the Currents in Indian Ocean.** (East West Centre Press, Honolulu) pp 68.
- Duing W (1972) The structure of sea surface temperature in monsoonal areas. In **Studies in Physical Oceanography**, A L Gordon (Ed.) 1-18.
- Duing W and A Leetmaa (1980) Arabian Sea cooling : A preliminary Heat Budget. *Journal of Physical Oceanography*, 10, 307-312.
- Ellison T H and J S Turner (1959) Turbulent entrainment in stratified flows. *Journal of Fluid Mechanics*, 6, 423-448.
- Eriksen C (1979) An equatorial transect of the Indian Ocean. *Journal of Marine Research*, 37, 215-232.
- Emery W J (1976) The role of vertical motion in the heat budget of the upper northeastern Pacific Ocean. *Journal of Physical Oceanography*, 6, 299-305.
- Esbensen S K and R W Reynolds (1981) Estimating monthly averaged air-sea transfer of heat and momentum using bulk aerodynamic method. *Journal of Physical Oceanography*, 11, 457-465.
- Etter P C (1983) Heat and fresh water budgets of the Gulf of Mexico. *Journal of Physical Oceanography*, 13, 2058-2069.
- Friehe C A and K F Schmitt (1976) Parameterisation of air-sea interface fluxes of sensible and moisture by the bulk aerodynamic formulas. *Journal of Physical Oceanography*, 6, 801-809.
- Gallagher J F (1966) The variability of watermasses in the Indian Ocean. **Publication National Oceanographic Data Centre**, G-11, 1-74.
- Garwood R W (1977) An oceanic mixed layer capable of simulating cyclic states. *Journal of Physical Oceanography*, 7, 455-468.

- Godfrey J S and K R Ridgway (1985) The large scale environment of the poleward flowing Leeuwin Current, western Australia : Longshore steric height gradients, wind stress and geostrophic flow. *Journal of Physical Oceanography*, **15**, 481-495.
- Hareesh Kumar P V, T Pradeep Kumar, Basil Mathew and M X Joseph (1990) Upper ocean thermal structure off Karwar (west coast of India) during the withdrawal phase of monsoon-1987. *Indian Journal of Marine Sciences*, **19**, 36-41.
- Hareesh Kumar P V, N Mohan Kumar and B Mathew (1991) Insolation over the Arabian Sea during the southwest monsoon. *Boundary Layer Meteorology*, **56**, 197-203.
- Hart T J and R I Currie (1960) The Benguela Current. *Discovery Report*, **8**, 437-457.
- Hastenrath S and P Lamb (1979a) *Climatic Atlas of the Indian Ocean - Part I : Surface Climate and Atmospheric Circulation* (Wisconsin University Press, Madison) pp 1 and Figs 97.
- Hastenrath S and P J Lamb (1979b) *Climatic Atlas of the Indian Ocean - Part II : The Oceanic Heat Budget*. (Wisconsin University Press, Madison) pp 17 and Figs 91.
- Hastenrath S and P J Lamb (1980) On the Heat Budget of Hydrosphere and Atmosphere in the Indian Ocean. *Journal of Physical Oceanography*, **10**, 694-708.
- Howe M R and R I Tait (1969) Some observations of the diurnal heat wave in the ocean. *Limnology and Oceanography*, **14**, 16-22.
- Hsiung J (1986) Mean surface energy fluxes over the global oceans. *Journal of Geophysical Research*, **91**, 10585-10606.
- Huyer A and R L Smith (1974) A surface ribbon of cool water over the continental shelf of Oregon. *Journal of Physical Oceanography*, **4**, 381-391.
- Jerlov N G (1968) *Optical Oceanography*. (Elsevier, London). pp 194.
- Johannessen O M, G Subbaraju and J Blindheim (1981) Seasonal variation of the oceanographic conditions off the southwest coast of India during 1971-75. *FiskeriDir. Skr. Ser.*, **18**, 247-261.

- Joseph M G, P V Hareesh Kumar and B Mathew (1990) Short term pre-onset southwest monsoonal transformations in upper western equatorial Indian Ocean. *Indian Journal of Marine Sciences*, 19, 251-256.
- Joseph P V (1990) Warmpool over the Indian Ocean and monsoon onset. *Tropical Oceans Global Atmosphere Newsletter*, 53, 1-5.
- Kato H and O M Phillips (1969) On the penetration of a turbulent layer into stratified fluid. *Journal of Fluid Mechanics*, 37, 643-655.
- Kondo J, Y Sasano and R T Ishii (1979) On wind driven current and temperature profiles with diurnal period in the oceanic planetary boundary layer. *Journal of Physical Oceanography*, 9, 360-362.
- Kraus E B and C Rooth (1962) Temperature and steady state vertical heat flux in the ocean surface layers. *Tellus*, 13, 231-238.
- Kraus E B and J S Turner (1967) A One-dimensional model of the seasonal thermocline II The general theory and its consequences. *Tellus*, 19, 98-106.
- Krishnamurti T N (1981) Cooling of the Arabian Sea and the onset vortex during 1979 In: **Recent Progress in equatorial oceanography**, Report of final meeting of SCOR Working Group 47 (Venice, Italy).
- Kundu P K (1980) A numerical investigation of the mixed layer dynamics. *Journal of Physical Oceanography*, 10, 220-236.
- Lamb P J and Bunker (1982) The annual march of heat budget of the northern and tropical Arabian Sea. *Journal of Physical Oceanography*, 12, 1388-1410.
- Leetmaa A and H Stommel (1980) Equatorial Current Observations in the Western Indian Ocean in 1975 and 1976. *Journal of Physical Oceanography*, 10, 258-269.
- Leetmaa A, D R Quadfasel and D Wilson (1982) Development of the flow field during the onset of the Somali Current, 1979. *Journal of Physical Oceanography*, 12, 1325-1342.
- Levitus S (1982) **Climatological Atlas of the world ocean**. (US Government Printing Office, Washington DC) pp 213.

- Levitus S (1986) Annual cycle of salinity and salt storage in the world ocean. *Journal of Physical Oceanography*, **16**, 322-343.
- Lukas R (1991) The Diurnal Cycle of Sea Surface Temperature in the Western Equatorial Pacific. *Tropical Oceans Global Atmosphere Notes*, **2**, 1-5.
- Lumb F E (1964) The Influence of Cloud on Hourly Amount of Total Solar Radiation at the Sea Surface. *Quarterly Journal of the Royal Meteorological Society*, **90**, 43-56.
- Mathew B (1983) **Studies on upwelling and sinking in the seas around India**, Ph.D Thesis, University of Cochin, pp 159.
- McCreary J P (1981) *Phil. Roy. Soc. Lond.* 355.
- McCreary J P and S Y Chao (1985) Three-dimensional shelf circulation along an eastern ocean boundary. *Journal of Marine Research*, **43**, 13-36.
- McCreary J and P K Kundu (1989) A numerical Investigation of Sea Surface Temperature Variability in the Arabian Sea. *Journal of Geophysical Research*, **94**, 16097-16114.
- McPhaden M J (1982a) Variability in the central equatorial Indian Ocean, I, Ocean Dynamics. *Journal of Marine Research*, **40**, 157-176.
- McPhaden M J (1982b) Variability in the central equatorial Indian Ocean, II, Oceanic heat and turbulent energy balances. *Journal of Marine Research*, **40**, 403-419.
- Mellor G L and P A Durbin (1975) The structure and dynamics of the ocean surface layer. *Journal of Physical Oceanography*, **5**, 718-728.
- Miles J W (1961) On the stability of heterogeneous shear flows. *Journal of Fluid Mechanics*, **10**, 496-508.
- Miller J R (1976) The salinity effects in a mixed layer ocean model. *Journal of Physical Oceanography*, **6**, 29-35.
- Molinari R L (1983) Somali Basin response to the monsoon and the feed back effect of the atmosphere. (CCCO Panel on Indian Ocean Climatic Studies, First Session, Paris)
- Molinari R L, J F Festa and J C Swallow (1986a) **Mixed layer and thermocline climatologies in the western Indian Ocean** (Atlantic Oceanographic and Meteorologic Laboratory, Miami), pp 40.

- Molinary R L, J C Swallow and J F Festa (1986b) Evolution of near surface thermal structure in the western Indian Ocean during FGGE 1979. *Journal of Marine Research*, **44**, 739-763.
- Murthy P G K, P V Hareesh Kumar (1991) Response of coastal waters off Karwar to a deep depression. *Continental Shelf Research*, **11**, 239-250.
- Munk W H and E R Anderson (1948) Notes on a theory of the thermocline. *Journal of Marine Research*, **7**, 276-295.
- Murthy V S N, D P Rao and J S Sastry (1983) The lowering of sea surface temperature in the east central Arabian Sea associated with a cyclone. *Mahasagar*, **16**, 67-71.
- Narayana Pillai V, P K Vijayarajan and A Nandakumar (1980) Oceanographic investigations off the southwest coast of India. *FAO/UNDP Report*, (FAO, Rome), pp 51.
- Niiler P P and E B Kraus (1977) One dimensional models. In **Modeling and prediction of the Upper Layers of the Ocean**, E B Kraus (Editor) (Pergamon Press, New York) 143-172.
- Noble A (1968) Studies on sea water off the north Canara coast. *Journal of Marine Biological Association India*, **10**, 197-227.
- Ostapoff F and S Worthem (1974) The intra-diurnal variations in the upper ocean layers. *Journal of Physical Oceanography*, **4**, 601-612.
- Oke T R (1987) **Boundary Layer Climatology**. (Methuen, USA) pp 435.
- Pankajakshan T and D V Ramaraju (1987) In **Contributions in Marine Sciences**. T S S Rao et al (Editors) 237-
- Patil M R, C P Ramamirtham, P U Varma, C P Nair, and P Myrland (1964) Hydrography of the west coast of India during the pre-monsoon period of the year 1962. Part I- Shelf water of Maharashtra and southwest Sourashtra coasts. *Journal of Marine Biological Association India*, **6**, 151-166.
- Paulson C A and J J Simpson (1977) Irradiance measurements in the upper ocean. *Journal of Physical Oceanography*, **7**, 952-956.
- Payne R E (1972) Albedo of Sea Surface. *Journal of Atmospheric Sciences*, **29**, 959-970.

- Pedlosky J (1974) Longshore currents, upwelling and bottom topography. *Journal of Physical Oceanography*, **4**, 214-226.
- Phillips O M (1977) *The dynamics of the upper ocean*. (Cambridge University Press, New York) pp 336.
- Piat J F and E J Hopfinger (1981) A boundary layer topped by a density interface. *Journal of Fluid Mechanics*, **113**, 411-443.
- Pickard G L and W J Emery (1982) *Descriptive Physical Oceanography. An Introduction*, (Pergamon Press, Oxford), pp 249.
- Pollard R T (1977) Observations and models of the structure of the upper ocean. In *Modelling and Prediction of the Upper Layers of the Ocean*, Ed. E B Kraus, Pergamon, New York, 102-117.
- Pollard R T, R B Rhines and R O R Y Thompson (1973) The deepening of the wind mixed layer. *Geophysical Fluid Dynamics*, **4**, 381-404.
- Price J F (1979) Observations of rain formed mixed layer. *Journal of Physical Oceanography*, **9**, 643-649.
- Price J F, C N K Mooers and J C Van Leer (1978) Observation and Simulation of Storm-Induced Mixed-Layer Deepening. *Journal of Physical Oceanography*, **8**, 582-599.
- Price J F, R A Weller and R Pinkel (1986) Diurnal cycling Observations and Models of the Upper Ocean Response to Diurnal Heating, Cooling and Wind Mixing. *Journal of Geophysical Research*, **91**, 8411-8427.
- Quadfasel D R (1982) Low frequency variability of the 20°C isotherm topography in the western equatorial Indian Ocean. *Journal of Geophysical Research*, **87**, 1990-1996.
- Quadfasel D R and F Schott (1982) Watermass distribution at intermediate layers off the Somali Coast during the southwest monsoon 1979. *Journal of Physical Oceanography*, **12**, 1358-1372.
- Ramam K V S, P G K Murthy and C K B Kurup (1979) Thermal structure variations in the Arabian Sea (May-June). *Mausam*, 105-112.

- Ramamirtham C P and R Jayaramam (1960) Hydrographic features of the continental shelf waters off Cochin during the years 1958-59. *Journal of Marine Biological Association India*, 2, 155-168.
- Ramamirtham C P and M R Patil (1965) Hydrography of the west coast of India during the pre-monsoon period of the year 1962, Part 2 In and offshore waters of the Konkan and Malabar coasts. *Journal of Marine Biological Association India*, 7, 150-168.
- Ramamirtham C P and D S Rao (1973) On upwelling along the west coast of India. *Journal of Marine Biological Association India*, 15, 306-317.
- Rama Sastry A A and P Myrland (1959) Distribution of temperature, salinity and density in the Arabian Sea along the South Malabar Coast (South India) during the post-monsoon season. *Indian Journal of Fisheries*, 6, 223-255.
- Ramamurthy S (1963) Studies on the hydrological factors in the North Kanara coastal waters. *Indian Journal of Fisheries*, 10, 79-53.
- Ramesh Babu V and J S Sastry (1984) Summer cooling in the east central Arabian Sea - A process of dynamic response to the southwest monsoon. *Mausam*, 35, 17-26
- Ramesh Babu V, M J Varkey, V Kesavadas and A D Gouveia (1980) Watermass and general hydrography along the west coast of India during early March. *Indian Journal of Marine Sciences*, 9, 82-89.
- Rao D P, R V N Sarma, J S Sastry and K Premchand (1976) On the lowering of the surface temperature in the Arabian Sea with the advance of southwest monsoon. Proceeding of the symposium on *Tropical Monsoons* (Indian Institute of Tropical Meteorology, Pune) 106-115.
- Rao R R (1984) A case study on the influence of summer monsoon vortex on the thermal structure of upper central Arabian Sea during the onset phase of MONEX-79. *Deep-Sea Research*, 31, 1511-1521.
- Rao R R (1986) Cooling and deepening of the mixed layer in the central Arabian Sea during MONSOON-77 : Observations and simulations. *Deep-Sea Research*, 33, 1413-1424.

- Rao R R (1987) The observed variability of the cooling and deepening of the mixed layer in the central Arabian Sea during monsoon-77. *Monsoon*, **38**, 43-48.
- Rao R R (1988) Seasonal heat budget estimates of the upper layers in the central Arabian Sea. *Monsoon*, **39**, 241-248.
- Rao R R and B Mathew (1990) A case study on the mixed layer variability in the south central Arabian Sea during the onset phase of MONEX-79. *Deep-Sea Research*, **37**, 227-243.
- Rao R R, P V Hareesh Kumar and B Mathew (1990) Watermass modification in the upper layers of the Arabian Sea during ISMEX-73. *Monsoon*, **41**, 611-620.
- Rao R R, P V Hareesh Kumar and B Mathew (1991) Surface layer warming in the Arabian Sea before the onset of summer monsoon during MONEX-79. Submitted to *Oceanologica Acta*
- Rao R R, R L Molinari and J F Festa (1989) Evolution of the Climatological Near-Surface Thermal Structure of the Tropical Indian Ocean I Description of Mean Monthly Mixed Layer Depth, Sea Surface Temperature, Surface Current and Surface Meteorological Fields. *Journal of Geophysical Research*, **94**, 10801-10815.
- Rao R R, R L Molinari and J F Festa (1991) **Surface meteorological and near surface oceanographic Atlas of the tropical Indian Ocean.** (NOAA Technical Memorandum, ERL AOML-69) pp 59.
- Rao R R and K V Sanil Kumar (1991) Evolution of salinity field in the upper layers of the east central Arabian Sea and northern Bay of Bengal during summer monsoon experiments. *Proceedings of the Indian Academy of Sciences (Earth and Planetary Sciences)*, **100**, 69-78.
- Reed R K (1977) On Estimating Insolation over the Ocean. *Journal of Physical Oceanography*, **7**, 482-485.
- Robinson M K, R A Baur and E H Schroeder (1979) **Atlas of North Atlantic-Indian Ocean monthly mean temperature and mean salinities of the surface layer.** (Naval Oceanographic Office, Washington DC) pp 213.
- Rochford D J (1964) Salinity maxima in the upper 1000m of the north Indian Ocean. *Australian Journal of Marine and Freshwater Research*, **15**, 1-24.

- Saddler J C, M A Lander, A M Hori and L K Oda (1987) **Tropical Marine Climatic Atlas**, Vol I. Indian Ocean and Atlantic Ocean. (University of Hawaii, Honolulu)
- Saha K R (1974) Some aspects of the Arabian Sea summer monsoon. *Tellus*, **26**, 464-476.
- Sastry J S and R S D'Souza (1970) Oceanography of the Arabian Sea during southwest monsoon season - Part I Thermal structure. *Indian Journal of meteorology and Geophysics*, **21**, 367-382.
- Sastry J S and R S D'Souza (1971) Oceanography of the Arabian Sea during southwest monsoon season - Part II : Stratification and Circulation. *Indian Journal of meteorology and Geophysics*, **22**, 23-34.
- Sastry J S and R S D'Souza (1972) Oceanography of the Arabian Sea during southwest monsoon season - Part III Salinity. *Indian Journal of Meteorology and Geophysics*, **23**, 479-490.
- Sastry J S and V Ramesh Babu (1979) Convergence of Ekman wind driven layer and surface circulation in the Arabian Sea during southwest monsoon. *Mahasagar*, **12**, 201-211.
- Schott F (1983) Monsoon response of the Somali Current and associated upwelling. *Progress in Oceanography*, **12**, 357-381.
- Seckel G R and F H Beaudry (1973) Radiation from sun and sky over the Pacific Ocean. *Transaction of the American Geophysical Union*, **54**, 1114.
- Seetaramayya P and A master (1984) Observed Air-Sea Interface Conditions and a Monsoon Depression During MONEX-79. *Archives for Meteorology, Geophysics and Bioclimatology*, **33**, 61-67.
- Sharma G S (1966) Thermocline as an indicator of upwelling. *Journal of Marine Biological Association of India*, **3**, 8-19.
- Sharma G S (1968) Seasonal variation of some hydrographic properties of the shelf water off the west coast of India. *Bulletin of the National Institute of Sciences*, **38**, 263-275.
- Sharma G S (1972) Water characteristics at 200 cl/t in the intertropical Indian Ocean during the southwest monsoon. *Journal of Marine Research*, **30**, 102-111.

- Sharma G S (1976) Transequatorial movement of watermass in the Indian Ocean. *Journal of Marine Research*, **34**, 143-154.
- Sharma G S (1978) Upwelling off the southwest coast of India. *Indian Journal of Marine Sciences*, **7**, 207-218.
- Shetye S R (1984) Seasonal variability of the temperature field off the southwest coast of India. *Proceeding of the Indian Academy of Sciences (Earth and Planetary Sciences)*, **93**, 129-137.
- Shetye S R (1986) A model study of the seasonal cycle of the Arabian Sea surface temperature. *Journal of Marine Research*, **44**, 521-542.
- Shetye S R, A D Gouveia, S S C Shenoi, D Sundar, G S Michael, A M Almeida and K Santanam (1990) Hydrography and circulation off the west coast of India during the Southwest Monsoon 1987. *Journal of Marine Research*, **48**, 359-378.
- Shonting D H (1964) Some observations of short term heat transfer through the surface layers of the ocean. *Limnology and Oceanography*, **7**, 576-588.
- Simpson J J and T D Dickey (1981) Alternative parameterization of downward irradiance and their dynamical significance. *Journal of Physical Oceanography*, **11**, 876-882.
- Simpson J J and C A Paulson (1979) Mid-ocean observations of atmospheric radiation. *Quarterly Journal of Royal Meteorological Society*, **105**, 487-502.
- Smith R L and J S Bottero (1977). On upwelling in the Arabian Sea. In : *A voyage of Discovery*, M Angel (Ed.), Pergamon Press, 291-304.
- Stevenson J W and P P Niiler (1983) Upper ocean heat budget during Hawaii to Tahiti shuttle experiment. *Journal of Physical Oceanography*, **13**, 1894-1907.
- Stommel H and A H Woodcock (1951) Diurnal heating on the surface layers of the Gulf of Mexico in the spring of 1942. *Transaction of the American Geophysical Union*, **32**, 565-571.
- Swallow J C and J G Bruce (1966) Current measurements off the Somali Coast during the southwest monsoon in 1964. *Deep-Research*, **13**, 861-888.

- Swallow J C, R L Molinari, J G Bruce, O B Brown and R H Evans (1983) Development of near-surface flow pattern and watermass distribution in the Somali Basin in response to the southwest monsoon of 1979. *Journal of Physical Oceanography*, 13, 1398-1415.
- Taft B A and J A Knauss (1967) The Equatorial Undercurrent of the Indian Ocean as observed by the Lusiad expedition. *Bulletin of Scripps Institution of Oceanography*, 9, pp 163.
- Thompson R O R Y (1976) Climatological numerical models of the surface mixed layer of the ocean. *Journal of Physical Oceanography*, 6, 496-503.
- Thorpe S A (1971) Experiments on the instability stratified shear flows: miscible fluids. *Journal of Fluid Mechanics*, 46, 299-320.
- Tunnel G A (1963) Sea temperature fluctuations in the Red Sea, The Gulf of Aden and the Arabian Sea. *Marine Observer*, 33, 192-201.
- Turner J S (1969) A note on wind mixing at the seasonal thermocline. *Deep-Sea Research*, 16 (Supplement), 297-300.
- Varadachari V V R, C S Murthy and V N Sankaranarayanan (1974) Physical characteristics of waters and watermasses off the west coast of India during late spring. *Indian Journal of Marine Sciences*, 3, 1-4.
- Varma K K, V Kesavadas and AD Gouveia (1980) Thermohaline Structure and Watermass in the Northern Arabian Sea during February-April. *Indian Journal of Marine Sciences*, 9, 149-155.
- Warren B, H Stommel and J C Swallow (1966) Watermasses and patterns of flow in the Somali Basin during the southwest monsoon of 1964. *Deep-Sea Research*, 13, 825-860.
- Weare B C, P T Strub and M D Samuel (1981) Annual mean surface heat flux in the tropical Ocean. *Journal of Physical Oceanography*, 11, 705-717.
- Wooster W S and M Gilmartin (1961) The Peru-Chile Undercurrent. *Journal of Marine Research*, 19, 97-112.
- Wooster W S and W H Jones (1970) California Undercurrent off Northern Baja California. *Journal of Marine Research*, 28, 235-250.

- Wooster W S and J L Reid (1961) Eastern boundary currents. In *The Sea*, Volume II. M N Hill (Editor), 253-280.
- Wooster W S, M B Schaefer and M K Robinson (1967) *Atlas of the Arabian Sea for Fishery Oceanography* (Institute of Marine Resources, University of California) pp 37 and 72 charts.
- Wyrtki K (1971) *Oceanographic Atlas of the International Indian Ocean Expedition* (US Government Printing Office, Washington DC) pp 531.
- Wyrtki K (1973) An equatorial Jet in the Indian Ocean. *Science*, 11, 262-264.
- Yoshida K (1955) Coastal upwelling off the California Coast. *Records of Oceanographic Works in Japan*, 2, 8-20.
- Yoshida K and H L Mao (1957) A theory of upwelling of large horizontal extent. *Journal of Marine Research*, 16, 40-54.
- Yoshida K and M Tsuchiya (1957) Northward flow in lower layers as an indicate of coastal upwelling. *Records of Oceanographic Works Japan*, 4, 14-22.